Recent developments in organic redox flow batteries: a critical review

P. Leung [1], A.A. Shah [2*], L. Sanz [3], C. Flox [3], J. R. Morante [3], Q.Xu [4], M.R. Mohamed [5],

C. Ponce de León [6], F.C. Walsh [6*]

1. *Department of Materials, University of Oxford, Oxford, OX 3PH, UK*

2. *School of Engineering, University of Warwick, Coventry, CV4 7AL, UK.*

3. *Insitut de Recerca en Energia de Catalunya (IREC), Barcelona, 08939, Spain.*

4. Institute for Energy Research, Jiangsu University, Zhenjiang, China

5. *Sustainable Energy & Power Electronics Research Group, Faculty of Electrical & Electronics Engineering, Universiti Malaysia Pahang, Pekan, Pahang 26600, Malaysia.*

6. *Electrochemical Engineering Laboratory, Energy Technology Group, University of Southampton, Highfield, Southampton, SO17 1BJ, UK.*

*****Authors for correspondence: ; Akeel.Shah@warwick.ac.uk; F.C.Walsh@soton.ac.uk

Abstract

Redox flow batteries (RFBs) have emerged as prime candidates for energy storage on the medium and large scales, particularly at the grid scale. The demand for versatile energy storage continues to increase as more electrical energy is generated from intermittent renewable sources. A major barrier in the way of broad deployment and deep market penetration is the use of expensive metals as the active species in the electrolytes. The use of organic redox couples in aqueous or non-aqueous electrolytes is a promising approach to reducing the overall cost in long-term, since these materials are low-cost and abundant. The performance of such redox couples can be tuned by modifying their chemical structure. In recent years, significant developments in organic redox flow batteries has taken place, with the introduction of new groups of highly soluble organic molecules, capable of providing a cell voltage and charge capacity comparable to conventional metal-based systems. This review summarises the fundamental developments and characterization of organic redox flow batteries from both the chemistry and materials perspectives. The latest advances, future challenges and opportunities for further development are discussed.

Keywords: Aqueous, non-aqueous, organic, redox couples.

Contents

1. Introduction

One of the hurdles to achieving an increased share of intermittent renewables at the grid scale is the need to provide a stable energy output to end-users. This will require robust energy storage devices, to deliver stable and flexible electricity that adheres to accepted standards for voltage and frequency, whether grid-connected or off-grid [1-8]. Over the last 30 years, a number of energy storage technologies have been introduced and successfully demonstrated, including thermal (i.e. latent or sensible heat), mechanical (i.e. pump hydro, compressed air) and chemical/electrochemical (i.e. fuel cells and rechargeable batteries). Amongst these technologies, electrochemical devices are attractive because they can be installed anywhere, free from the geological/geographical restrictions [3, 4]. To ensure that energy storage devices are economically viable in the long term, the US Department of Energy (DoE) has set a system capital cost target of USD$ 150 $(kW\ h)^{-1}$ by 2023, alongside a target of USD$ 100 $(kW)^{-1}$ to match with existing physical energy storage technologies [9]. This is expected to be in line with the requirements of the EU [10].

With regards to both economic and safety considerations, redox flow batteries (RFBs) are recognized as one of the most realistic candidates amongst electrochemical technologies for energy storage in the range of several kW/ kW h up to tens of MW / MW h [3, 4]. In contrast to conventional rechargeable batteries, redox flow batteries store all or part of the charge in electrolytes recirculated through the cell, while in conventional batteries such as lead acid and lithium-ion batteries, charge is stored entirely within the cell (as active materials in the electrode structures) and the electrolyte remains in the cell at all times [3, 4]. This method of charge storage enables redox flow batteries to be scaled more easily, economically and safely than conventional batteries. In RFBs, the electrolytes are

typically stored in separate reservoirs and circulated through the batteries during charge and discharge (Figure 1a); exceptions include the soluble lead acid battery, which operates with a single electrolyte in a single reservoir [11]. In contrast, a fuel cell (FC) is a purely Galvanic cell, in which catalytic oxidation of an externally stored fuel and reduction of an oxidant (typically oxygen from an air-breathing cathode) take place continuously. As in a fuel cell, an ion exchange membrane is usually required in a RFB to minimize losses associated with cross-contamination of the two half-cell electrolytes (internal currents). In a few cases, undivided cells are possible, subject to the stability of the positive active species in contact with the negative electrode materials [3].

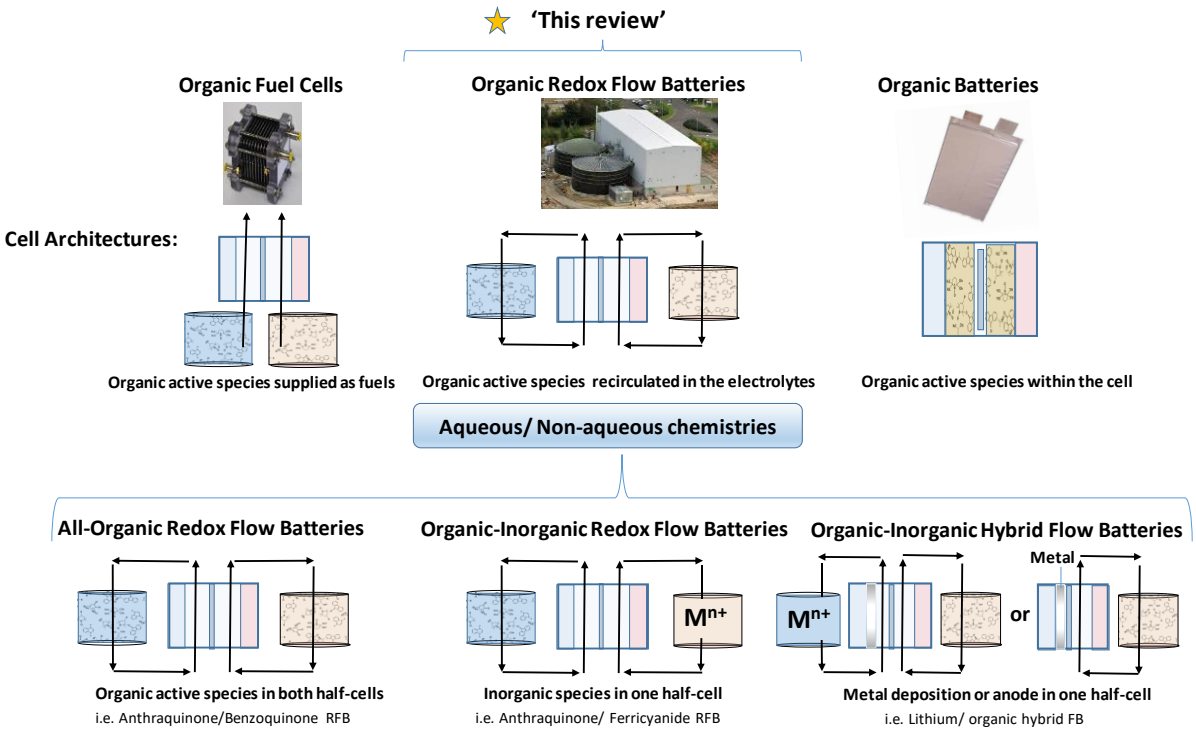

Figure 1a

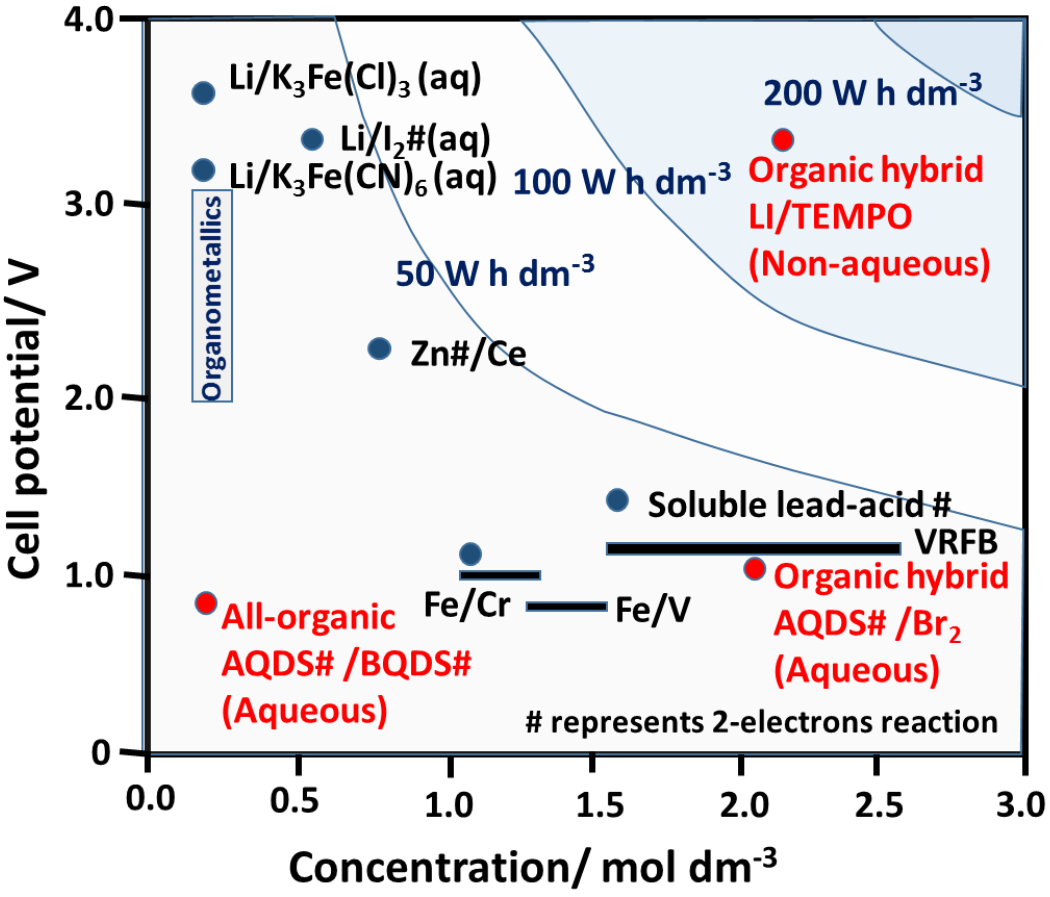

Figure 1b

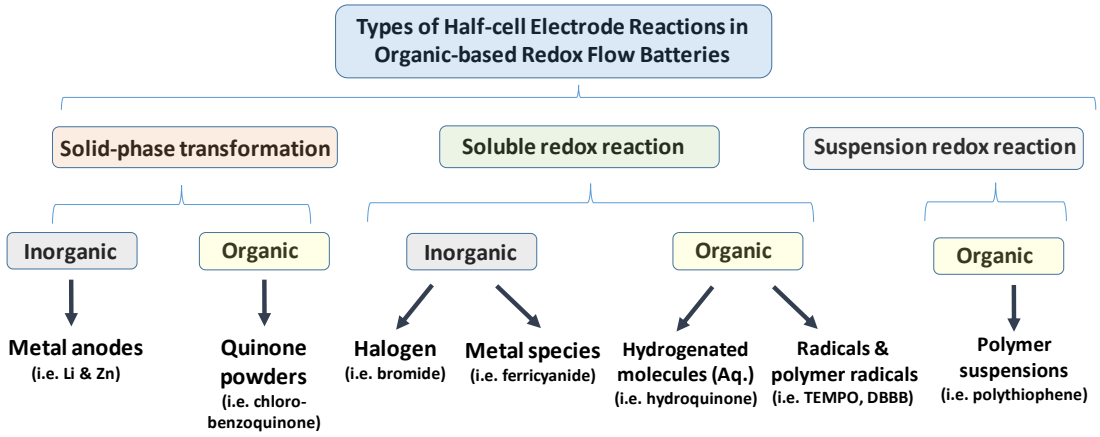

Figure 1c

Figure 1 Overview of organic redox flow batteries considered in this review: (a) general classification of organic-based electrochemical power sources; (b) summary of the performance and energy density of the reported

organic flow battery systems; and (c) various types of half-cell electrode reactions in existing organic flow battery systems.

Redox flow batteries can be more scalable than conventional batteries without incurring losses in the power density. Scale-up of power can be achieved by increasing the electrode active surface area or the number of electrodes in a cell stack. The storage capacity of conventional RFB is can be increased by increasing the volume of the electrolytes and/or the concentrations of active species.

The overall cost per kW h of the redox flow battery not only depends on the costs of the cell components but also on the molar mass and the corresponding chemistries of the electroactive species. For example, higher concentrations of electrolytes are desired for active species with lower molar mass. If the selected chemistry is reversible and yields a higher cell voltage and/or multi-electron transfers, a larger energy capacity is expected for a given electrolyte concentration [1-8]. A high solubility of the redox couple is needed to maintain a high current while minimizing mass transport losses; ideally, the majority of charge and discharge should take place under charge transfer control at both electrodes.

Various metal-based redox flow battery chemistries have been proposed with the use of aqueous and non-aqueous electrolytes [12-29]. Some successful systems have received significant industrial investment and have reached the stage of commercialization, mainly for grid-scale applications due to their relatively low energy densities (<40 W h dm^{-3}) [3]. At present, the all-vanadium redox flow battery is the most developed system, primarily as a consequence of the active species remaining in solution at all times during charge/discharge cycling, its high reversibility and its relatively large power output. Compared to the DoE target, however, the capital cost of these systems (USD$ 300 – 800

kW h^{-1}) remains far too high for deep market penetration [30, 31]. For example, the cost of vanadium redox flow battery electrolytes is as high as USD$ 80 (kW h)$^{-1}$, while the ion-exchange membrane can account for up to 40% of the total cost of the battery [32, 33].

In order to meet the proposed cost target of USD$150 (kW h)$^{-1}$ [9], recent investigations have highlighted the use of organic active materials in solid-state organic batteries [34-38], in which energy is stored within the cell, mainly in the form of a radical polymer. In general, the advantages of using organic molecules are their abundance and the possibility of extraction from various sources. These compounds are based on common elements, such as carbon, hydrogen, oxygen and sulfur. Even in the early stages of development, the electrolyte cost of some organic-based flow batteries has been demonstrated to be lower than USD$ 35 (kW h)$^{-1}$ (based on half-cell estimates) [39-42]. With advances in synthetic chemistry, the properties of these organic molecules can be further tailored to provide fast kinetics and high solubility, and to yield high cell voltages in batteries [43-47]. The electrolyte cost per kW h can be lowered further by selecting active species based on the cell voltage and/or on multi-electron transfers. In the presence of non-aqueous electrolytes, the operating cell voltage is no longer limited to 1.5 V due to the evolutions of hydrogen and oxygen in the water electrolysis. In contrast, the electrochemical stability window of typical non-aqueous solvents, such as acetonitrile and propylene carbonate, can exceed 5 V [48]. As suggested by fundamental electrochemical behaviour, some redox couples exhibit better electrochemical performance at more negative potentials than is possible in aqueous electrolytes [49, 50], and a cell voltage of 4.5 V might be achieved by the use of a suitable pair of organic redox couples [43].

Organic electroactive species can provide the possibility of a higher solubility in both aqueous and non-aqueous electrolytes. Before the introduction of all-organic redox flow batteries, organic molecules contained in aqueous electrolytes (with reasonable solubilities (> 1 mol dm^{-3})) were used in early studies of regenerative fuel cells [51] and organic fuel cells [52, 53]. In the case of quinoxaline, the solubility is up to 4.0 mol dm^{-3} in potassium hydroxide solution (0.9 mol dm^{-3} potassium chloride + 0.1 mol dm^{-3} potassium hydroxide, pH 12.9) and the redox potential in such an electrolyte is more negative than – 0.70 V *vs.* SHE [54], although the addition of salts and solvents could reduce the solubility significantly (e.g., solubilities of quinoxaline: 4.5 mol dm^{-3} at at *c.a.* 1.0 mol dm^{-3} potassium chloride and 0.01 mol dm^{-3} potassium hydroxide; 0.5 mol dm^{-3} at *c.a.* 0.5 mol dm^{-3} potassium sulphate and 0.01 mol dm^{-3} potassium hydroxide). High solubilities of organic compounds have been reported in selected non-aqueous electrolytes [43]. For instance, methyl-para benzoquinone (molar mass: 122.12 g mol^{-1}) has a solubility of up to 6 mol dm^{-3} in acetonitrile [55].

In the most ideal scenario, if these organic compounds could function as reversible redox species in a rechargeable battery, the specific energy of 150 W h kg^{-1} or energy density of 240 W h dm^{-3} could be similar to, or higher than conventional lithium-ion batteries (120 W h kg^{-1}; 240 W h dm^{-3} (Table 1)).

Parameters	Conventional all-vanadium RFB	Conventional lithium-ion batteries	Projected organic RFB*
Electron stoichiometry	1	< 1	2
V Concentration / mol dm^{-3}	2	0	6 mol dm^{-3}
Cell potential / V	1.4 – 1.8	3.6	1.5
% Energy efficiency	75	90	75
Charge capacity	54 A h dm^{-3}	70 A h dm^{-3}	320 A h dm^{-3}
Energy density	35 W h dm^{-3}	240 W h dm^{-3}	210 W h dm^{-3}
Specific energy	31 W h kg^{-1}	120 W h kg^{-1}	150 W h kg^{-1}

Table 1 Comparison of the projected organic redox flow battery characteristics with those of the conventional all-vanadium redox flow and lithium-ion batteries. *Assumed performance of projected organic flow battery system: 2-electron transfers, 1.5 V and 75% round trip energy efficiency.

This assumption is based on a realistic performance scenario for an existing flow battery, namely, a molecular weight of 120 g mol^{-1}, a 2-electron transfer, a cell potential of 1.5 V and a 75% round trip energy efficiency [56]. To obtain these desirable properties for all-organic flow batteries, tremendous improvements need to be made in existing systems, considering that the energy densities are still lower than 15 Wh dm^{-3} in both aqueous and non-aqueous systems (i.e. aqueous methyl viologen/ hydroxyl-TEMPO flow batteries: 8.4 W h dm^{-3} [57]; non-aqueous fluorine-DBMMB: 11 Wh dm^{-3} [58]). For aqueous systems, it is still a challenge to obtain high solubility and high cell voltage simultaneously. In contrast, non-aqueous systems often suffer from high electrolyte/separator resistances, low utilization, chemical instability and crossover of the active materials. For both types of systems, it is also important to use lower molar mass molecules (< 200 g mol^{-1}) to obtain higher specific capacity (i.e. 1,4-benzoquinone: 108 g mol^{-1}; *c.a.* 496 Ah Kg^{-1} (2 e^-); 9,10-anthraquinone-2,6-disulfonic acid disodium: 412 g mol^{-1}; *c.a.* 129 Ah Kg^{-1} (2 e^-)), although synthesizing active materials with molar masses of lower than 100 g mol^{-1} is unlikely [59].

Despite these hurdles, the energy densities of several organic-inorganic systems (aqueous anthraquinone-bromide flow batteries: 16 W h dm^{-3} [40]; non-aqueous lithium-meo-TEMPO flow batteries: 200 W h dm^{-3} (static) [60]) are already comparable to their commercial counterparts in aqueous (e.g., all-vanadium redox flow batteries: 35 W h dm^{-3}) and non-aqueous (e.g., lithium-ion batteries: 240 W h dm^{-3}) chemistries, as indicated in Figure 1b).

The major hurdles to the widespread adoption of electrochemical energy storage as the main power source in electric vehicles are strongly related to cost and safety, as well as the slow recharging of existing devices, such as lithium-ion batteries. Considering that

the architecture of a redox flow battery enables the charge to be stored largely within the electrolytes, ultra-fast recharging could be possible by simply ´refueling´ with charged electrolytes in the reservoirs [61]. Automobile applications open up an important new research direction for RFBs (including organic systems) and require further developments in performance (energy/power density), system architectures and durability, alongside an overall cost per kW h of USD$150 $(kW\ h)^{-1}$ or lower.

Recently, Dmello *et al.* [59] have evaluated the design pathways of redox flow batteries in both aqueous and non-aqueous electrolytes by considering a number of parameters in the design iterations. It was found that decreasing the active material cost could provide the most drastic savings in aqueous systems, since the cost of the supporting electrolyte is extremely low (*c.a.* USD$ 0.1 Kg^{-1}) and is not likely to increase or decrease in the future due to an already mature and high-volume production. In contrast, the costs of organic active materials are estimated to decrease from USD$ 20 Kg^{-1} (in 2014) down to USD$ 3 – 7 Kg^{-1} in the future [41]. The cost of vanadium (USD$ 20 Kg^{-1} in 2014) is predicted to be between USD$ 7 – 37 Kg^{-1} [41].

For aqueous systems, a more ambitious cost target of USD$ 100 $(kW\ h)^{-1}$ can be achieved with the combination of USD$ 2 Kg^{-1} active material cost, 100 g mol^{-1} molar mass of active material, 0.5 Ω cm^2 area specific resistance of the battery and 0.79 V cell voltage. For non-aqueous systems, the cost is not particularly sensitive to the active material cost (future-state cost: *c.a.* USD$ 5 Kg^{-1}), since they often use expensive solvents (e.g. nitriles, glymes, and carbonates) and fluorinated salts (e.g.. tetrafluoroborates, hexafluorophosphates and bis(tri-fluoromethylsulfonyl)imides). The future-state costs of salts and solvents are expected to be as expensive as USD$ 20 Kg^{-1} and USD$ 2 Kg^{-1}, respectively [59].

Therefore, increasing the cell voltage is the most effective approach to reduce the overall cost of the non-aqueous battery, since this simultaneously decreases the cost contributions of both the electrolyte and reactor. Other recommendations include reducing the area specific resistance of the battery, selecting low molar mass active materials with multiple electron-transfers, and using a low salt ratio. For instance, a cost target of USD$ 100 (kW h)$^{-1}$ is achievable with the combination of 100 g mol^{-1} molar mass of active material, 2.5 Ω cm^2 area specific resistance of the battery, 3.0 V cell voltage, a 0.2 salt ratio and a 3.3 mol kg^{-1} active molarity [59].

In order to lower the cost and advance organic redox flow battery technology, it is essential to improve our understanding of organic redox couples. Regarding the redox chemistries [1-5, 17, 43, 62], cell-architectures [63], cell components/structures [3, 64, 65], mathematical modelling [66] and cost analyses [31, 41], several review articles have been published for typical metal-based systems using aqueous and non-aqueous electrolytes. More recently, Gong *et al.* [43] provided a perspective for selection of organic solvents for non-aqueous systems, including the use of metal-free, organic redox couples. Brushett *et al.* [43, 59, 67] evaluated the materials-level requirement and the overall cost of both aqueous and non-aqueous systems. Schon *et al.* [44] reviewed the organic active materials used in supercapacitors and metal-ion/redox-flow batteries. Zhao *et al.* [56] summarised recent developments in lithium-based redox flow batteries for high energy density applications. Kowalski *et al.* [68] reviewed recent advances in molecular engineering of organic molecules for non-aqueous systems. Winsberg *et al.* [69] and Park *et al.* [70] have recently provided an overview of redox flow batteries, ranging from those based on transition metals to those based on organic active materials. In contrast to previous reviews, the present contribution provides a comprehensive summary of all existing organic redox flow batteries with an emphasis on their electrode reactions in both

aqueous and non-aqueous electrolytes. Remaining challenges are highlighted and directions for future development are discussed.

2. Organic-based redox flow batteries

Organic redox flow batteries use active materials based on organic active molecules for at least one electrode reaction. Systems using these active species in both electrode reactions are referred to as 'all-organic redox flow batteries'. In most cases, these active species dissolve in either aqueous or non-aqueous electrolytes, akin to metal-based redox flow batteries. Some organic active materials can be incorporated in polymers [71], or appear as solid electrodes mixed with porous carbon and binders [72]. General classifications of various half-cell electrode reactions of the existing organic based redox flow batteries are summarised in Figure 1c.

To further increase the cell voltage and/or specific energy, some systems incorporate inorganic redox couples in organic-inorganic systems. Common approaches to the latter include the use of highly electronegative metals, e.g. zinc (E^o = −0.76 V *vs.* SHE) [73] and lithium (E^o = −3.00 V *vs.* SHE) [74]) in hybrid systems using either aqueous and non-aqueous electrolytes. Figure 1a provides a schematic of all-organic redox flow batteries and organic-inorganic hybrid flow batteries using metallic anodes. Positive redox couples, such as ferricyanide/ferrocyanide (E^o = + 0.36 V *vs.* SHE), have been used to increase the cell potential in certain electrolytes that lack electropositive organic active materials (>0.5 V *vs.* SHE in alkaline media) at reasonable solubility (>0.6 mol dm^{-3}) [75].

Recent research and development in the redox flow battery community has focused on the identification, synthesis and modification of novel redox active molecules [43-47, 76]. The majority of studies have utilized metallic species in either aqueous and non-aqueous systems. In non-aqueous electrolytes, active molecules mainly take the form of ligand modified inorganic species or metal coordination complexes [18-23, 77] in anion-exchange systems. Although they can achieve relatively high overall cell voltages (>2.0 V), these systems are still based on expensive metals (e.g.., nickel, ruthenium and cobalt [18-23, 77]) and are restricted by the limited solubilities of the complexes, as well as low efficiencies. Recent research efforts have been broadened to include tailored organic molecules that possess higher solubilities in non-aqueous electrolytes (>1.0 mol dm^{-3}). Enabled by recent advances in synthetic chemistry, organic molecules can be tailored to have the necessary properties required of active species in redox flow batteries [43-47, 76, 78]. Several of these synthetic or tailored molecules have exhibited high cell voltages and fast kinetics, in addition to being low cost. However, further major challenges from the current status are to achieve all of the aforementioned benefits in addition to high solubility, long cycle life and low toxicity [43]. While early research focused on the use of organic active molecules in non-aqueous electrolytes, several recent investigations have demonstrated promising levels of performance of aqueous systems (in terms of solubilities and efficiencies) using innovative approaches described in the following sections.

2.1. Organometallic materials and organic ligand complexes

Flow batteries with organic ligand complexes and organometallic materials are good examples of the evolution from metal-based to organic-based redox flow battery systems

[70]. The electrochemical behaviour of a number of transition metal complexes (iron, cobalt, vanadium, cerium, chromium and ruthenium) with ligands, e.g., ethylenediaminetetraacetate (EDTA) [79, 80], phenanthroline [80, 81], triethanolamine [82] and diethylenetriaminepentaacetic acid (DTPA) [83, 84], was reported in the 1980s in both aqueous and non-aqueous electrolytes. Non-aqueous rechargeable cells using tris(2,21 -bipyridine)ruthenium(II) ($[Ru(bpy)_3]^{2+}$) tetrafluoroborate were first demonstrated by Matsuda [18] in 1988. Subsequently, a non-aqueous system based on the use of ruthenium acetylacetonate ($Ru(acac)_3$) was introduced by Chakrabarti *et al.* [85] and several other metal complexes were investigated by the research groups of Lee [86] and Thompson [19-21]. Metal methanesulfonates, such as cerium [87], lead [88] and vanadium [89], have significantly higher solubilities than their sulphate counterparts, while zinc methanesulfonate [90] effectively reduces the formation of dendrites in the electrodepositions. In the zinc-bromine redox flow battery, organic quaternary ammonium bromide [91], such as 1-ethyl-1-methylmorpholinium bromide or 1-ethyl-1-methylpyrrolidinium bromide, and other ionic liquid additives [92], were used as bromine sequestration agents to complex the evolved bromine gas into a separate phase from the aqueous electrolytes. Investigations have broadened to include metal-centred ionic liquids as active species in non-aqueous electrolytes [76, 93].

The use of organometallic materials can be traced back to the 1970s, when ferricyanide was used in the aqueous zinc-ferricyanide flow battery [94]. Since then, organometallic materials such as metallocene derivatives (e.g., methoxymethylferrocene, carbomethoxyferrocene) have been studied extensively (in non-aqueous electrolytes) as redox shuttle additives for overcharge protection of lithium-ion batteries [95]. Metallocene is a compound consisting of two cyclopentadienyl (Cp) ligands, C_5H_5, bound to a metal centre in the oxidation state of II on opposite sides. It is known that the π–

orbitals of the Cp rings and the d-orbitals in the metal centre are primarily in charge of the coordination and chemical reactivity. In general, ferrocene is an air-stable, sublimable compound, while cobaltocene is a structural analogue of ferrocene but is highly reactive toward air [96].

Different from the aforementioned systems using metal chelates, molecular design on Cp rings can tune both the redox potential and solubility using molecular engineering methods [97]. For instance, ferrocene has a low solubility in organic solvents and electrolytes, e.g., 0.2 mol dm^{-3} in a carbonate mixture and only 0.04 mol dm^{-3} when lithium bis(trifluoromethanesulfonyl)imide (LiTFSI) salt is used in the same solvent mixture. By modifying the molecular structure, Wei *et al.* [97] prepared ferrocenylmethyl dimethyl ethyl ammonium bis(trifluoromethanesulfonyl)imide, which showed significantly enhanced solubility of up to 1.7 mol dm^{-3} in the carbonate mixture and 0.85 mol dm^{-3} with the addition of a lithium bis(trifluorowmethanesulfonyl)imide (LiTFSI) salt [97]. This material was coupled with a lithium anode in a lithium-organic hybrid cell, which attained a cell voltage of 3.49 V and an energy density of 50 W h dm^{-3}.

Recently, a non-aqueous all-metallocene flow battery was proposed by Yu and co-workers [96, 98] using cobaltocene and ferrocene as the negative and positive electrode materials. In N,N-dimethylformamide (DMF), these redox species have electrode potentials of *c.a.* 2.0 V *vs.* Li^+/Li and *c.a.* 3.7 V *vs.* Li^+/Li, respectively. The solubility of cobaltocene was up to 1.5 mol dm^{-3}, higher than in many other negative electrolytes used in non-aqueous systems, in which active species of metal acetylacetonate (derivatives of quinoxaline and anthraquinone) are lower than 1.2 mol dm^{-3} [96]. The resulting chemistry had a cell voltage of 1.7 V with an energy efficiency of > 85 % (at 0.4 C). The reaction

rate constants were up to two orders of magnitude higher than those of conventional active species in aqueous systems (VO_2^+/VO^{2+}, Fe^{3+}/Fe^{2+}) [96].

2.1.1. Organometallic mediators used in flow battery systems

In contrast to previous flow battery architectures using soluble active species or semi-solid suspensions, Wang and co-workers introduced organometallic materials for redox-mediated reactions [63, 99-103]. This concept was inspired by their earlier work of redox targeting in 2006 [104], in which the material was lithiated (reduced) by a molecule with a low redox potential and delithiated (oxidized) by another molecule with a high redox potential. The active materials of these systems are immobile and exposed to the electrolyte. This configuration could avoid the use of a solid suspension and a large mass of conductive carbon [63, 99-103]. Redox mediators such as metallocene and iodide were dissolved in the electrolytes, which were recirculated during the charge-discharge processes. Half-cell studies of using $LiFePO_4$ [99] and Li_xTiO_2 [100, 101] as active materials were conducted by oxidizing or reducing with metallocene mediators as follows:

Charge-discharge of the Li_xTiO_2 negative electrode reactions [63]:

$$xLi^+ + TiO_2 + xCoCp^*_2 \rightarrow Li_xTiO_2 + xCoCp^*_2{}^+ \text{ (in the reservoir)} \quad (1)$$

$$CoCp^*_2{}^+ + e^- \rightarrow CoCp^*_2 \text{ (on the electrode)} \quad (2)$$

$$Li_xTiO_2 + xCoCp_2^+ \rightarrow xLi^+ + TiO_2 + xCoCp_2 \text{ (in the reservoir)} \quad (3)$$

$$CoCp_2 \rightarrow CoCp_2^+ + e^- \text{ (on the electrode)} \quad (4)$$

$CoCp_2$ is cobaltocene with a chemical formulae of $Co(C_5H_5)_2$.

Charge-discharge of the $LiFePO_4$ positive electrode reactions [63]:

$$FcBr_2^+ + LiFePO_4 \rightarrow FcBr_2 + FePO_4 + Li^+ \text{ (in the reservoir)} \quad (5)$$

$$FcBr_2 \rightarrow FcBr_2^+ + e^- \text{ (on the electrode)} \quad (6)$$

$$Fc + FePO_4 + Li^+ \rightarrow Fc^+ + LiFePO_4 \text{ (in the reservoir)} \quad (7)$$

$$Fc^+ + e^- \rightarrow Fc \text{ (on the electrode)} \quad (8)$$

Fc is ferrocene with a chemical formulae of $Fe(C_5H_5)_2$.

The capacities of these systems are based on the active materials stored in the immobile electrodes in the reservoirs rather than the dissolved redox mediators in the electrolytes. The areas of the immobile electrodes exposed to the electrolytes are critical for the redox targeting reactions. In the presence of mediator molecules, *c.a.* 5 times in excess of $LiFePO_4$, the delithiation process still requires more than 15 minutes to form $LiFePO_4$, while the lithiation process was an even slower process [102]. Therefore, higher concentrations of the mediator molecules could facilitate the kinetics of these reactions and reduce mass transport losses. The latter were believed to be the main cause of the low power density, along with the separator resistance.

To address these issues, the same research group demonstrated a new system using inorganic mediators (I^-/I^{3-} and l^{3-}/I_2; solubility of LiI: > 2 mol dm^{-3}) [102] and Nafion/PVDF separators [102, 103], which exhibited a very high coulombic efficiency (> 99 %) and capacity retention (c.a. 90 %) at 0.075 mA cm^{-2} over 40 cycles. The resulting energy density was as high as 500 W h dm^{-3}, about 10 times that of the conventional all-

vanadium system based on one tank calculations (*c.a.* 50 Wh dm^{-3} for one tank). This concept allows flow-battery configuration to be extended to other chemistries, including lithium-oxygen [105-107] and lithium-sulfur [108, 109], as well as to solar cells [110], as demonstrated by several other research groups.

2.1.2. Organometallic based immiscible electrolyte batteries

In most of the above systems, the cell voltage of the battery is attributed to the difference in the redox potentials of the redox couples. Peljo *et al.* [111] proposed an ion-transfer battery based on the potential differences of the two phases. The proposed battery consists of two organic redox electrolytes of decamethylferrocene (DMFc, $C_{20}H_{30}Fe$) and decaethylferrocene tetrakis (penta-fluorophenyl)borate (DMFcTB, $C_{44}H_{30}BF_{20}Fe$) (0.1 mol dm^{-3}), which are separated by an immiscible aqueous phase (1 mol dm^{-3} LiClO4 and 0.1 mol dm^{-3} LiOH). The energy is stored by transferring a salt from the aqueous phases to organic phases in ion transfer coupled electron transfer reaction. During the discharge process, the battery reactions are as follows:

$$DMFcTB - e^- \leftrightarrow DMFcTB^+ \qquad E^o = -0.7 \text{ V } vs \text{ Ag|AgCl} \qquad (9)$$

$$DMFc^+ + e^- \leftrightarrow DMFc \qquad E^o = -0.12 \text{ V } vs. \text{ Ag|AgCl} \qquad (10)$$

In such process, DMFc is oxidized to $DMFc^+$ on the negative electrode and $DMFc^+$ is reduced to DMFc on the positive electrode, while the lithium and perchlorate ions are transferred from the electrolytes to the aqueous solutions, ensuring electroneutrality of the electrolytes. The redox potential between these phases results in a cell voltage of up to 0.8 V. The advantage of this system is that both reactions are highly reversible and no separator is required.

The charge-discharge cycling experiment was carried out in a static H-cell with porous reticulated vitreous carbon electrode on both electrodes (3 mm diameter). Organic solvents were either 1,2-dichloroethane (DCE) or trifluoro-toulene (TFT). At 0.3 mA (*ca.* 4.2 mA cm^{-2}), the energy efficiencies were 83% and 65% for DCE and TFT solvents, respectively. However, after several cycles, the normalized charge capacity tended to decrease in DCE, while remaining more stable in TFT due to a slower rate of solvent evaporation. The main limitation of this work was that the cell geometry did not allow for complete separation of the organic phases.

3. Organic couples in aqueous electrolytes

Aqueous electrolytes have significant advantages in terms of cost and ionic conductivity. The ionic conductivities of both the electrolyte and separator are significantly higher in aqueous electrolytes than in non-aqueous electrolytes. For instance, 1 mol dm^{-3} tetraethylammonium tetraflueroborate in acetonitrile has an ionic conductivity of 55.5 mS cm^{-1}, which is 65 %, 27 % and 14 % of 1 mol dm^{-3} sodium chloride (85.76 mS cm^{-1}), 1 mol dm^{-3} potassium hydroxide (209 mS cm^{-1}) and 1 mol dm^{-3} sulfuric acid (394.5 mS cm^{-1}), respectively [43]. The ionic conductivity of a commercial anion-exchange membrane is around 0.2 – 0.5 mS cm^{-1}; for instance, 0.16 mS cm^{-1} for the Neosepta AHA membrane from Tokuyama Co. in 0.1 mol dm^{-3} tetraethylammonium tetraflueroborate containing acetonitrile solution; 0.48 mS cm^{-1} for Fumatech FAP4 in 1.0 mol dm^{-3} tetraethylammonium tetraflueroborate containing propylene carbonate solution. In contrast, the conductivities of commercial anion-exchange membranes are around 15 mS cm^{-1} for Cl^- and 40 mS cm^{-1} for OH^-, and the ionic conductivity of commercial cation-exchange membranes in water are around 20 mS cm^{-1} for Na^+ and 100 mS cm^{-1} for H^+. A

conductivity level of 0.5 mS cm^{-1} leads to a membrane resistance of 2.0 Ohm cm^2 per 10 µm thickness. [43]

Electrochemical investigations of organic molecules in aqueous solutions can be traced back to the 1920s [112, 113]. The use of organic active species for redox flow batteries was reintroduced in 2009 [51, 72, 114-116]. The chemistries were based on aqueous electrolytes and involved organic substances of at least one aromatic group. When the organic compound is used as the positive-electrode active species, energy can be released by forming dehydrogenated products during the oxidation process.

Compared to non-aromatic products, aromatic products (forming aromatic rings upon dehydrogenation) tend to have higher redox potentials, suitable for positive-electrode reactions [51, 116]. These substances are invariably cyclic structures having 4n+2 delocalized electrons and appear as, e.g., phenyl (n=1), thienyl (n=1), furanyl (n=2), azulenyl (n=2) and anthraceneyl (n=3) groups. For instance, the oxidation of cyclohexane or cyclohexadiene to the corresponding aromatic benzene structure exhibits a high open-circuit potential of more than 1.0 V vs. SHE [116]. Some of these reactions are not reversible, however, and their applications have been limited to liquid organic fuel cells.

Certain organic molecules, particularly quinones, containing secondary hydroxyl groups exhibit high reversibility for energy storage applications. These hydroxyl groups serve as liquid carriers of hydrogen in aqueous electrolytes. In such cases, electrical energy can be released by oxidizing the hydroxyl group(s) to form the corresponding hydrogen depleted carbonyl compound(s). It is important to note that not all of these structures are electrochemically reversible during the reduction and oxidation processes.

As summarized in Table 2, some of these structures have gravimetric hydrogen storage capacities of more than 6 wt. %, which is sufficient for mobile/automobile applications [51].

Hydrogen density and ΔG of dehydrogenation of linear and alicyclic polyolsas organic liquid carriers of hydrogen				
Hydrogenated form	**Dehydrogenated form**	**Hydrogen % wt.**	**Volumetric density / g dm^{-3}**	***ΔG* dehydrogenation / kcal mol^{-1} of hydrogen**
Decaline	Naphtalene	7.29	65.3	20.6
Dehydro-N-ethylcarbazole	N-Ethylcarbazole	5.83	64.2	16.2
2-Propanol	Acetone	3.35	26.4	13.9
2,3-Butanediol	Diacetyl	4.47	44.2	15.2
2,4-Pentanediol	Acetylacetone	3.87	37.2	14.2
2,5-Hexanediol	hexane-2,5-dione	3.41	33.1	12.8
3,5-Hexanediol	1- methylacetylacetone	3.41	33.1	14.9
3-Methyl-2.4-pentanediol	3-methylacetylacetone	3.41	n/a	13.1
5,5-Dimethyl-l,3-cyclohexanediol	Dimedone	2.8	n/a	13.9
1,3-Cyclohexanediol (trans)	1,3-cyclohexanedione	3.47	40.1	14.9

1,3-Cyclohexanediol (cis)	1,3- cyclohexanedione	3.47	40.1	14.9
1,4-Cyclohexanediol trans (quinitol)	1,4-cyclohexanedione	3.47	40.6	15.8
1,4-Cyclohexanediol (cis)	1,4-cycloheXanedione	3.47	40.6	15.6
Heptane-2,4,6-triol	heptane-2,4,6-trione (diacetylacetone)	4.08	45.8	13.9
3,5-Dimethyl-2,4,6-heptanetriol	3,5-dimethyl-2,4,6-heptanetrione	3.43	n/a	14.6
Nonane-2,5,8-triol	nonane-2,5,8-trione	3.43	n/a	12.9
3-Ethylhydroxypentane-2,5-diol	Triacetylmethane	4.08	n/a	13.6
9,10-DihydroXy-9,10-dihydroanthracene	Anthraquinone	1.98	n/a	5.2
Hydrogen density and ΔG dehydrogenation of heterocyclic polyols as an organic liquid carrier of hydrogen				
3-Methyltetrahydrofuran-2,5-diol	3-Methylfuran-2,5-dione	5.12	n/a	-14.8
3,4-Di-methyltetrahydrofuran-2,5-diol	3,4-Dimethylfuran-2,5-dione	4.58	n/a	-12.4
Pyranol-2,4,6-triol	Pyranol-2,4,6-trione	4.51	68.1	-10.8

3,5-Dimethylpyranol-2,4,6-triol	3,5-Dimethylpyranol-2,4,6-trione	3.78	n/a	-10.5
Thiotetrahydrofuran-2,5- dial	Thiofuran-2,5-dione	5.04	n/a	-17.2
Perhydropyromellitic dianhydride	Pyromellitic dianhydride	6.08	n/a	-12.0
1,4-Dioxane-2,3,5-triol	1,4-Dioxane-2,3,5- trione	4.44	76.0	-10.8
1,4-Dioxane-2,3,5,6-tetrol	1,4-Dioxane-2,3,5,6-tetrone	5.30	n/a	-12.9
Hydrogen Density and ΔG dehydrogenation of amino alcohols as organic liquid carrier of hydrogen				
1,1'-Iminobisethanol	N-Acetylacetarnide	5.23	n/a	5.0
1-(1-Hydroxyethyl-methyl-amino)ethanol	N-Methyl-N-acetylacetarnide	4.42	46.2	5.8
1,2-Diarninoethane-1,2-diol	Oxarnide	4.47	63.7	-4.9
1,3-Diarninopropane-1,3- diol	Propanediarnide	3.80	49.4	-2.4
1,3-Diarninopropane-1,2- diol	1,3-Diarninopropane-1,2-dione	3.80	49.7	9.8
Perhydro-N-carbarnoylacetarnide	N- Carbarnoylacetarnide	3.80	n/a	2.3

2-Hydroxy-1,4-diarninobutane-1,4-diol	2-Oxopentanediarnide	4.03	53.5	4.6
Piperazine-2,3,5,6-tetrol	Piperazine-2,3,5,6- tetrone	5.37	93.2	6.3
1-Methylpyrrolidine-2,3 ,4,5-tetro	1-Methylpyrrolidine- l 2,3,4,5-tetrone	5.41	n/a	14.9
Piperidine-2,3,4,5-tetrol	Piperidine-2,3,4,5- tetrone	5.41	89.1	18.7
1-(1-Hydroxyethylarnino)ethanol	N-Acetylacetarnide	3.83	40.6	5.0
1-(1-Hydroxyethyl-methyl-arnino)ethanol	N-Acetyl-N-methyl-acetarnide	3.38	35.3	5.8
1H-Tetrahydropyrrole-2,5-diol	1H-Pyrrole-2,5-dione (maleimide)	5.86	76.8	12.4
Perhydropyrornellitic diimide	Pyrornellitic diimide	6.13	n/a	8.8

Table 2. Hydrogen density and ΔG of dehydrogenation of linear and alicyclic polyols, heterocyclic polyols and amino alcohols [51].

For aqueous redox flow battery applications, the main concerns over these compounds remain the reversibility of the redox reactions and their solubilities in water. In some cases, the redox reactions of these molecules may require catalysts or elevated temperatures. Compared to the hydrogenation (reduction) process, the dehydrogenation (oxidation) of these compounds is expected to have slow kinetics and require temperatures up to 150 – 250 ^{o}C, which is not practical for many redox flow battery applications.

The dehydrogenation energies of different aromatic compounds, including single and fused five- and six-membered rings and different heteroatoms (O, N and S), as well as organic substances containing one or more hydroxyl group have been estimated using density functional theory (DFT) (see Table 2) [51, 116]. Since these calculations are based on the Gibbs free energy change, the open-circuit potential is related to the heat of dehydrogenation. In many cases, a higher heat of dehydrogenation leads to a lower open-circuit potential than would be expected.

For compounds having six-membered rings, introducing a nitrogen atom in the heterocyclic structure may increase the redox potential by 30 – 40 mV relative to the carbocyclic analogue. Further addition of a second nitrogen atom was predicted to increase the redox potential by 30 mV. Similarly, in the case of a five-membered ring structure, the effect of incorporating a nitrogen atom should be even more pronounced, leading to an estimated redox potential increase of 100 mV (e.g., imidazole *vs.* pyrrole); however the hydrogen volumetric capacity is reduced. Structures with single N–N bonds tend to have even more positive redox potentials but are also less stable than their C–C bond counterparts due to the possible hydrogenolysis process. For some fused ring compounds (e.g., fused six-membered ring), further addition of nitrogen atoms are not

expected to increase the redox potentials substantially [116]. It was also reported that the introduction of at least two secondary hydroxyl groups in some organic compounds reduces the dehydrogenation energy below that of cyclic hydrocarbons with no hydroxyl group (decaline ↔ naphthalene, dehydro-N- ethylcarbazole ↔ N-ethylcarbazole) [51]. Compounds with at least two secondary hydroxyl groups have higher hydrogen and energy densities than those having a single hydroxyl group (i.e., 2-propanol ↔ acetone). In some molecules, the replacement of the CH_2 group for an oxygen heteroatom in the heterocyclic polyols tends to decrease the dehydrogenation energy and increase the volumetric hydrogen capacity. On the other hand, the dehydrogenation energy is increased when the heteroatom is sulfur (e.g., thiotetrahydrofuran-2,5-diol ↔ thiofuran-2,5-dione). For amino alcohol compounds, the presence of the nitrogen heteroatom in linear and cyclic polyols in the position next to hydroxyl also improves both features [51].

Regarding the redox potential, solubility and stability, selection or modification of some of these molecules has been facilitated by high-throughput computational screening *via* an automated molecule generator [45-47, 117-119]. This was achieved by creating derivatives of molecules under investigation in the literature, or by proposing new molecules. The chemistries of aqueous organic redox flow batteries are still limited to the groups of quinones [40, 75, 120-125], quinoxalines [54, 126], and several polymer-based [71] chemistries. The reaction mechanisms of these molecules have been studied extensively in the literature. In aqueous electrolytes, one of the important factors in governing the reaction process is the pH of the solution, which has a significant influence on the electrochemical performance and water solubility of the molecules as well as the chemical stability of the reaction products [40, 127-129]. In proton-rich electrolytes, the redox reactions often involve proton-coupled electron transfer(s) and lead to the formation of hydrogenated or dehydrogenated products. The corresponding redox

potential is pH dependent, moving to more negative values as the pH increases. Pourbaix diagrams are used to define the range of potential and pH over which the species is thermodynamically stable. Through the linear relationship between the potential and pH, the number of protons and electrons can be estimated *via* the Nernst equation for a particular electrode reaction [127]. In alkaline electrolytes, the proton concentration may not be sufficiently high to form hydrogenated compounds. Instead, charge-containing radicals may form in the electrolytes, depending on their chemical stability. The solubility and chemical stability of some organic molecules may improve in acidic and alkaline electrolytes, respectively [40, 127-129].

3.1. All-organic redox flow batteries: quinone-based chemistries

All-organic redox flow batteries involve organic active species for both the negative and positive electrode reactions [45-47, 117] (Table 3).

All-organic redox flow batteries									
Chemistries	**Negative active material (in discharged state)**	**Positive active material (in discharged state)**	**Electrolyte & flow conditions**	**Cell components**	**Experimental OCV / V**	**Approx. % System efficiencies**	**Energy density / W h dm^{-3}**	**Number of cycles**	**Year [Ref:]**
Anthraquinone/ benzoquinone (acid)	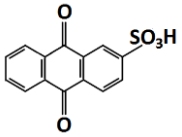	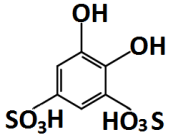	1 M H_2SO_4; 0.2 M active materials; up 1.0 M active materials in recent work; flowing	Carbon papers/ Nafion 117	0. 76 (100 % SOC)	Coulombic: > 95% (8 – 10 mA cm^{-2})	4.1	> 12	2014 [121]
Quinoxaline/ benzoquinone (alkaline-acid)	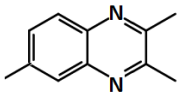	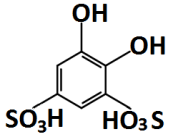	0.2 M KOH + 0.067 M KCl + 0.5 M K_2SO_4 ; 0.4 M H_2SO_4 + 0.5 M K_2SO_4; 0.1 M active materials; static	Carbon felts / lithiated Nafion 117	1.4 – 1.5	Coulombic: > 70% (0.35 mA cm^{-2})	N.G.	> 10	2015 [126]
Polymer-based viologen/ TEMPO (neutral)	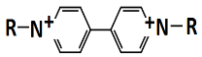	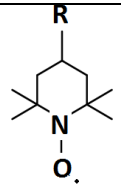	2 M NaCl; 15 mL negative active materials; 10 mL positive active materials; flowing	Carbon felts/ cellulose-based dialysis membrane	1.1	Coulombic: 99% Energy: > 75% (20 – 40 mA cm^{-2})	8.0	10,000 cycles (static cell)	2015 [71]
Methyl viologen / hydroxyl-TEMPO (neutral)	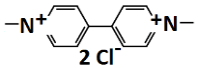	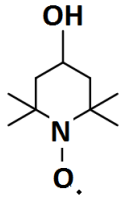	1 M NaCl; 0.1 M active materials; flowing.	Carbon felts / Selemion	1.25	Coulombic. 99% Energy: 45 – 82% (20 – 100 mA cm^{-2})	8.4	100	2016 [57]

Table 3. Operational parameters and performance of all-organic redox flow battery systems in aqueous electrolytes. N.G.: not given.

The energy densities listed in Table 3 are based mainly on the energy density of the electrolyte and do not take account of the flow cell and electrolyte piping. Some organic active species, particularly quinones [40, 75, 121, 125], are highly reversible and relatively stable in aqueous electrolytes. The incorporation of these materials enables a reasonable approach to achieving low-cost redox flow batteries with performance characteristics that are comparable to conventional metallic systems. However, the energy densities of existing systems are still lower than 10 Wh dm^{-3}, which is significantly lower than the energy density of commercial all-vanadium systems (*c.a.* 35 Wh dm^{-3}). The identification or synthesis of organic active species with reasonable solubility, electrode potential and chemical stability remains a major challenge. Such developments will be necessary to meet the demanding cost, durability, and sustainability requirements for grid-scale applications [43-47, 117].

Among different families of organic compounds, several investigations have focused on the use of quinones, due to their relatively reversible and stable natures in aqueous media [39, 40, 128, 129]. These molecules are a class of aromatic-derived compounds (e.g. benzene or naphthalene) synthesized by converting an even number of –CH=groups into –C(=O)– groups with any necessary rearrangement of double bonds, resulting in a fully conjugated cyclic dione structure [18-23, 77]. A classical member of this group is para-benzoquinone, known as cyclohexadienedione. When protons are freely available in aqueous electrolytes, the reduction of quinone molecules involves one proton and one electron for the formation of each hydroxyl group, resulting in the reduction product of a hydroquinone molecule. Taking into consideration that most hydroquinone molecules have two hydroxyl groups, the reductions of quinone undergo two-proton-two-electron

transfers subject to the availability of protons in the electrolytes. This feature enables quinone-based redox flow batteries to achieve higher energy densities than conventional metal-based flow batteries that utilize one electron-transfer reactions, e.g. vanadium, chromium and iron. In addition to enhanced energy conversion [51, 114], the hydroxyl groups of the quinone molecules also enhance the corresponding solubilities in aqueous electrolytes [45, 117].

Following the introduction of quinone-based redox flow batteries in 2014 [39, 40, 121], the selection of further quinone molecules, including benzoquinones, naphthoquinones and anthraquinones, has been facilitated by computational screening based on DFT. Through such computational studies, the equilibrium potentials and the solubilities of up to 1700 quinone based redox couples have been evaluated by Er *et al.* [117].

Without modifying the functional groups, the equilibrium potentials of the parent iomers of the 1-, 2-, and 3- ring quinone molecules (benzoquinones, naphthoquinones, and anthraquinones, respectively) are usually between E^o = +0.05 and +1.1 V *vs.* SHE. Computational modelling data is shown in Figure 2a). The addition of aromatic rings lowers the electrode potential. For the case of 1,4-benzoquinone (one aromatic ring), the redox potential is +0.7 *vs.* SHE. 1,4-naphthoquinone (two aromatic rings) and 9,10-anthraquinone (three-aromatic rings) have redox potentials of *ca.* +0.45 and *ca.* +0.10 V *vs.* SHE, respectively. In most cases, these unmodified quinones have limited solubility in water, but the solubility can be increased substantially with functional groups, such as $–SO_3H$, $–PO_3H_2$, –COOH, –OH, $–O^-M^+$, $–SO_3^-M^+$, $–PO_3^{2-}M^+_2$, $–COO^-M^+$, pyridinyl, imidazoyl, or pyrrole, as shown in Figure 2b) [117]. For instance, 1,2-benzoquinone disulfonic acid has a solubility of 1.7 mol dm^{-3} compared to 0.1 mol dm^{-3} for unmodified 1,2-benzoquinone [121, 125]. The hydrogen bonding ability, acidity and polarity of

suitable functional groups are important in terms of achieving high aqueous solubility [40, 130]. For example, the solubility of 9, 10-anthraquinone 2, 6-disulfonic acid was increased from less than 0.1 mol dm^{-3} in pure water [131] to 0.5 mol dm^{-3} in 1 mol dm^{-3} sulfuric acid [40, 121].

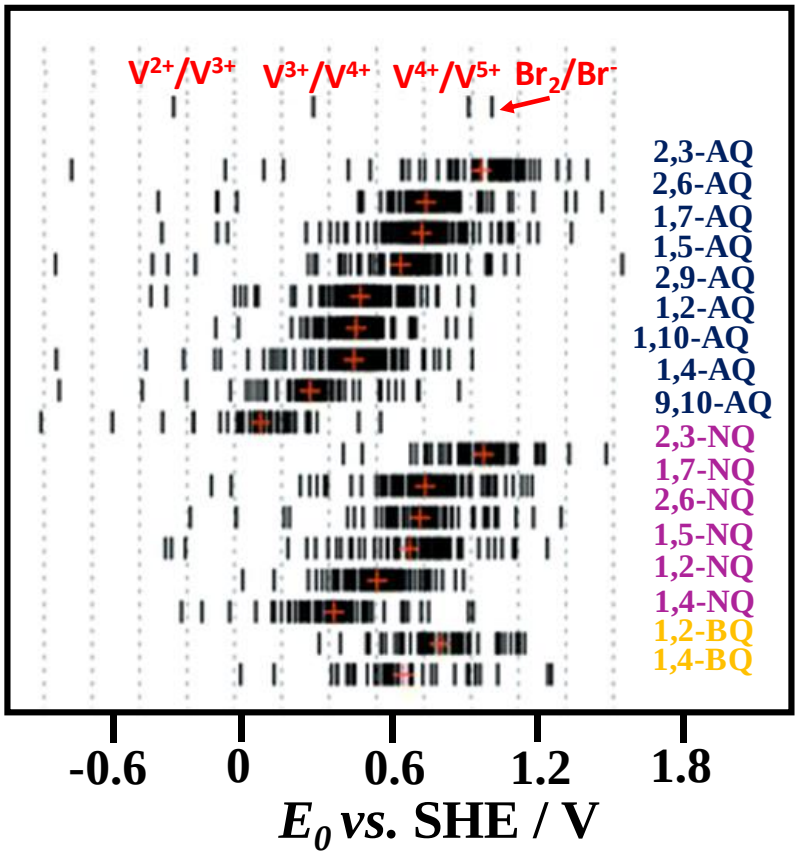

Figure 2a

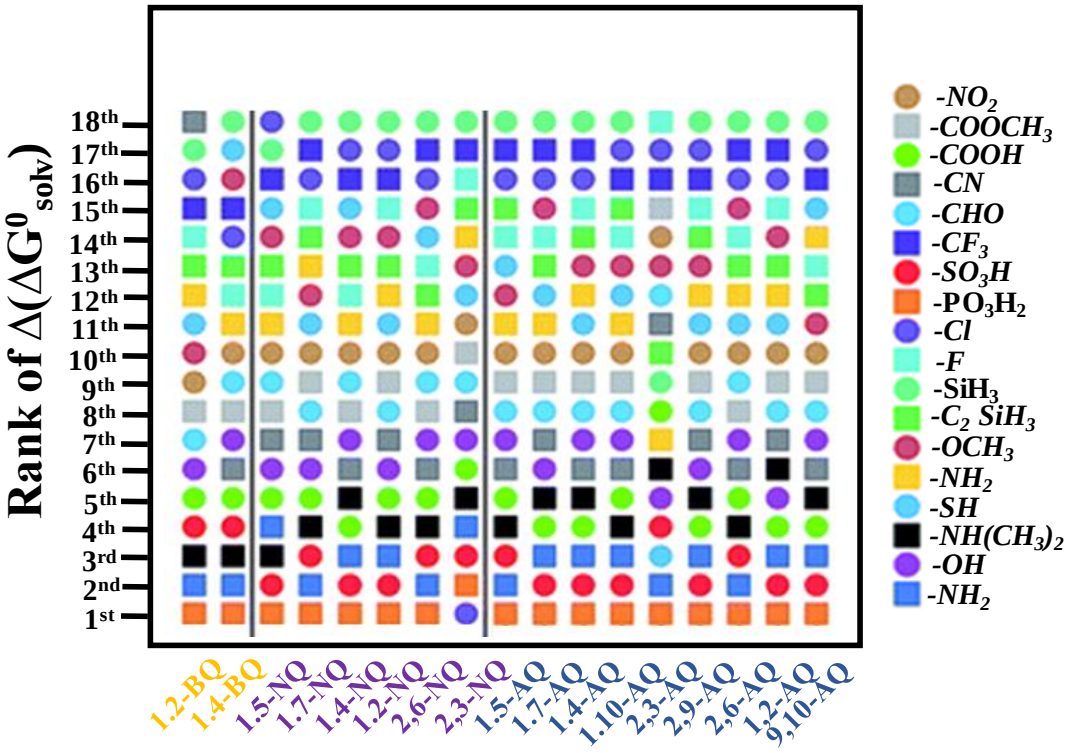

Figure 2b

Figure 2. Computational modelling results for quinone molecules (benzoaquinor naphthoaquinone and anthraquinone) using density functional theory: predicted equilibrium potential (red) and b) the ranking of substituents in terı of the effect on ΔG^0_{sol}.

Among the various quinone molecules, computational studies have suggested that the group containing 9-10-anthraquinone (E^o = *ca.* + 0.1 V *vs.* SHE) provides the most suitable redox couples for the negative electrode reaction, whereas more than 300 quinones, particularly 1,2- benzoquinone, 2,3-naphthoquinones and 2,3-anthraquinone, have electrode potentials of more than + 0.7 V *vs.* SHE, making them suitable for positive electrode reactions [117]. The suggested 9-10-anthraquinones have been tested experimentally in laboratory-scale flow cells as the negative electrode reactions, with

different chemistries based on metal-free compounds (anthraquinone/bromine [39, 40, 120]; anthraquinone/benzoquinone [121, 122]). Furthermore, an alkaline system based on anthraquinone and inorganic ferricyanide has been proposed, achieving a high cell voltage (1.2 V) and reasonable solubility (0.6 mol dm^{-3}) [75].

For a number of quinone molecules, including parabenzoquinone and 2,6-dihydroxyanthraquinone, the formation of the protonated hydroquinone through the reduction processes takes place over a wide range of pH (i.e. pH $0.5-10$). At certain high values of pH, the formation of hydroquinone is unlikely to take place as described in the Pourbaix diagrams (Figures 3a), 3b) and 3c) for 1,4-benzoquinone, 9,10-anthraquinone, 2,7-disulfonic acid and 2,6-dihydroxylanthraquinone, respectively) [40, 127-129]. The reduction may result in charge-containing radicals, which may exist as free radicals or further react to form complexes with other compounds, depending on their chemical stabilities in the electrolytes. Although radicals are often reactive and short-lived, this remains a major challenge for the use of high pH values in aqueous organic flow batteries [40, 127-129].

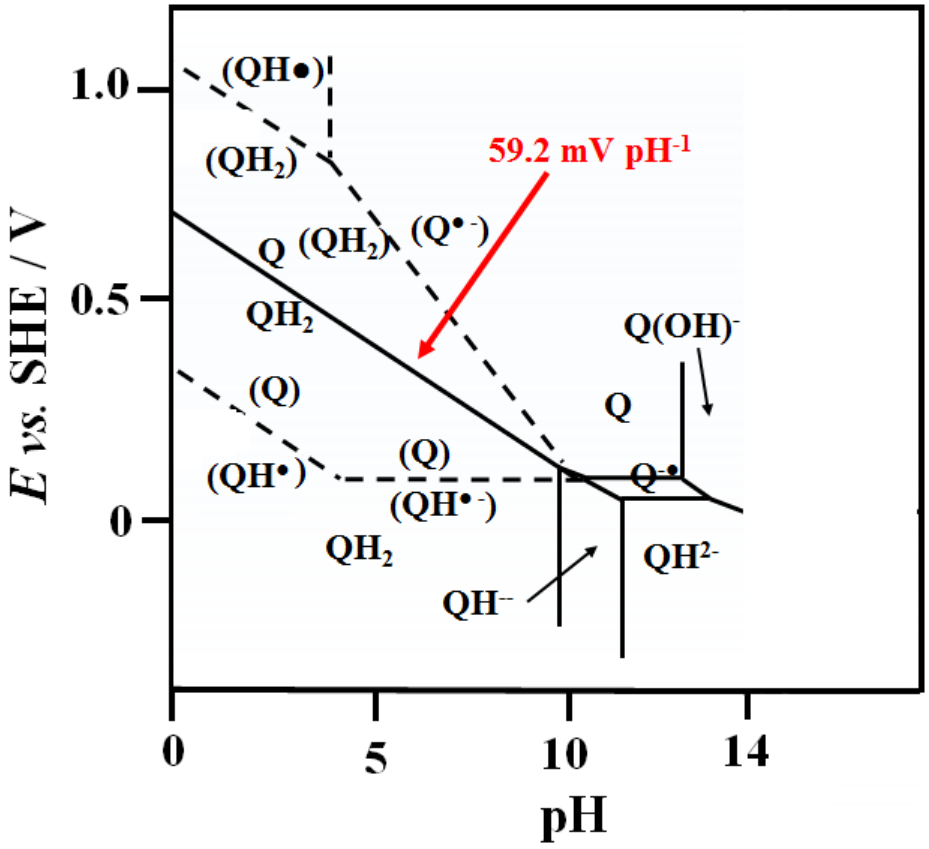
1.0
0.5
0
E vs. SHE / V
0
5
10
14
pH
(QH•)
(QH2)
59.2 mV pH-1
Q
(QH2)
(Q•-)
QH2
Q(OH)-
(Q)
Q
(QH•)
(Q)
Q-•
(QH•-)
QH2
QH2-
QH--

Figure 3a

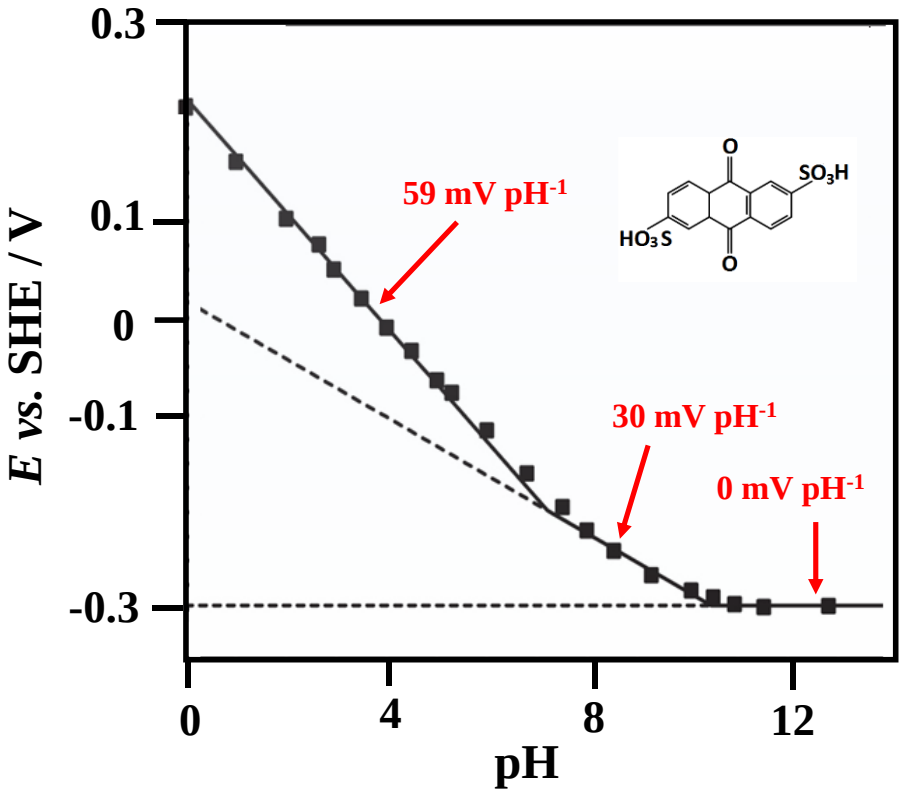
0.3
0.1
0
-0.1
-0.3
E vs. SHE / V
0
4
8
12
pH
59 mV pH-1
30 mV pH-1
0 mV pH-1
SO3H
HO3S
O

Figure 3b

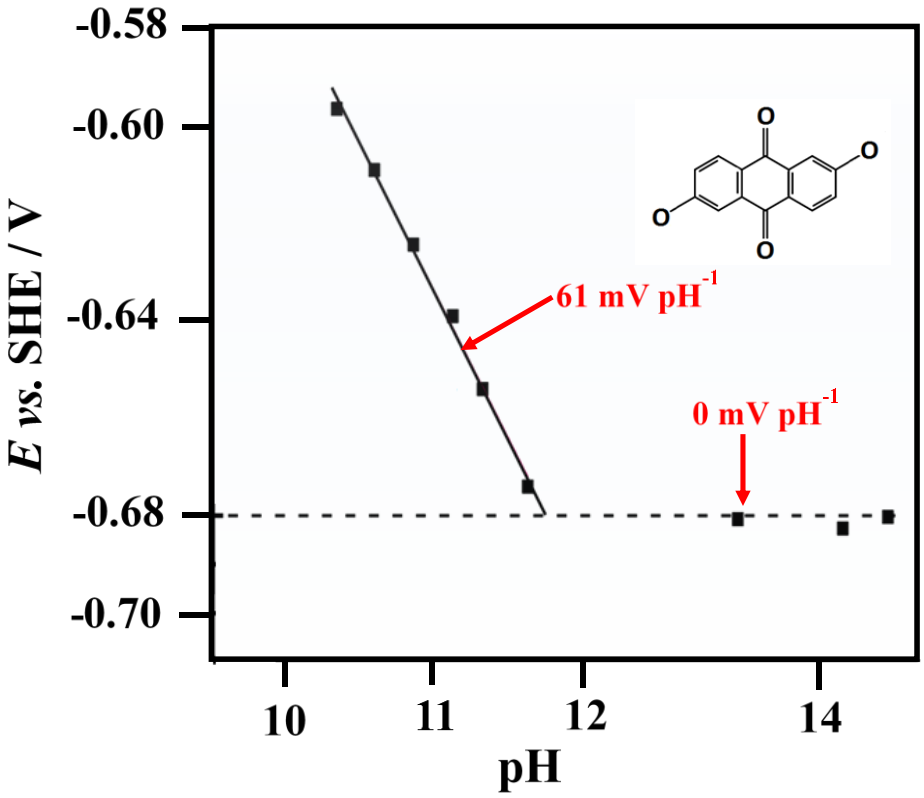
-0.58
-0.60
-0.64
-0.68
-0.70
E vs. SHE / V
10
11
12
14
pH
61 mV pH-1
0 mV pH-1
O

Figure 3c

Figure 3. *E vs.* pH relationship for quinone-based molecules: a) Pourbaix diagram of prototypical 1,4-benzoquinone from the literature; measured *E vs.* pH plot of b) 9,10-anthraquinone, 2,7-disulfonic acid; and c) 2,6-dihydroxylanthraquinone. A gradient of –59 mV pH^{-1}, –30 mV pH^{-1} and 0 mV pH^{-1} could correspond to two-proton-two electron, one-proton-one electron and zero-proton processes, respectively.

3.1.1. Acidic anthraquinone-benzoquinone redox flow battery

The first all-organic redox flow battery was introduced by Yang and co-workers [121, 122, 132]. The negative and positive electrode half-cells were based on solutions of 9,10-anthraquinone-2 sulfonic acid and 1,2-benzoquinone-3,5-disulfonic acid, respectively. The battery chemistries involve the transformation of quinone to hydroquinone and *vice versa*:

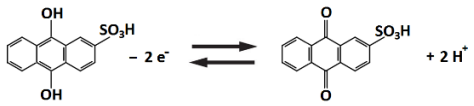

E^o = + 0.09 V *vs.* SHE

(11)

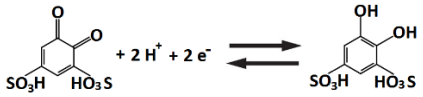

E^o = + 0.85 V *vs.* SHE

(12)

This battery was inspired by earlier studies of flow battery systems [40, 72, 125], in which anthraquinone and benzoquinone were used as the negative and positive redox couples,

respectively. The addition of aromatic rings in the case of anthraquinone lowers the redox potential [133]. These redox couples [134, 135] have relatively high rate constants for the charge-transfer processes (at least an order of magnitude higher than those of vanadium). Quinone molecules also contain conjugated carbon-carbon bonds and keto- and enol-groups that allow delocalization and rearrangement of the pi-electrons to undergo these transformations with extraordinary facility [136]. For the two-electron transfer process, the intermediate formation of semi-quinone with the addition of one electron is often assumed to be the rate-determining step [137]. The addition of sulfonic acid and hydroxyl groups are necessary to enhance the aqueous solubility of these quinone molecules, considering that unsubstituted forms of 9,10-anthraquinone [138] and 1,2-benzoquinone [125] are either insoluble or near insoluble. The aqueous solubility of AQDS is *ca.* 0.5 mol dm^{-3}, while that of AQS is *ca.* 0.2 mol dm^{-3}. In the form of sodium sulfonate salts, the aqueous solubilities of these quinones can be up to *c.a.* 1.0 mol dm^{-3} and could be further increased to 1.5 mol dm^{-3} (9,10-anthraquinone-2 sulfonic acid) and 4.0 mol dm^{-3} (1,2-benzoquinone-3,5-disulfonic acid) when transformed to the free acid forms (sulfonic acid) by passing through an ion-exchange column [122]. The higher solubilities allow the cell voltage to be maintained at a higher value due to more efficient mass transport of the active species from the bulk to the electrode surface.

The flow battery was operated with a membrane electrode assembly (MEA) similar to that used in a direct methanol fuel cell [121]. Two sheets of carbon paper without precious metal catalysts were coated with inks containing Vulcan carbon black and Nafion® ionomer solution. The Nafion® membrane was hot pressed with the coated electrodes to form the MEA. The battery survived more than 12 cycles with a charge capacity retention of more than 90% at 10 mA cm^{-2} (Figure 4a). The open-circuit voltage was *ca.* 0.7– 0.8 V and the coulombic efficiency was >95%, while the cell voltage dropped rapidly with

decreased state-of-charge (Figure 4b) [121]. The 1,2-benzoquinone-3,5-disulfonic acid molecule was assumed to be converted to 1,2,4,6-tetrahydroxybenzene-3,5-sulfonic acid in the initial cycles *via* two steps of electrochemical oxidation and two steps of water addition *via* the Michael reaction. Once this conversion was complete, no further change in the composition of the positive electrolyte was observed.

Improvements were subsequently made by incorporating flow fields, carbon-coated electrodes and high concentrations of active materials in the acidic form (1.0 mol dm^{-3} sulfuric acid), to yield a power density of 100 mW cm^{-2} [122]. This power density is still much lower than that of the all-vanadium redox flow battery (200 – 300 mW cm^{-2} in a similar battery configuration, since the discharge cell voltage (0.5 V) is less than a half of the all-vanadium counterpart (*c.a.* 1.25 V) at 200 mA cm^{-2} [139]. Based on the active materials in the electrolytes, the theoretical energy density and specific energy are *c.a.* 16 Wh dm^{-3} and *c.a.* 11 Wh Kg^{-1}, respectively. Despite the involvement of two-electron transfers, these values are still around half those of the all-vanadium systems (*c.a.* 26 Wh dm^{-3} and *c.a.* 22 Wh Kg^{-1} for 1 mol dm^{-3} electrolytes). This is because the specific capacities of the molecules (150 – 170 Ah Kg^{-1} *vs. c.a.* 526 Ah Kg^{-1} of vanadium) are relatively small, which can be attributed to the large molecular weights (300 – 330 g mol^{-1} *vs. c.a.* 50.9 g mol^{-1} of vanadium). Further studies of this system are needed to understand the behaviour of the redox couples, especially the influence of substituent groups on battery performance.

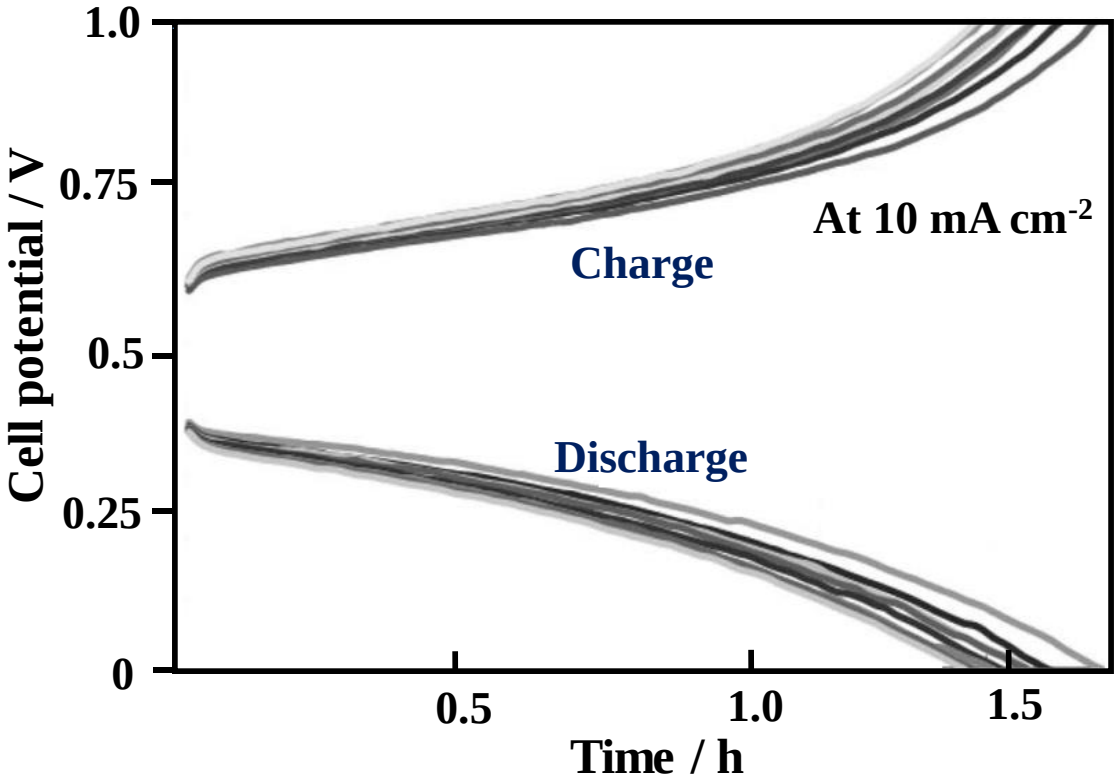
1.0
0.75
0.5
0.25
0
Cell potential / V
At 10 mA cm-2
Charge
Discharge
0.5
1.0
1.5
Time / h

Figure 4a

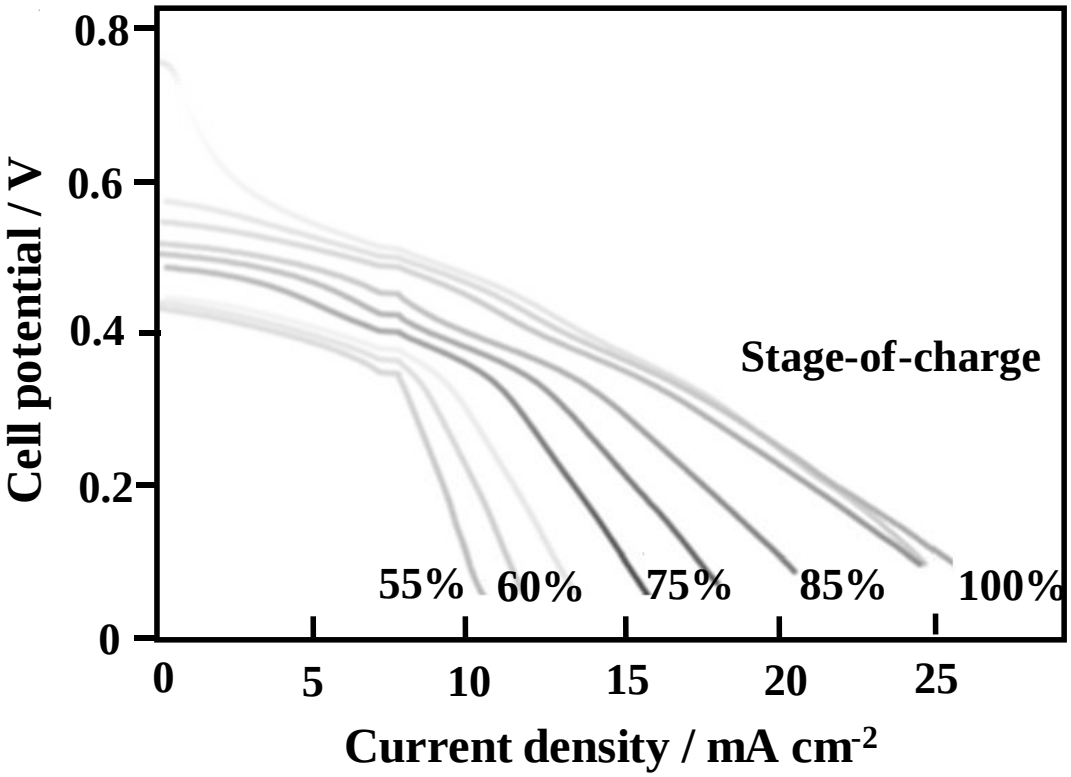
0.8
0.6
0.4
0.2
0
Cell potential / V
Stage-of-charge
55%
60%
75%
85%
100%
0
5
10
15
20
25
Current density / mA cm-2

Figure 4b

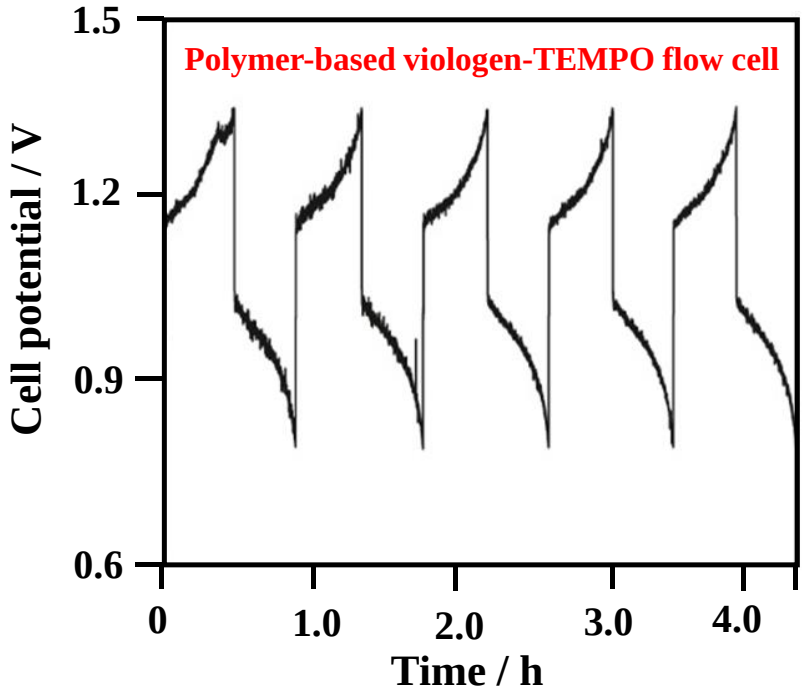
Polymer-based viologen-TEMPO flow cell
1.5
1.2
0.9
0.6
Cell potential / V
0
1.0
2.0
3.0
4.0
Time / h

Figure 4c

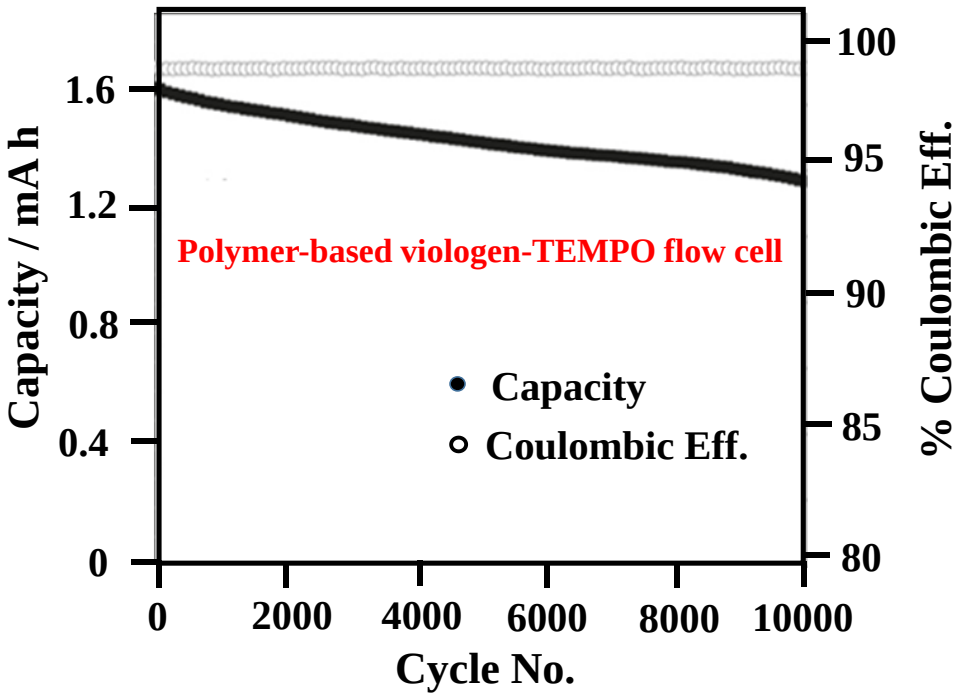

Figure 4d

Figure 4 Charge-discharge cycling performance of all-organic redox flow batteries (flow & static): (1) acidic anthraquinone-benzoquinone redox flow battery: (a) charge-discharge profile at 10 mA cm^{-2}; b) cell voltage *vs.* current density curve; and (2) polymer-based viologen-TEMPO redox flow battery: (c) charge-discharge profile at 40 mA cm^{-2}; (d) long-term cycling test over 10,000 cycles at 20 mA cm^{-2} in a static cell.

3.1.2. Alkaline quinoxaline- acidic benzoquinone redox flow battery

In aqueous chemistries, several organic-based redox flow batteries have been based on anthraquinones at the negative electrode. In recent studies, Brushett and co-workers [54, 126] instead proposed the use of quinoxaline, also in aqueous systems. Quinoxaline is a class of organic compounds characterized by a benzene ring and a –C–N=C– containing

pyrazine ring. These derivatives have been used as component materials in dye-sensitized solar cells and non-aqueous flow batteries. Quinoxaline has high solubility in pure water (up to 4.5 mol dm^{-3}). The low molar mass (130.15 g mol^{-1}) and the capacity for a two-electron transfer lead to a theoretical specific energy of 410 mA h g^{-1}. As a low potential redox active compound, quinoxaline has a redox potential of < –0.5 *vs.* SHE, dependent on the electrolyte composition and pH [54]. On the other hand, 1,2-dihydrobenzoquinone-3,5-disulfonic acid (1,2-BQDS or Tiron) is electropositive (E^o = *ca*. 0.85 V *vs.* SHE) and has an aqueous solubility of up to 1.0 mol dm^{-3}. It has been used in the positive electrodes in this and other systems [121].

Compared to 1,2-BQDS, studies of the aqueous electrochemical behaviour of quinoxaline were until recently very limited [140, 141]. More than 30 electrolyte compositions have been evaluated to identify the influence of pH, the cation and the anion [54]. Redox potentials were found to shift towards more negative values at increased pH values, while exhibiting a weak dependency on pH in acidic and neutral electrolytes. This implies the involvement of protons in the reaction mechanisms, which was also observed in other electrolytes [140, 141].

In near-neutral alkaline electrolytes (5< pH <10), the redox potential is shifted by –47 mV pH^{-1} leading to the hypothesis that quinoxaline was reduced to an equilibrium combination of protonated neutral species, monovalent anions and divalent anions [54] . However, the electrochemical reversibility in terms of peak separation and current density was observed to decrease rapidly at lower pH (pH < 5.4) after 10 cyclic voltammetry cycles, suggesting that this reaction is not suitable for acidic conditions. Although anions do not affect the electrochemical behaviour, the aqueous solubilities increased by nearly an order of magnitude when switching from sulphate to chloride anions. The solubility of

quinoxaline is as high as 4.0 mol dm^{-3} in 1 mol dm^{-3} potassium chloride and 0.01 mol dm^{-3} potassium hydroxide [54].

For the aforementioned reasons, the reported work [126] used quinoxaline at the negative electrode in an alkaline electrolyte (0.2 mol dm^{-3} potassium hydroxide), while BQDS was used in an acidic electrolyte (0.4 mol dm^{-3} sulphuric acid) at the positive electrode. Rather than using a flow cell, the studies were carried out in a stainless-steel Swagelok cell, in which a Nafion® membrane was placed between two graphite felt electrodes. The charge-discharge reactions are [126]:

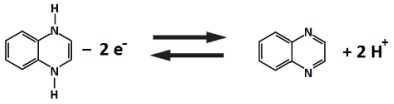

E^o = *ca.* –0.5 V *vs.* SHE

(13)

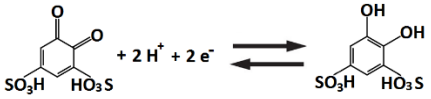

E^o = + 0.85 V *vs.* SHE

(14)

The involvement of two-proton and two-electron transfers for the quinoxaline reactions was inspired by previous studies in acidic electrolytes [140, 141]. The battery was charge-discharge cycled in the static Swagelok cell at 0.35 mA cm^{-2} between the voltage limits of 1.6 and 0.6 V and more than 10 cycles were achieved within 180 minutes. Carbon felts and lithiated Nafion® cation exchange membrane were used as the electrodes and separators, respectively. The coulombic and energy efficiencies were relatively stable, remaining at *ca.* 82% and 63%, respectively. However, a significant decrease in capacity was observed, possibly attributable to the cell architecture [126]. Furthermore, maintaining the alkalinity and acidity for the negative and positive electrolytes appears to be challenging when a proton-exchange membrane is used in the system.

3.1.3. Polymer-based viologen-TEMPO redox flow battery

Organic polymers as the active materials for aqueous redox flow batteries were first proposed by Janoschka and co-workers [71]. These polymers had previously been studied for application in solid-state batteries [34, 35] and consist of two components, namely a redox-active moiety and a unit providing sufficient aqueous solubility to prevent precipitation [34, 142, 143]. The use of a redox-active moiety was inspired by previous organic systems using non-aqueous electrolytes. The negative and positive active materials are viologen (4,4'-bipyridine derivative – N-methyl-bipyridinium iodide) [144-146] and TEMPO (2,2,6,6,-tetramethylpiperidinyloxyl), respectively. The organic polymers were prepared by free radical polymerization and subsequent functionalization (negative electrode) or polymer-analogous oxidation (positive electrode). The aqueous solubility of these polymers is enabled by the quarternary ammonium cation. The proposed configuration has a theoretical capacity of up to 10 A h dm^{-3}. With the use of such a high molar mass active material (*c.a.* 20,000 g mol^{-1}), it is important to minimize the dynamic viscosity of the electrolytes as much as possible. In the proposed studies, the viscosities of the negative and positive electrolytes were 5 mPa s and 17 mPa s, respectively. These values are in the shear rate range, typical of pipe flow. Upon charging the battery, the divalent viologen cation ($Viol^{++}$) is reduced to a monovalent radical cation ($Viol^{+\bullet}$) in the negative electrode, while the TEMPO molecule is oxidized and forms an oxammonium cation ($TEMPO^{+}$) in the positive electrode. This is accompanied by a strong colour shift from ochre to blue and orange to yellow for $Viol^{++}/Viol^{+\bullet}$ and $TEMPO/TEMPO^{+}$, respectively. The reverse reactions take place during the discharge process as follows [71]:

E^o = *ca.* –0.30 V *vs.* SHE

(15)

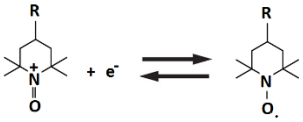

E^o = *ca.* +0.90 V *vs.* SHE

(16)

As estimated by cyclic voltammetry, the redox potentials of the negative and positive electrode reactions in sodium chloride solutions were *ca.* +0.7 and –0.6 V *vs.* Ag|AgCl, respectively. A typical test was conducted in a parallel flow cell, in which carbon felts were used as the electrodes and a cellulose-based dialysis membrane was used as the separator. Since the active polymers have a hydrodynamic radius of 2 nm, dialysis membranes with < 1 nm pore size can effectively prevent crossover of the active polymers across the two electrolytes compartments [147]. Furthermore, these membranes are chemically stable in sodium chloride electrolytes in the long term [71]. The resulting separator is only 5 to 10% of the cost of perfluorinated ion-exchange membranes, which are commonly used in systems with highly oxidative and corrosive electrolytes (e.g., all-vanadium [13], zinc-bromine [15]). As shown in Figure 4c), the battery achieved an open-circuit voltage of 1.1 V and was charge-discharge cycled at 40 mA cm^{-2} within a voltage window of 0.85 – 1.35 V. It was able to retain most of its capacity, with an energy efficiency of 75 – 85%. In a static cell, 10,000 charge-discharge cycles were achieved at 20 mA cm^{-2} with coulombic efficiencies in excess of 98% (Figure 4d). The main research challenge for this system is the increased viscosity of the electrolyte caused by dissolving a considerable amount of polymeric species. Therefore, specifically shaped polymers,

such as dendrimeric or miscellar structures, are more favourable over regular, linear polymers. Furthermore, the energy density of this system (10 W h dm^{-3}) is slightly lower than that of the conventional all-vanadium redox flow batteries (15–40 W h dm^{-3}), but may be further improved with active species involving more than one-electron transfers [71].

3.1.4. Methyl viologen-hydroxyl-TEMPO redox flow battery

Following the introduction of the polymer-based viologen-TEMPO redox flow batteries [71], Liu and co-workers [57] proposed a system using similar active species that dissolve directly in aqueous electrolytes. In order to obtain a comparable energy density (10 W h dm^{-3} [71]), it is necessary to incorporate active species with reasonable solubilities. The aqueous solubilities of several commercially available viologen and TEMPO compounds have been evaluated. In the class of viologen compounds, 4,4-dimethyl bipyridinium dichloride (m-Viol) has an aqueous solubility of up to 3.0 mol dm^{-3}, significantly higher than the others (40×10^{-3} to 1.5 mol dm^{-3}) [57]. On the other hand, 4-hydroxyl-TEMPO (HO-TEMPO) has a solubility of *ca.* 2.1 mol dm^{-3} in water, compared to <0.1 mol dm^{-3} for unsubstituted TEMPO, attibuted to the hydrophillic hydroxyl functional group at the para position. These two materials (4,4-dimethyl bipyridinium and 4-hydroxyl-TEMPO), with redox potentials of –0.45 and +0.80 V *vs.* SHE, respectively, were used as the negative and positive electrode materials. During charge-discharge cycling, stable radicals are involved in the battery reactions as shown below [57]:

E^o = –0.45 V *vs.* SHE (17)

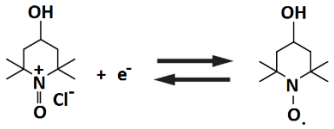

E^o = +0.80 V *vs.* SHE (18)

The charge-discharge cycling was conducted in a flow cell employing an anion-exchange membrane to transport chloride anions, due to the natures of the methyl viologen (4,4-dimethyl bipyridinium dichloride) and sodium chloride supporting electrolyte. Carbon felts were used as both the negative and positive electrode materials. The negative electrolyte was 0.1 mol dm^{-3} 4,4-dimethyl bipyridinium dichloride (m-$Viol^{++}Cl_2$) in 1.0 mol dm^{-3} sodium chloride solution, while the positive electrolyte was 0.1 mol dm^{-3} 4-hydroxyl-TEMPO (HO-TEMPO) in 1.0 mol dm^{-3} sodium chloride solution. The open-circuit voltage was 1.25 V, which is the highest among organic redox couples in aqueous electrolytes [57].

The battery was charge-discharge cycled at 40 mA cm^{-2} between the voltage limits of 1.77 V and 0.65 V for 100 cycles. The charge-discharge cycling can be visualized by the colour changes of the two active species. Throughout cycling, the coulombic efficiency was close to 100% and the capacity retention was more than 99% with a negligible loss for each cycle. The resulting system was also investigated at a higher concentration, 0.5 mol dm^{-3}, for both redox materials in 1.5 mol dm^{-3} sodium chloride solutions to yield a higher energy density of 8.4 W h dm^{-3}. The energy density is limited by the solubility limit of the 4-hydroxyl-TEMPO in 1.5 mol dm^{-3} sodium chloride solutions (0.5 mol dm^{-3} compared to 2.1 mol dm^{-3} in pure water) [57]. Since the charged species in both negative and positive electrode reactions are radicals, their stability after prolonged charge needs to be examined for future applications.

3.2. Organic-inorganic redox flow batteries

Organic-inorganic redox flow batteries involve one organic and one inorganic active material for the two electrode reactions (Table 4). The energy densities given in Table 4 are mainly based on the energy contents of the electrolyte and do not take account of the flow cell and electrolyte piping. The inorganic redox couples, such as zinc, bromine and ferricyanide, are based on low-cost elements that have been used in conventional redox flow batteries, which often have higher specific energy (e.g., zinc: 820 A h Kg^{-1}; bromine (Br_2): 335 A h Kg^{-1}). These systems (< 20 W h dm^{-3}) tend to have higher energy densities than the all-organic systems (< 10 W h dm^{-3}). Given the well-established knowledge of inorganic redox couples [15, 88, 94], several of these systems had been proposed before the all-organic systems described in Section 3.1. The inorganic active materials were selected to increase the cell voltages and in some cases the reversibilies were comparable to organic counterparts. Despite these benefits, significant improvements in terms of cell performance (cell voltage, current density, coulombic efficiency) and tuning of physical/electrochemical properties (number of electron-transfers, solubility, molar mass) are still required before these systems can compete with conventional all-vanadium systems (*c.a.* 35 W h dm^{-3}), which have cell voltages of around 1.5 V, a solubility of up to 2.0 mol dm^{-3} and high specific capacity of active materials (vanadium: 526 Ah Kg^{-1}). However, the costs of organic-inorganic systems are still likely to be lower than their all-vanadium counterparts in near term.

Organic-inorganic redox flow batteries									
Chemistries	**Negative active (in discharged state)**	**Positive active material (in discharged state)**	**Electrolyte & flowing condition**	**Cell components**	**Experimental OCV / V**	**Approx. % System efficiencies**	**Energy density /W h dm^{-3}**	**Number of cycles**	**Year [Ref]**
Cadmium / chloro-benzoquinone (acid)	Cd^{2+}	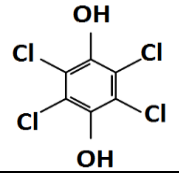	1 M $(NH_4)_2SO_4$ + 0.5 M H_2SO_4; 0.5 M negative active materials; flowing	Cadmium, chloranil/ No separator	*c.a.* 1.2	Coulombic: 99 Energy: 82 (10 mA cm^{-2})	N.G.	100	2009 [72]
Lead/ benzoquinone (acid)	$PbSO_4$	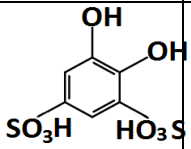	1 M H_2SO_4; 0.25 M positive active materials; flowing	Carbon felts/ Nafion 115	*c.a.* 1.1	Coulombic: > 99 Energy: > 80 (10 mA cm^{-2})	7.2	10	2010 [148]
Anthraquinone-bromide (acid)	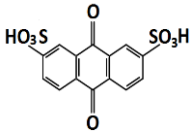	HBr	1 M H_2SO_4; 0.1 – 1 M negative active material; 0.5 – 2.5 M positive active material; flowing	Carbon papers/ Nafion 212	*c.a.* 0.86	Coulombic: 99 (200 – 500 mA cm^{-2})	12 - 16	> 10	2014 [40]
Anthraquinone-ferricyanide (alkaline)	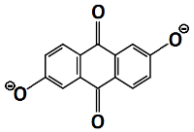	$Fe(CN)_6^{4-}$	1 M KOH; 0.5 M negative active material; 0.4 M positive active material; flowing.	Carbon papers/ Nafion 212	*c.a.* 1.2	Coulombic: > 99 Energy: 84 (100 mA cm^{-2})	6.8	100	2015 [75]
Flavin mononucleotide/ ferricyanide (alkaline)	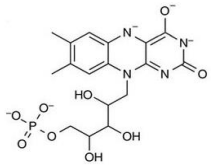	$Fe(CN)_6^{4-}$	1 M KOH & 1 M nicotinamide; 0.24 M negative active material; 0.4 M positive active material; flowing	Carbon felts/ Nafion 212	*c.a.* 1.3	Coulombic: > 99 (80 mA cm^{-2})	4.8	200	2016 [149]

Quinoxaline/ ferricyanide (alkaline)	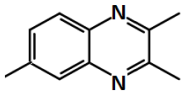	$Fe(CN)_6^{4-}$	0.2 M KOH + 0.067 M KCl + 0.5 M K_2SO_4 ; 0.2 M KOH + 0.5 M K_2SO_4; 0.1 M negative active material; 0.08 M positive active material; flowing.	Carbon felts / lithiated Nafion 117	*c.a.* 1.4	Coulombic: > 92 Energy: > 83 (1.76 mA cm^{-2})	N.G.	200	2015 [126]
Alloxazine/ ferricyanide (alkaline)	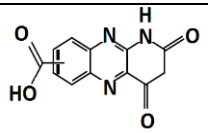	$Fe(CN)_6^{4-}$	pH 14 adjuested by KOH; 0.5 M negative active material; 0.08 M positive active material; flowing.	Carbon papers/ Nafion 212	1.1 – 1.2	Coulombic: > 99 Energy: > 60 (100 mA cm^{-2})	N.G.	400	2016 [150]
Zinc/ polymeric-TEMPO	Zn^{2+}	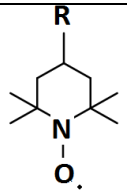	1 M $ZnCl_2$, 1 M NH_4Cl; flowing	Carbon paper, carbon felt/ cellulose-based dialysis membrane	*c.a.* 1.7	Coulombic: > 80 Energy: > 50 (5 – 20 mA cm^{-2})	> 3	50 (static cell)	2016 [151]
Zinc/ benzoquinone	Zn^{2+}	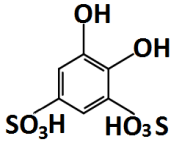	pH 7, 1.5 M $ZnCl_2$; 1.5 M negative active material; 50 mM positive active material	Carbon, carbon felt (membrane-less)	*c.a.* 1.52	Coulombic: > 78 Energy: > 70 (30 mA cm^{-2})	N.G.	12	2016 [152]

Table 4. Operational parameters and performance of organic-inorganic redox flow battery systems in aqueous electrolytes.

3.2.1. Acidic cadmium-chloro-benzoquinone hybrid flow battery

The first organic-inorganic hybrid flow battery was introduced by Xu and co-workers [72]. It used cadmium and chloranil as the negative and positive active electrode species, respectively. This system was also the first organic-based system proposed for flow battery applications, and arose from early investigations in the 1970s using soluble tetrachloro-1,4-benzoquinone (chloranil) as the cathode species [153]. The use of solid-state electrodes sets this system apart from other organic-based flow batteries using soluble organic active species, and it does not allow capacity to be increased by using concentrated electrolytes or higher electrolyte volumes. Using this configuration, the capacity of the battery was limited by insoluble chlorobenzoquinone at the positive electrode, in the form of a flexible film of active carbon black and binders. The resulting reactions of these organic materials exhibit excellent electrochemical reversibility and positive electrode potentials (*ca.* 0.7 *vs.* SHE) in highly acidic electrolytes. On the other hand, cadmium is used at the negative electrode to minimize side reactions due to its relatively high hydrogen overpotential. Cadmium ions are used as an electrolyte additive in commercial batteries to suppress hydrogen evolution [154].

The main novelty of this system is the single electrolyte, i.e. no membrane or separator is required for the system. This is because the charged products are in the solid state on both the negative and positive electrodes. Direct self-discharge reactions are not possible between the two charged products [3]. Since ion-exchange membranes are expensive, this configuration reduces the overall cost significantly [32, 33, 155]. Charge-discharge experiments were performed in a parallel flow cell. During charge, chlorobenzoquinone is reduced to its hydroquinone form, while cadmium is electro-deposited. The reverse reactions take place during discharge [72]:

$$Cd - 2e^- \leftrightarrow Cd^{2+} \qquad E^o = -0.42 \text{ V } vs. \text{ SHE} \qquad (19)$$

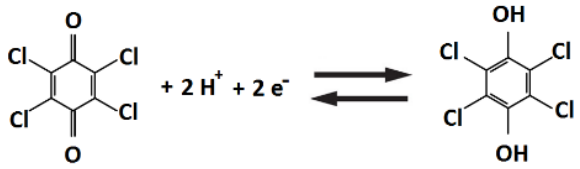

$$E^o = +0.71 \text{ V } vs. \text{ SHE} \qquad (20)$$

The supporting electrolyte was based on sulphate electrolytes of cadmium, ammonium and acid. The battery was typically charge-discharge cycled at 10 mA cm^{-2} for 100 cycles within a voltage window of 0.5 – 1.3 V. The open-circuit voltage was around 1.2 V with average charge and discharge voltages of 1.18 V and 0.97 V, respectively. In the first few cycles, the coulombic and energy efficiencies were relatively low, indicating a low utilization of the chlorobenzoquinone. Average coulombic and energy efficiencies of 99 % and 82% were obtained in the remaining cycles. Regarding the potential drop, the cadmium redox couple exhibits reversible charge-discharge behaviour at low overpotential. The main polarization of the system is attributed to the chlorobenzoquinone electrode. Prolonged cycling had an insignificant effect on the capacities of both electrodes [72]. The main drawback of this system is its limited capacity at the chlorobenzoquinone electrode, which may be replaced by soluble organic species while minimizing its direct reaction with the metallic electrodeposit at the negative electrode.

3.2.2. Acidic lead-benzoquinone hybrid flow battery

Following the introduction of the cadmium-chloro-benzoquinone hybrid flow battery, Xu and co-workers [148] proposed a similar system using soluble benzoquinone species as

the positive electrode. The negative and positive active species were lead and 1,2-benzoquinone-3,5-disulfonic acid (1,2-BQDS or Tiron), respectively. The proposed work was the first to use 1,2-benzoquinone-3,5-disulfonic acid as the positive redox couple for redox flow battery applications. As described in Section 3.1, this type of benzoquinone is electropositive (*ca.* 0.85 V *vs.* SHE) and has an aqueous solubility of up to 1.0 mol dm^{-3}. The work evaluated the electrochemical behaviour of this active species in aqueous electrolytes for a wide range of pH values. Cyclic voltammetric data showed that the reactions are electropositive and highly reversible in acidic electrolytes (pH < 4). The proposed battery reactions are:

$$Pb + SO_4^{2-} - 2e^- \leftrightarrow PbSO_4 \qquad E^o = -0.35 \text{ V } vs. \text{ SHE} \qquad (21)$$

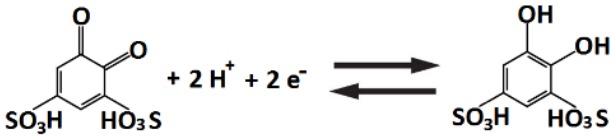

$$E^o = +0.85 \text{ V } vs. \text{ SHE} \qquad (22)$$

Experiments were carried out in a flow cell at 10 mA cm^{-2} using asymmetric electrodes. The negative electrode was metallic lead extracted from a commercial valve-regulated lead-acid battery, while the positive electrode was a conventional carbon felt electrode contacted against the graphite plate current collector. Unlike the single flow system [72] described in Section 3.2.1, this system employs a cation exchange membrane to avoid crossover of the negative and positive electrolytes. The negative electrolyte was solely 3.0 mol dm^{-3} sulphuric acid since the active species undergo solid-state transformation at the electrode surface [88], while the positive electrolyte contained 0.25 mol dm^{-3} 1,2-benzoquinone-3,5-disulfonic acid dissolved in 3.0 mol dm^{-3} sulphuric acid. In typical

half-cell and full-cell experiments, the charge potential of the positive benzoquinone reaction in the first few cycles was higher than in subsequent cycles. This suggested that the first electro-oxidation may be a four-electron reaction, while in subsequent cycles it is a two-electron reaction. A possible explanation is that the first charge-transfer reaction is followed by a chemical reaction with water, which is followed by a secondary charge-transfer reaction (an ECE process) [122, 156]. As a result of these reactions, the structure of the organic compound was changed. The secondary oxidation/reduction reaction, involving two-protons and two-electrons, takes place only in the subsequent cycles.

For these reasons, the coulombic efficiency of the first cycle was only 38%, showing that a portion of the charge transfer is not reversible due to the positive benzoquinone reaction. The coulombic efficiencies of the subsequent cycles were over 90%. The resulting open-circuit voltage was around 1.10 V with an energy efficiency of up to 82%. Since the negative electrode reaction does not involve metal deposition from soluble active species, the overall capacity is still limited by the mass of the active species within the negative electrodes [148].

3.2.3. Acidic anthraquinone-bromide redox flow battery

A metal-free redox flow battery based on anthraquinone and bromine was introduced by Aziz *et al.* [39, 40, 120, 157, 158]. Both redox species undergo rapid and reversible two-proton-two-electron reduction on a glassy carbon electrode (without costly precious metal catalysts) in sulfuric acid electrolytes. The Br_2/Br^- redox couple has been used for the positive electrode reaction in commercial zinc-bromine hybrid flow batteries, which were developed in the 1970s [15]. The negative electrode reaction was based on the redox

chemistry of 9,10-anthraquinone-2,7-disulphonic acid (AQDS). The redox reactions of this batteries are expressed as follows:

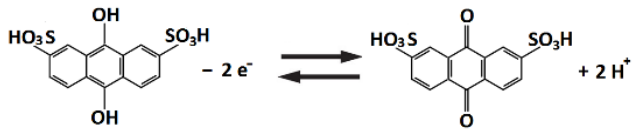

E^o = + 0.09 V *vs.* SHE

(23)

$Br_2 + 2H^+ + 2e^- \leftrightarrow 2HBr$ E^o = + 1.09 V *vs.* SHE

(24)

The proposed AQDS can be synthesized from inexpensive commodity chemicals [159, 160]. Its precursor molecule, anthracene, is abundant in crude oil and has been oxidized to anthraquinone at large scale in industrial processes. The estimated costs of anthraquinone and bromine are \$21 kW h^{-1} [39] and \$6 kW h^{-1} [161], respectively.

Among the various quinones, anthraquinones have low electrode potentials and are more suitable as negative redox couples. However, these molecules are relatively large and exhibit limited aqueous solubilities. Tuning of the properties, such as the reduction potential and solubility, are possible by adding suitable functional groups as described in Section 3.1. The addition of hydroxyl groups is calculated to lower the redox potential by an average of –50 mV (per group) and enhance the solubility due to the hydrogen bonding. The two hydroxyl groups in AQDS increased the overall cell voltage by around 11% (118 mV) and yield an aqueous solubility of >1 mol dm^{-3} at pH 0, resulting in relatively high energy density (>50 W h kg^{-1}, >50 W h dm^{-3}) compared to conventional all-vanadium redox flow batteries (10–20 W h kg^{-1}; 15–40 W h dm^{-3}) [40, 161].

The anthraquinone-bromide redox flow battery was constructed using a Nafion® membrane sandwiched between carbon papers without any catalysts. The open-circuit

voltage of the battery increased linearly from 0.69 V to 0.92 V going from 10% to 90% state-of-charge. As shown in Figure 5a) and 5b), the battery was charge-discharge cycled at 200 mA cm^{-2} and 500 mA cm^{-2}, respectively, for more than 10 cycles in each experiments (at 40 ^{o}C). The capacity retention was up to 99%, indicating minimal capacity fade and high coulombic efficiency. This can be attributed to the fast reaction kinetics of the redox species in both the negative and positive electrode reactions and the minimal crossover of the active species across the membranes due to their relatively large size as well as charge in aqueous solution as a sulphonate anion [40]. By further optimizing the electrolyte composition, flow rate, operating temperature and cell components, it is possible to obtain a peak power density in the region of 1.0 W cm^{-2} [120]. However, the major drawback of this system is the toxicity of the bromine species. Further improvements should be made by optimizing the cell design and operating parameters, such as the flow-field geometry, electrode design, membrane/separator and temperature.

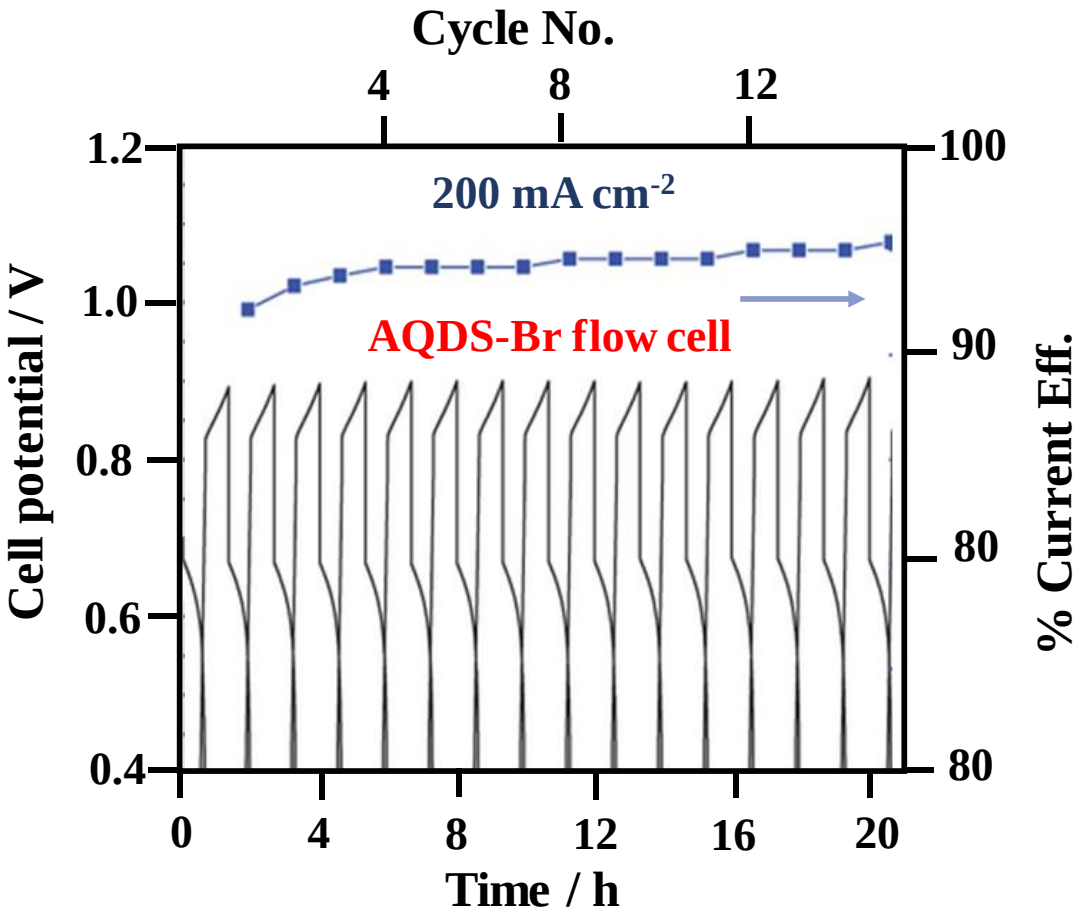
Cycle No.
4
8
12
1.2
1.0
0.8
0.6
0.4
100
90
80
80
200 mA cm-2
AQDS-Br flow cell
Cell potential / V
% Current Eff.
0
4
8
12
16
20
Time / h

Figure 5a

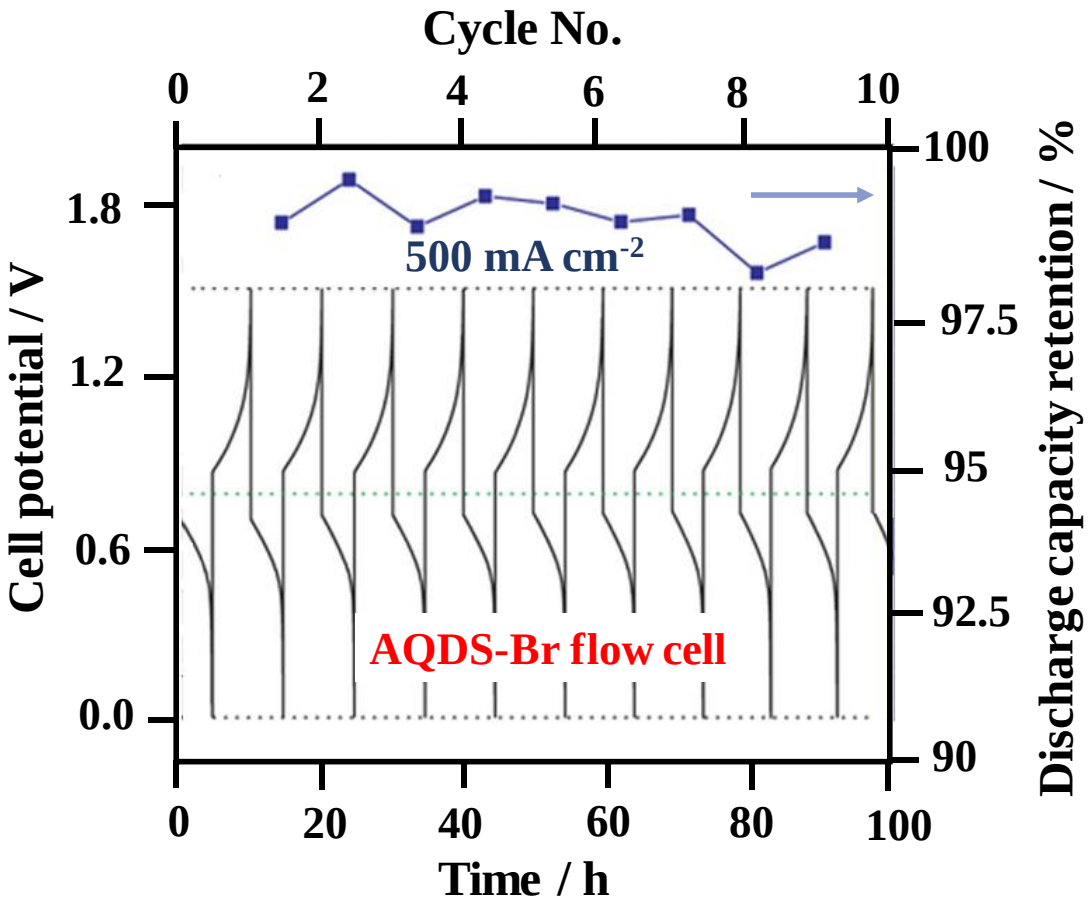
Cycle No.
0
2
4
6
8
10
1.8
1.2
0.6
0.0
Cell potential / V
100
97.5
95
92.5
90
Discharge capacity retention / %
500 mA cm-2
AQDS-Br flow cell
0
20
40
60
80
100
Time / h

Figure 5b

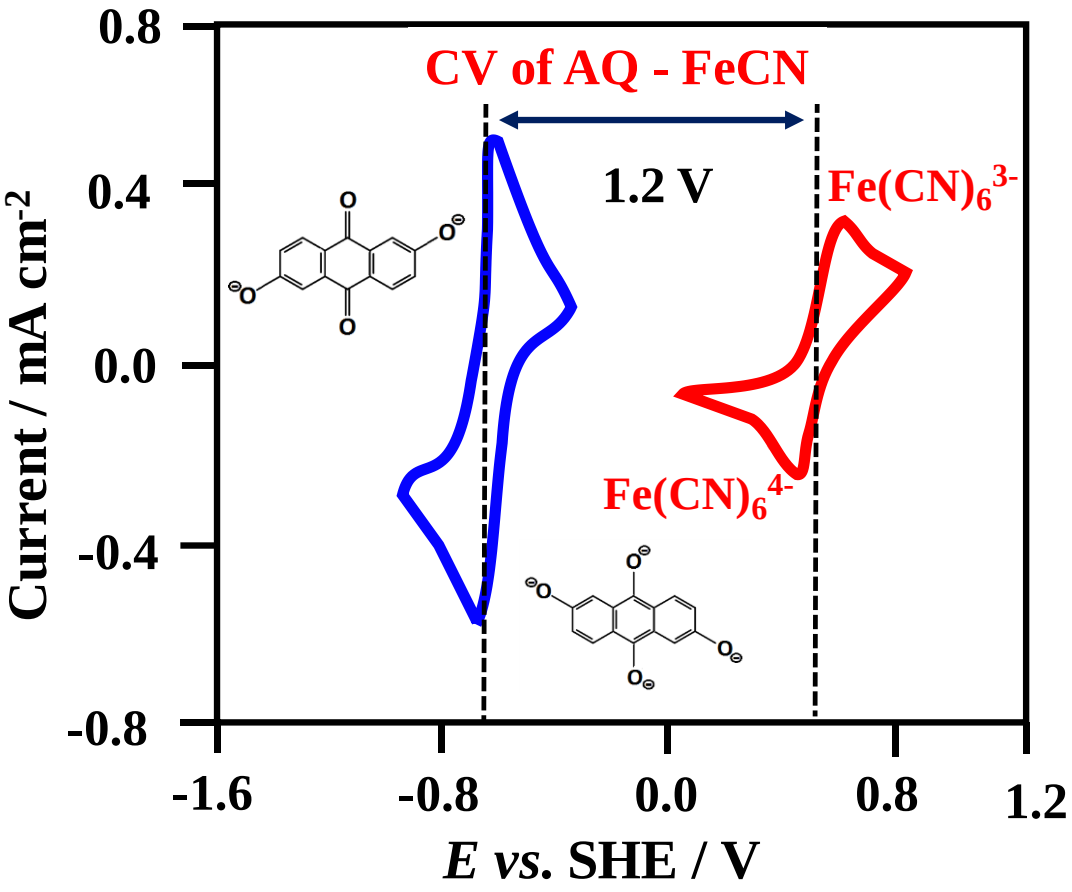
CV of AQ - FeCN
1.2 V
Fe(CN)6 3-
Fe(CN)6 4-
Current / mA cm-2
E vs. SHE / V
0.8
0.4
0.0
-0.4
-0.8
-1.6
-0.8
0.0
0.8
1.2

Figure 5c

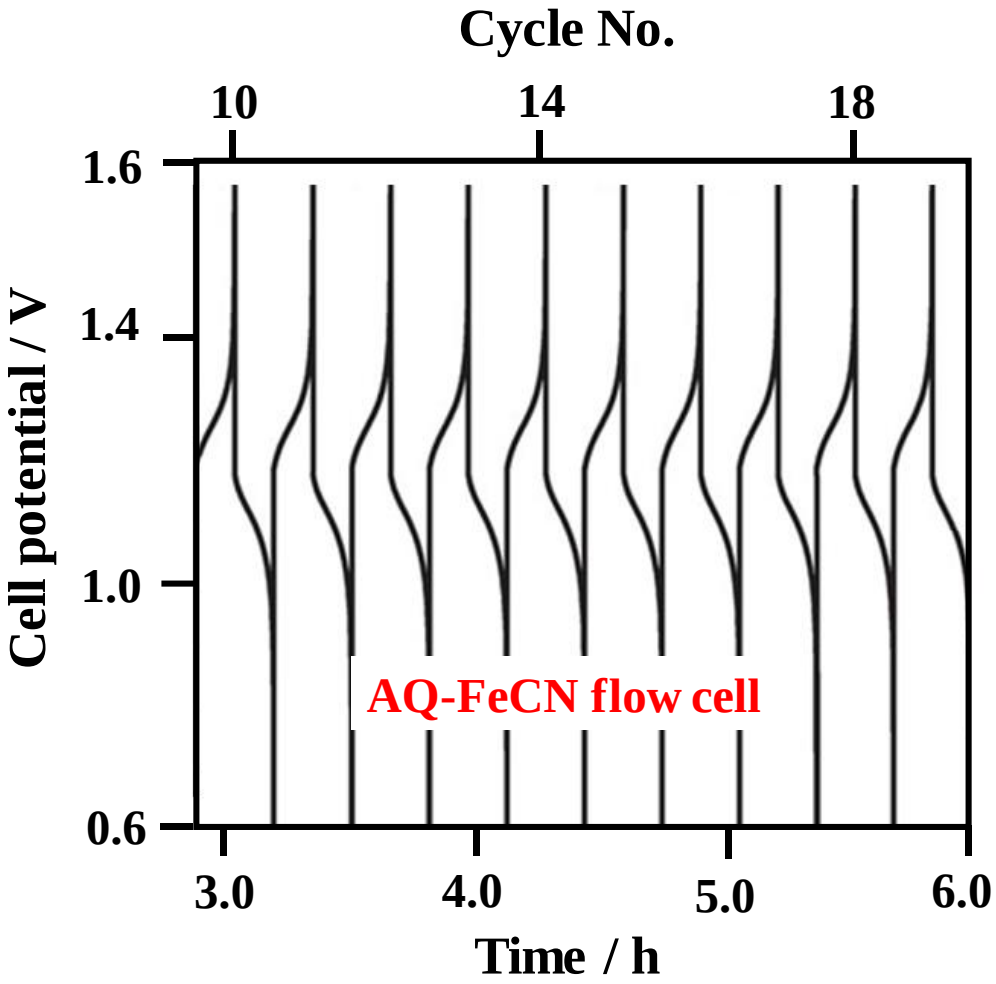
Cycle No.
10
14
18
1.6
1.4
1.0
0.6
Cell potential / V
AQ-FeCN flow cell
3.0
4.0
5.0
6.0
Time / h

Figure 5d

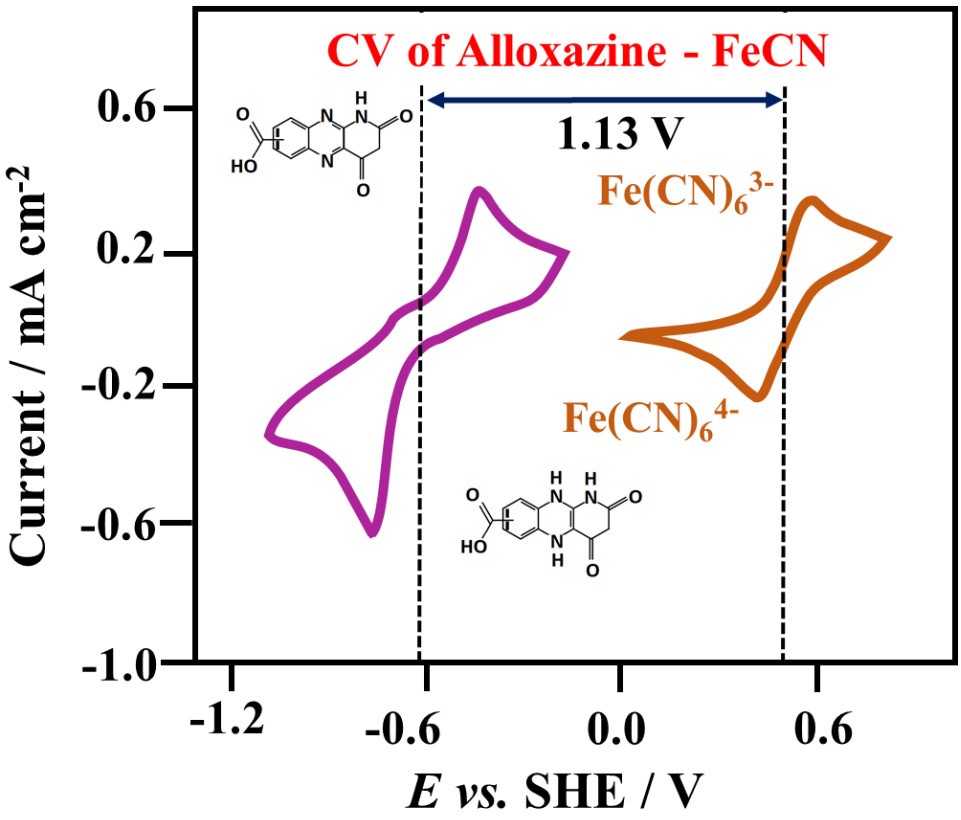
CV of Alloxazine - FeCN
1.13 V
Fe(CN)6 3-
Fe(CN)6 4-
Current / mA cm-2
E vs. SHE / V
0.6
0.2
-0.2
-0.6
-1.0
-1.2
-0.6
0.0
0.6

Figure 5e

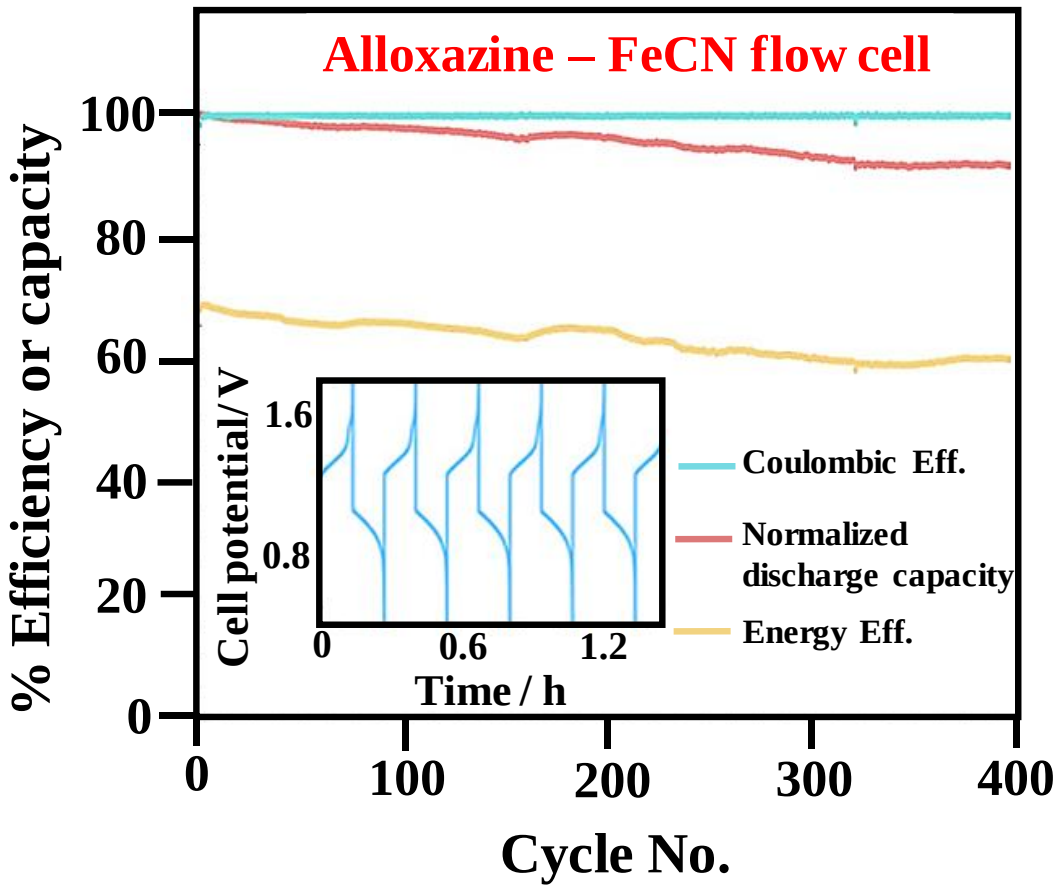

Figure 5f

Figure 5 Electrochemical performance and charge-discharge cycling performance of organic-inorganic redox flow batteries: (1) anthraquinone-bromide redox flow battery (40 ^{o}C): (a) charge-discharge profile at 200 mA cm^{-2} using a lower concentration of active species; (b) charge-discharge profile at 500 mA cm^{-2} using a higher concentration of active species; (2) anthraquinone-ferricyanide redox flow battery (20 ^{o}C): (c) cyclic voltammogram of 2 mmol dm^{-3} 2,6-dihydroxyl anthraquinone and ferrocyanide at 100 mV s^{-1} on glassy carbon electrode in 1.0 mol dm^{-3} KOH; (d) charge-discharge profile during 100 charge-discharge cycles at 100 mA cm^{-2}; (3) alloxazine-ferricyanide redox flow battery (20 ^{o}C): (e) cyclic voltammogram of 2 mmol dm^{-3} alloxazine 7/8-carboxylic acid and ferricyanide at 100 mV s^{-1} on glassy carbon electrode in KOH solution

(pH 14); (f) capacity retention, current efficiency and energy efficiency values over 400 cycles at 100 mA cm^{-2}.

3.2.4. Alkaline anthraquinone-ferricyanide redox flow battery

Lin and co-workers [75] proposed another organic-inorganic system based on alkaline electrolytes. The selected redox couples were 2,6-dihydroxylanthraquinone and ferricyanide, both of which are commercially available. In alkaline electrolytes, both the reduced and oxidized species on both sides have reasonable solubilities (>0.6 mol dm^{-3}). Inorganic ferricyanide as the positive electrode species is less hazardous than bromine [162-164]. Similar to most quinone-based systems in aqueous electrolytes, the hydroxyl groups of the anthraquinone molecules are shown to lower the reduction potential and enhance the solubility. For the negative electrode reaction, the use of an alkaline electrolyte exploits the pH as a parameter to shift the thermodynamic potentials of proton-dependent reactions to more negative values. In acidic electrolytes, anthraquinone molecules undergo two-proton-two-electron transfers, which shift to more negative potentials as the pH increases [75].

In the proposed system, 0.5 mol dm^{-3} 2,6-dihydroxyl anthraquinone and 0.4 mol dm^{-3} ferrocyanide were dissolved in 1 mol dm^{-3} potassium hydroxide as the negative and positive electrolytes, respectively. In such a high pH electrolyte (pH > 12), the anthraquinone reaction no longer involves protons and the reduction potential becomes pH-independent. The reduced species is in fully deprotonated form as negatively charged-radicals. The corresponding negative and positive electrode reactions are expressed as follows [75]:

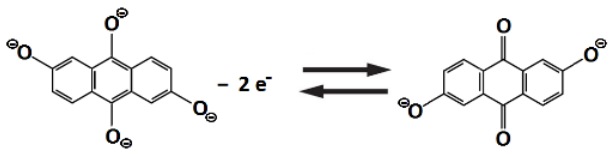

E^o = *ca.* – 0.65 V *vs.* SHE (25)

$$Fe(CN)_6^{3-} + e^- \leftrightarrow Fe(CN)_6^{4-} \qquad E^o = ca. + 0.36 \text{ V } vs. \text{ SHE} \quad (26)$$

In contrast to the pH-dependent anthraquinone reactions, the positive ferro/ferricyanide redox couple has a pH-independent redox potential. The low-reduction potential of the anthraquinone molecule (more negative than –0.6 V *vs.* SHE) at high pH results in an open-circuit voltage of up to 1.2 V at 50% state-of-charge, which is comparable to the conventional vanadium redox flow battery (1.4 V) and is about 50% higher than the previous-developed anthraquinone-bromine flow battery (0.8 V). The open-circuit voltage is consistent with the values observed in the cyclic voltammograms of Figure 5c). A preliminary study showed that a slight increase in cell potential is possible by using other hydroxyl-substituted anthraquinones, namely 2,3,6,7-tetrahydroxyanthraquinone (1.33 V) and 1,5-dimethyl-2,6-dihydroxyanthraquinone (1.34 V) [75].

Evaluation was performed at 20 ^oC in a parallel flow cell, in which carbon papers were used as the electrodes and a Nafion® membrane was used as the separator. As shown in Figure 5d), the resulting battery was charge-discharge cycled at 100 mA cm^{-2} for 100 cycles. During these cycles, the round-trip energy efficiency was 84% with a current efficiency of more than 99 %. The capacity loss was around 0.1% for each cycle, typically attributed to the chemical decomposition, crossover of the active species across the separators and leakage from the pumping system. The chemical stability of the cycled negative electrolytes, however, has been evaluated by heating at 100 ^oC for 30 days and

no degradation product was detected by proton nuclear magnetic resonance (NMR). The active species are all negatively charged in the alkaline electrolytes and are electrostatically repulsed by the cation exchange membrane, leading to reduced crossover during cell cycling [75]. The chemical stability and ionic conductivity of the cation exchange membrane in alkaline electrolytes remains, on the other hand, a major challenge. A better understanding of the reaction mechanism and the long-term stability of these deprotonated molecules in alkaline electrolytes are essential.

3.2.5. Alkaline quinoxaline-ferricyanide redox flow battery

Based on the introduction of quinoxaline as the negative electrode species in aqueous electrolytes, another organic-inorganic system has been proposed by Brushett and coworkers involving the use of a positive ferricyanide redox couple [75, 94, 148, 155-162, 165]. As discussed in Section 3.1.2, quinoxaline tends to provide improved performance in terms of electrode potential (*ca.* –0.5 V *vs.* SHE) and the peak separations in cyclic voltammograms [54, 126]. More importantly, the electrochemical behaviour is much more stable in alkaline electrolytes than in acidic media. In contrast, voltammograms in neutral/acidic electrolytes exhibit significant decay in peak current and larger peak separations within 10 voltammetric cycles. The above features suggest that quinoxaline is mainly suitable for alkaline electrolytes, in which ferricyanide is known to be safe and highly reversible. In the case of the alkaline-acidic system [126] described in Section 3.1.2, the alkalinity and acidity of the two half-cell electrolytes are difficult to maintain and both become neutralized in the long-term, especially when a proton-exchange membrane is used. In this proposed system, the supporting electrolytes

(0.2 mol dm^{-3} potassium hydroxide and 0.5 mol dm^{-3} potassium sulfate) are similar in both the negative and positive half-cell [126].

Similar to the alkaline-acidic system, the battery testing was conducted in a stainless-steel Swagelok cell, in which a Nafion® membrane was placed between two graphite felt electrodes. The charge-discharge reactions are as follows [126]:

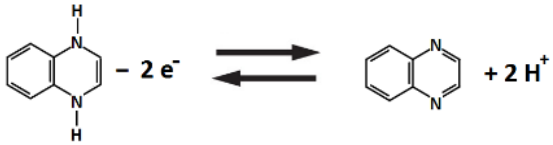

E^o = *ca.* –0.5 V *vs.* SHE (27)

$Fe(CN)_6^{3-} + e^- \leftrightarrow Fe(CN)_6^{4-}$ E^o = *ca.* +0.36 V *vs.* SHE (28)

The battery was charge-discharge cycled in the static Swagelok cell between the voltage limits of 0.6 and 1.6 V and 200 cycles were achieved within 170 minutes. The current density (1.76 mA cm^{-2}) was higher than that in the alkaline-acidic system (0.35 mA cm^{-2}). The coulombic and energy efficiencies remained steady at *ca.* 95 and *ca.* 82 %, respectively. Unlike the alkaline-acidic system, the capacity of each cycle appeared to be similar, which can be attributed to the similar supporting electrolyte content and the reduced crossover in the short (*ca.* 1 min) charge/discharge cycles [126].

3.2.6. Alkaline Flavin mononucleotide -ferricyanide redox flow battery

Orita and co-workers [149] proposed the use of flavin mononucleotide (FMN-Na) as the negative electrode reaction coupling with ferrocyanide in alkaline electrolytes.

These kind of organic materials often act as a cofactor in many enzymes and used in a wide variety of biological reactions. Flavins, such as riboflavin and lumichrome, have also been used as active materials in solid-state lithium-organic batteries [166].

. Compared with other flavins, such as riboflavin (vitamin B2) and lumiflavin, flavin mononucleotide has relatively higher solubilitity in water. With the addition of nicotinamide (NA, also known as vitamin B3) as a hydrotropic agent, the solubilities can reach up to 0.4 mol dm^{-3} and 1.5 mol dm^{-3} in neutral and alkaline electrolytes, respectively. The higher water solubility in alkaline electrolytes can be explained by the higher polarity of flavin mononucleotide than in acidic or neutral solution due to the large negative charge (FMN^{3-}). In alkaline electrolytes, the electrode potential is also more negative (<− 0.726 V vs. Ag|AgCl) than its neutral counterpart (*c.a.* − 0.5 V vs. Ag|AgCl). The resulting battery reactions are [149]:

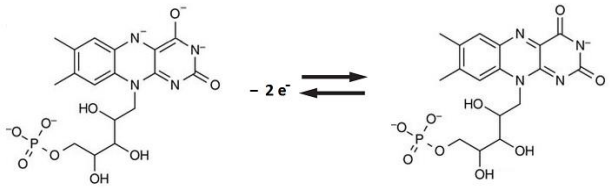

E^o = *ca.* − 0.5 to – 1.0 V *vs.* SHE (29)

$$Fe(CN)_6^{3-} + e^- \leftrightarrow Fe(CN)_6^{4-} \qquad E^o = ca. + 0.36 \text{ V } vs. \text{ SHE} \qquad (30)$$

The battery was charge-discharged cycled at 10 – 80 mA cm^{-2} for 100 between 0 and 2.0 V in a parallel plate flow cell with flow fields. Low and high concentrations of flavin mononucleotide (0.06 and 0.24 mol dm^{-3}) were used in the electrolytes at 1 mol dm^{-3} potassium hydroxide. At low current density (10 – 25 mA cm^{-2}), two charge

plateaus were observed and correspond to the reduction of monomer and dimer flavin mononucleotide.

At 25 mA cm^{-2}, the initial capacity was close to the theoretical capacity (5.03 Ah dm^{-3} *vs.* 5.36 Ah dm^{-3}) and the average discharge voltage was 0.96 V. When the current densities was increased to higher than 50 mA cm^{-2}, the coulombic efficiency was > 99% and the discharge capacity retention was up to 99 % after 100 cycles. The peak power density was determined to be 0.16 W cm^{-2} at 300 mA cm^{-2}. Considering that the maximum solubility of ferrocyanide is *c.a.* 0.5 mol dm^{-3}, alternatives of positive active materials should be further explored to enhance the energy and power densities [149].

3.2.7. Alkaline alloxazine -ferricyanide redox flow battery

Alloxazine-based molecules have been proposed by Lin and co-workers [150] for coupling with ferricyanide redox couples in alkaline electrolytes as a new flow battery chemistry. Similar to quinones and quinoxaline, alloxazine-based molecules are aromatic compounds, which can be synthesized *via* a simple and high-yield coupling reaction between *o*-phenylenediamine derivatives and alloxan in acetic and boric acid at room temperature and atmospheric pressure [167-169]. This group of materials has been used as the negative electrode species for both lithium-ion and sodium-ion batteries. Functionalization of these molecules with carboxylic acid group can result in a solubility of up to 2 mol dm^{-3} in an alkaline electrolyte (e.g., pH 14, potassium hydroxide solutions). DFT suggested that replacement of the carboxylic acid groups with solubility enhancing hydroxyl groups could further increase the battery voltage by nearly 10%. This can be achieved by coupling *o*-phenylenediamine-4-carboxylic acid with alloxane to form an isomeric mixture of alloxazine 7/8-carboxylic acid (ACA) at almost 100% yield. As

determined by voltammetric techniques, the synthesized product (alloxazine 7/8-carboxylic acid) has a reduction potential of −0.62 V *vs.* SHE with a rate constant of $1.2\pm0.2 \times 10^{-5}$ cm s^{-1} (an order of magnitude higher than that for vanadium) [2]. Furthermore, almost no decline in the voltammeric performance was observed over a two-week experiment.

As shown in Figure 5e), the combined cyclic voltammograms of alloxazine 7/8-carboxylic acid and ferricyanide showed that the estimated cell voltage could be as high as *ca.* 1.13 V. The resulting chemistry was further tested in a flow-cell to evaluate the charge-discharge cycling performance, with the following discharge reactions:

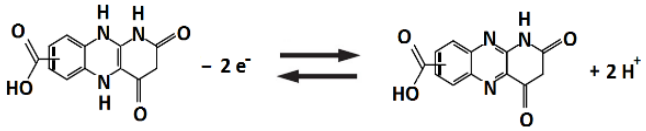

E^o = *ca.* – 0.62 V *vs.* SHE (31)

$$Fe(CN)_6^{3-} + e^- \leftrightarrow Fe(CN)_6^{4-} \qquad E^o = ca. + 0.36 \text{ V } vs. \text{ SHE} \quad (32)$$

In a typical experiment, the negative electrolyte was a solution of 0.5 mol dm^{-3} alloxazine 7/8-carboxylic acid, while the positive electrolyte contained 0.4 mol dm^{-3} ferrocyanide and 40 mmol dm^{-3} ferricyanide. Both electrolytes were adjusted to pH 14 by potassium hydroxide. The excess amounts of ferrocyanide and ferricyanide were used to ensure that the negative electrode reaction would be the capacity limiting factor of the battery. Carbon papers and Nafion® membrane were used as the electrodes and separators, respectively. The battery was charge-discharge cycled for more than 400 cycles with initial charge and discharge voltages of *ca.* 1.4 V and *ca.* 0.9 V, respectively. In this

prolonged cycling, the coulombic efficiency was over 99.7% at 100 mA cm^{-2}, which is indicative of negligible side reactions and insignificant crossover of the active species across the membrane (Figure 5f)). The system had an average energy efficiency of 63% and exhibited a capacity retention rate of more than 91% over 400 cycles, i.e., a capacity loss rate of 0.023% per cycle. Furthermore, another battery with adjusted cell compression was demonstrated at higher concentrations of up to 1.0 mol dm^{-3} active species. The energy efficiency was further increased to 74%, while retaining the same level of current efficiency (99.7%) and capacity retention per cycle (99.95%).

3.2.8. Neutral zinc – polymeric TEMPO hybrid flow battery

Following the polymer-based system introduced in Section 3.1.3, the same research group [151] proposed the use of electropositive polymeric TEMPO (up to +0.90 V *vs.* SHE) coupling with electronegative zinc anode (–0.76 V *vs.* SHE) in neutral chloride electrolytes. These active materials show lower toxicity compared with other ionic polymers (i.e. poly-L-lysine and poly(ethylene imine)) and other halogen cathodes (i.e. bromine and iodine). In the electrolytes, the soluble salt of zinc not only acts as the active species but also as the supporting electrolytes. Poly(ethylene glycol) methyl ether methacrylate (PEGMA) and [2-(methacryloyloxy)ethyl]trimethylammonium chloride (METAC) were used and compared as the copolymers with TEMPO as the positive active materials. The resulting battery has the following discharge reactions [151]:

$$Zn - 2\ e^- \leftrightarrow Zn^{2+} \qquad E^o = \ ca.\ -0.76\ V\ vs.\ SHE \tag{33}$$

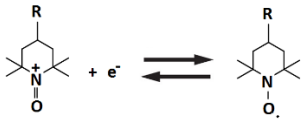

E^o = *ca.* +0.90 V *vs.* SHE

(34)

Between the two half-cells, dialysis membrane derive from regenerated cellulose was us ed as an effective separator, blocking the crossover of the large TEMPO containing poly mers. In order to increase the surface area and allow higher current densities/ prevent the formation of dendrites, carbon papers and carbon felts were used as the electrode materi als. The battery was charge-discharged cycled in a flow cell at a range of current densiti es (0.5 – 20 mA cm^{-2}) between 1.2 and 2.0 V. In aqueous systems, open-circuit voltages of c.a. 1.7 V were observed with two types of polymeric TEMPO. Compared to PEGM A-based polymers, METAC-based polymeric TEMPO was observed to have low solubil ities in concentrated zinc solutions regardless of anions. In contrast, PEGMA-based poly meric TEMPO has higher solubilities and does not precipitate in zinc chloride solutions of up to 1 mol dm^{-3} salt concentrations. For these reasons, zinc chloride can be used as t he supporting electrolytes and the capacity of up to 2.39 A h dm^{-3} was achieved. In gene ral, the charge-discharge capacity tend to decrease linearly with the increasing current d ensities. The capacity was up to *c.a.*18 mA h at < 2.5 mA cm^{-2} and decreased to *c.a.* 1 m A h at 20 mA cm^{-2}. However, the coulombic and energy efficiencies maintained over 80 % and 50 %, respectively [151].

3.2.9. Membrane-less neutral zinc-benzoquinone hybrid flow battery

The first membrane-less organic-inorganic redox flow battery was introduced by Leung and co-workers [42, 152]. The operating concept makes use of the slow dissolution of the

deposited metal in the presence of the soluble active species in the common electrolytes, which has been used in previous inorganic systems [88, 155]. The negative and positive half-cell electrode reactions were based on zinc electrodeposition and the redox reactions of benzoquinone species:

$$Zn - 2e^- \leftrightarrow Zn^{2+} \qquad E^o = -0.76 \text{ V } vs. \text{ SHE} \tag{35}$$

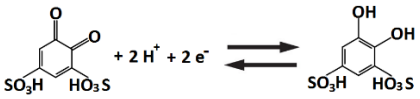

$$E^o = +0.85 \text{ V } vs. \text{ SHE} \tag{36}$$

These active materials are low-cost, abundant and show high electrode potentials in aqueous electrolytes. It should be noted that both electrode reactions undergo two electron-transfers processes. Based on this architecture and the low cost of the active materials, the capital cost of this system is estimated to be lower than USD$150 (kW h)$^{-1}$, reaching the cost target set by the US Department of Energy in the long-term, the cost of the active materials in the electrolytes is only USD$ 14 (kW h)$^{-1}$. In the absence of separator, the charged benzoquinone species are free to react with the metallic zinc anode as a self-discharge process. The corrosion current density has been calculated to be between 1.1 and 9.4 mA cm^{-2} depending on the quinone concentration (10 – 100 mmol dm^{-3}), which is still lower than the typical operating current density of 30 mA cm^{-2} used in hybrid redox flow batteries.

The proposed chemistry was further tested in a parallel-plate flow cell, in which carbon substrate and carbon felt were used as the negative and positive electrodes, respectively. The common electrolyte contained 1.5 mol dm^{-3} zinc chloride and 50 mmol dm^{-3} benzoquinone species. The battery was charge-discharge cycled with an average energy

efficiency of *ca.* 73 % at 30 mA cm^{-2} for more than 12 cycles. The charge and discharge voltages were around 1.52 and 1.24 V, respectively. The low concentration of benzoquinone implies a relatively low specific energy compared to conventional systems. Future work should focus on the use of higher applied current densities, facilitated by improved mass transport and cell architecture. Higher specific energy can also be achieved with the use of separators, with which reversible reactions at high concentrations (e.g., 1.0 mol dm^{-3}) have been demonstrated in previous work [90, 121]. This, however, would add further cost to the system, although the low cost of the active species would still keep the overall cost to a low level.

4. Organic couples in non-aqueous electrolytes

Non-aqueous electrolytes offer a wider window of electrochemical stability, which enables flow batteries to operate at higher cell voltages (>2 V). For high voltage systems with reasonable solubilities (>1 mol dm^{-3}), fewer unit cells and ancillary parts are required to achieve a given energy output. In the past few decades, a number of studies have focused on selecting suitable redox active species to obtain systems with higher energy densities and system efficiencies. The majority of the reported non-aqueous flow batteries are anion-exchange systems using single electrolytes composed of metal-centred coordination complexes [18-23, 77]. In 1988, Matsuda *et al.* [18] demonstrated the first non-aqueous redox flow battery based on a ruthenium bypyridine complex with an open-circuit cell voltage of 2.6 V. Following this, a number of non-aqueous systems (particularly anion-exchange systems) have been introduced, also using single electrolytes composed of metal coordination complexes [18-23, 77, 85, 86, 170]. Despite the relatively high cell potentials (>2 V), many of these systems suffer from poor

solubilities and low efficiencies of the metal complexes. Recent investigations have focused on metal-centred ionic liquids [76] and hybrid chemistries with electronegative anodes [97, 171, 172] to respectively improve the solubilities and the energy densities of the non-aqueous systems.

Among non-aqueous systems, the main research limitation is the low ionic conductivities (10^{-8} – 10^{-10} S cm^{-1}) of the pure electrolytes (without salts) compared to aqueous systems (6×10^{-8} S cm^{-1} for pure water) [18]. This can be attributed to the higher viscosity of organic solvents, as governed by Stokes' law. With the addition of salts, the ionic conductivities can be increased up to 10^{-2} S cm^{-1} with suitable combinations of salts and solvents [58]. However, it is important to note that different solutes are found to compete with each other, which can be explained well by the theory of partial molar volume for solutes. The effect of competing solubility with the active species needs to be considered when selecting the concentrations of supporting electrolytes. Several examples are given in the work of Gong *et al.* [43], in which a higher concentration of supporting electrolyte often leads to lower solubilities of the active materials.

Table 5 shows the ionic conductivities of a number of non-aqueous electrolytes with a salt concentration of 1 mol dm^{-3}. Ionic conductivities increase in the order: acetonitrile (MeCN) > dimethoxyethane (DME) > dimethyl sulfoxide (DMSO) > propylene carbonate (PC) [58, 173]. The addition of salts containing cations, e.g. tetraethylammonium (TEA^+) [58], and anions, e.g. hexafluorophosphate (PF_6^-), perchlorate (ClO_4^-) and trifluoromethane sulfonimide ($TFSI^-$), tends to increase the ionic conductivities. In certain cases, mixtures of linear and cyclic carbonates (i.e. propylene, ethylene and diethyl carbonates) also increase the ionic conductivity and the solubility of the active species [173, 174]. For instance, non-aqueous solvents containing 1.0 mol dm$^-$

^{3} tetraethylammonium salts in acetonitrile have ionic conductivities of more than 4×10^{-2} S cm^{-1}, which is comparable to that of salt water (*ca.* 10^{-2} S cm^{-1}) [48, 175]. With this type of electrolyte, it was possible to charge-discharge cycle a battery at a current density up to 15 mA cm^{-2} [58] or even at 100 mA cm^{-2} in recent work using interdigitated flow fields and carbon paper electrodes [176]. The current density value can be higher than the typical current densities (0.01 – 0.5 mA cm^{-2}) used in non-aqueous electrolytes. This phenomenon is also associated with the use of different types of ion-exchange membranes in particular solvents.

	Electrolytes	Conductivity / mS cm^{-1}
1	1 M TEA-BF_4/ acetonitrile	56
2	1.5 M TEA-BF_4/ acetonitrile	60
3	1 M TEA-TFSI/ acetonitrile	45
4	1 M $LiBF_4$/ acetonitrile	16
5	1 M LiClO/ acetonitrile	34
6	1 M $LiPF_6$/ acetonitrile	50
7	1 M LiTFSI/ acetonitrile	36
8	1 M LiTFSI/ diethylene glycol dimethyl ether	7
9	1 M LiTFSI/ 1,2-dimethoxyethane (DME)	14
10	1 M TEA-TFSI/ 1,2-dimethoxyethane (DME)	17
11	1 M TEA-TFSI/ dimethyl sulfoxide (DMSO)	9
12	1 M TEA-TFSI/ tetrahydrofuran (THF)	10

Table 5. Ionic conductivities of different supporting electrolytes and conducting salts used in non-aqueous systems.

In recent years, Shin *et al.* [17] have reviewed the status of separators for non-aqueous redox flow battery systems. The majority of the reported systems focused on positively charged redox species, and anion-exchange membranes have primarily been used to shuttle the counter ions between the electrodes [17, 177, 178]. Typical ionic conductivities of commercial anion-exchange membrane are in the range 0.2 – 0.5 mS cm^{-1} in non-aqueous electrolytes, significantly lower than those in aqueous electrolytes (> 10 mS cm^{-1}) [43]. With the use of these membranes, the overall resistance of incumbent systems is relatively high, ranging from a few tens to a few hundreds of Ω cm^2, restricting the discharge current density and power density to only a few mA cm^{-2} and a few mW cm^{-2}, respectively [43].

The anions used in non-aqueous electrolytes (e.g. PF_6^- or BF_4^-) are also the major cost contributors to the overall costs of the electrolytes. Therefore, negatively charged redox active species with inexpensive cations (i.e. Na^+ and Li^+) have been investigated in recent years [41]. For the case of lithiated Nafion® cation exchange membranes, a nearly linear relationship between diffusive crossover of neutral redox species and the ionic conductivity was observed [178]. This is due to the increased pore size and overall porosity, which facilitate the mass transfer of ions or molecules and, therefore, lead to increased conductivities and crossover rates. In comparison, the charge of the redox species is less important in terms of selectivity but still affects the crossover rate in accordance with Donnan exclusion [178]. Although sacrificing the selectivity of the active species, porous separators, particularly Daramic®, have relatively low area resistances in non-aqueous electrolytes (e.g., Daramic-175: 3.8 Ω cm^2 [179]), which allows charge-discharge cycling to take place at 15 – 100 mA cm^{-2} [58, 176, 179].

For some non-aqueous organic-inorganic systems, particularly lithium-based flow batteries, glass ceramic separators (e.g. Ohara LiCGC or LATP ($Li1+xAlxTi_{2-x}(PO_4)_3$)) are commonly used and effectively block the crossover of positive active species and aqueous electrolytes towards the lithium anode compartment. These separators may not, however, be chemically stable in the electronegative electrolyte and are prone to degradation due to their poor chemical stability. In contrast, polymeric separators, e.g., the cation-exchange Nafion®, appear to have more flexibility and better chemical stability. Modification of polymeric separators with chemically resistant polymers (e.g., polyvinylidene difluoride (PVDF)) has recently been demonstrated by Jia *et al.* to yield significant improvements in a full-cell study [102, 103].

Since the ionic conductivity is lower in non-aqueous electrolytes, energy storage devices require active species with certain desirable properties (e.g., multi-electron transfers, increased solubility and wide redox windows) to provide a reasonable energy density [41, 43]. Compared to their metallic counterparts, organic active species are attractive in these aspects. Similar to the aqueous systems, the selection of the organic active molecules has been facilitated by computational screening within the framework of DFT [45-47]. Cheng *et al.* [45] down-selected a pool of candidates based on successive property evaluations. The main three criteria were redox potential, solubility and stability, which correspond to selections of molecules with oxidation potentials >5.00 V, reduction potentials of <1.43 V and solvation energies below – 4.2 kcal mol^{-1} (– 17.58 kJ mol^{-1}). The selection process considered thousands of derivatives of quinoxalines, anthraquinone, thiane, thiophene and bipyridine.

In addition to computational screenings, electrochemical investigations of some of these organic active species, particularly the derivatives of quinoxaline [180], anthraquinone

[74, 181, 182] and thiophene [183], have been carried out experimentally in a parallel flow cell or a static type cell, as shown in Table 6. The use of other redox active species, including 2,5-Di-tert-bityl-1,4-bis(2-methoxyethoxy)benzene (DBBB) [78, 180], was inspired by their previous use for overcharge protection in lithium-ion batteries [184-187]. In aprotic electrolytes, proton-coupled electron-transfer is clearly not possible for the protonation [43, 128]. Electron transfer for most organic active molecules involves the formation of stable radicals. Neutral species form radical anions or radical cations by gaining or losing electrons, respectively. Since no bond formation or breakage is involved, the reaction kinetics are highly facile, resulting in a high rate constant [43]. Unlike their metallic counterparts, some organic active molecules have high solubility. For instance, unsubstituted quinoxaline has a solubility limit of up to 7 mol dm^{-3} in propylene carbonate [180].

Non-aqueous organic redox flow batteries							
Chemistries	**Negative active material (at disch. state)**	**Positive active material (at disch. state)**	**Electrolyte & flowing condition**	**Cell components**	**Exp. OCV / V**	**Approx. % System Efficiencies**	**Year [Ref]**
N-methyl-phtalimide / TEMPO	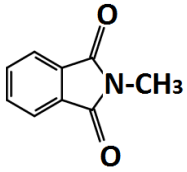	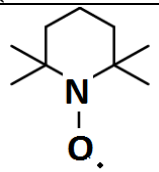	1 M $NaClO_4$ in acetonitrile; 0.1 M active materials; static.	Carbon papers/ Nepem-117	*ca.* 2.0	Coulombic: > 90 Energy: > 60 (0.35 mA cm^{-2})	2011 [188]
Camphoquinone/ oxo-TEMPO	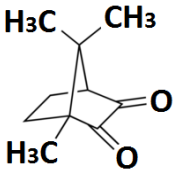	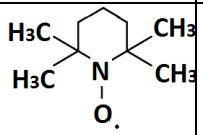	1.0 M $TEABF_4$ in propylene carbonate; 0.2 M active materials; static	Carbon felts/ Fumasep FAP	*ca.* 2.1 – 2.3	Coulombic: > 80 Energy: > 71 (1.0 mA cm^{-2})	2015 [189]
Trimethyl-quinoxaline/ DBBB	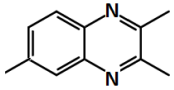	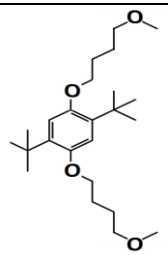	0.2 M $LiBF_4$ in propylene carbonate; 0.05 M active materials; static	Carbon papers/ Nafion 117	1.6 – 2.4	Coulombic: 70 Energy: 37 (0.0625 mA cm^{-2})	2012 [180]
Trimethyl-quinoxaline/ trifluoromethyl-ethyl-phenothiazine	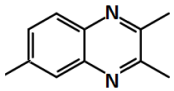	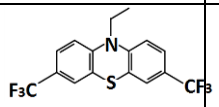	0.2 M $LiBF_4$ in propylene carbonate; 0.05 – 0.35 M active materials; static	Carbon felts/ Nafion	1.5 – 2.4	Coulombic: > 80 (0.14 mA cm^{-2})	2015 [190]

Fluorenone / DBMMB	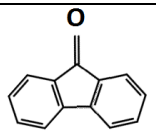	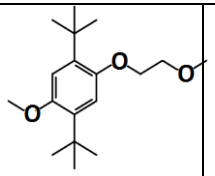	1.0 M TEA-TFSI in acetonitrile; 0.5 M active materials; flowing	Carbon felts/ Daramic microporous polyethylene / silica separator	2.2 – 2.7	Coulombic:. 86 Energy: 71 (15 mA cm^{-2})	2015 [58]
N-methyl-phthalimide/ DBMMB	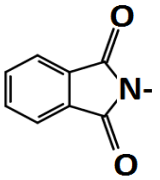	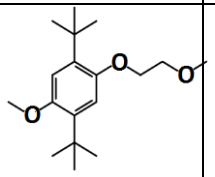	1 M LiTFSI in DME; 0.3 M active materials;	Carbon felts/ Daramic 175	2.0 – 2.4	Coulombic: 90 Energy: 69 (35 mA cm^{-2})	2016 [179]
Symmetric diamino-anthraquinone	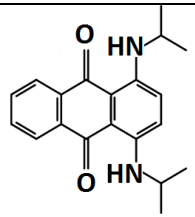	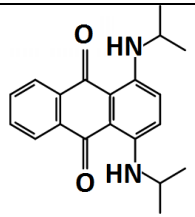	100 mM TBAP in acetronitrile /toluene; 50 mM active materials; static	Reticulated vitreous carbon / medium porosity glass frit	> 1.1	Coulombic: 60 – 80 Energy: 28 – 40 (0.66 mA cm^{-2})	2016 [181]
Symmetric PTIO	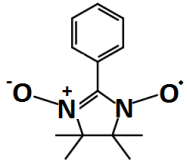	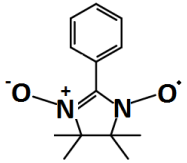	1 M $TBAPF_6$ in acetronitrile; 0.5 M active materials; flowing	Carbon felts/ Daramic porous separator	1.5 – 1.9	Coulombic: 90 Energy: 60 (20 mA cm^{-2})	2016 [191]
Symmetric polythiophene	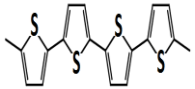	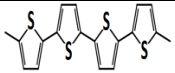	1.0 M $TEAPF_6$ in propylene carbonate; 8.41 g dm^{-3} active materials; flowing	Carbon & Ketjen black / Fumasep FAP	2.6 – 3.0	Coulombic: 78 Energy: 61 (0.5 mA cm^{-2})	2014 [183]

Zinc/ polymeric TEMPO	Zn	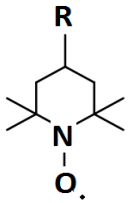	0.5 M $Zn(ClO_4)_2$ in EC:DMC:DEC; flowing	Zinc and carbon felt or paper / dialysis membrane	1.3 – 1.7	Coulombic: > 90 Energy: > 70 (1.0 mA cm^{-2})	2016 [73]
All-poly(boron-dipyrromethene)	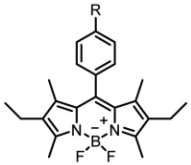	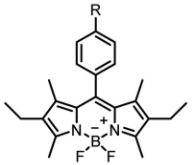	0.5 M Bu_4NClO_4 in propylene carbonate; static	Carbon felts/ dialysis membrane	> 1.28	Coulombic: 89 Energy: 55 (0.1 mA cm^{-2})	2016 [192]

Table 6. Operational parameters and performance of organic redox flow battery systems in non-aqueous electrolytes (excluding lithium-based systems).

Most of these radicals, however, are reactive and short-lived, implying challenges for long-term cycling and storage stability This is also a major technical hurdle in the way of exploiting the concentrations of active species in non-aqueous electrolytes. Since low concentrations of the active species [22-27] and relatively small current densities (0.01 – 0.5 mA cm^{-2}) [139, 148, 158] were used, many of the existing systems suffer from low power outputs and energy densities (< 15 W h dm^{-3}) [58]. Given that low power output also implies a higher number of cells and larger electrode areas, the overall costs of these systems are prohibitively expensive for any practical applications. From a structural aspect, it is still possible to stabilize radicals through electronic resonance, steric crowding and/or dimer formation [193]. In certain cases, some radicals are relatively stable and sometimes persistent. For instance, the TEMPO (2,2,6,6,-tetramethylpiperidinyloxyl) neutral radical is a persistent radical molecule, attributed to both steric crowding and electronic resonance [188]. The chemical stability of these radicals can also be influenced by the selections of the salts and solvents. For instance, 9-fluorenone (FL^-) was found to be more chemically stable in dimethoxyethane (DME) than in acetonitrile (MeCN) [58]. In terms of conductive salts, the tetraethylammonium (TEA^+) cation and the trifluoromethane sulfonimide ($TFSI^-$) anion provide better chemical stability than conventional ions, including the lithium cation (Li^+) and the tetrafluoroborate anion (BF_4^-). With suitable selections of radical active species and electrolyte compositions, it is possible to maintain 90 % of the initial capacity of the battery for over 50 cycles [58], with round-trip energy efficiencies (> 80 % at 10 mA cm^{-2} [58]) comparable to aqueous systems (> 80% at > 40 mA cm^{-2}). The promise shown by such systems should be balanced against the challenges associated with non-aqueous electrolytes, such as higher cost, lower ionic conductivity, and other unfavourable

physical properties, such as moisture sensitivity, flammability and toxicity [43]. Further understanding and progress towards these issues will be critical for the development of organic redox flow batteries in non-aqueous electrolytes.

4.1. All-organic redox flow batteries

Non-aqueous all-organic redox flow batteries were introduced in 2011, even before their aqueous counterparts. These systems involve organic active species as soluble species for both the negative and positive electrode reactions. The active species were mainly based on derivatives of quinoxaline [180], anthraquinone [181, 182], thiophene [183], TEMPO (2,2,6,6,-tetramethylpiperidinyloxyl) [188] and DBBB (2,5-Di-tert-bityl-1,4-bis(2-methoxyethoxy)benzene) [194]. Since the selected non-aqueous electrolytes are mainly aprotic, electron transfers in the reactions involve the formations of charged radicals, exhibiting facile reaction kinetics but also poorer chemical stability in the long-term. Other major concerns are the cost, moisture sensitivity, flammability and toxicity of the non-aqueous electrolytes [43].

4.1.1. N-methylphtalimide-TEMPO redox flow battery

The first non-aqueous all-organic redox flow battery was proposed by Li and co-workers [188] using N-methylphtalimide and TEMPO for the negative and positive electrode reactions, respectively. These active species were known to form stable radical molecules during the charging process and have also been used in lithium-ion batteries to prevent overcharge, which can lead to thermal runaway and catastrophic failure [35, 194, 195]. N-methylphtalimide has been used in electron-transfer studies since it undergoes

stoichiometric reduction to the corresponding stable anion radicals localized on the electron deficient rings [196], while the chemical stability of TEMPO is provided by the steric structures around the radical centre and/or by resonance structures. During charge-discharge, the reaction mechanisms at the negative and positive electrodes are as follows:

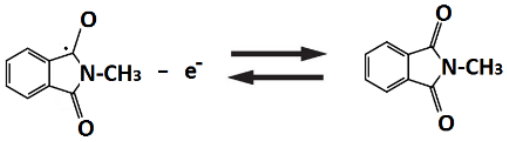

E^o = *ca.* –1.3 V *vs.* Ag

(37)

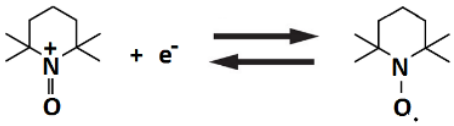

E^o = *ca.* +0.3 V *vs.* Ag

(38)

The redox reaction of TEMPO takes place between itself and the oxoammonium cation. In both cases, these active materials exhibit quasi-reversible electrochemical behaviour in acetonitrile electrolytes. As suggested by cyclic voltammetry, the reversible peaks of the negative (N-methylphtalimide) and positive (TEMPO) active species are centred at –1.3 and +0.3 V *vs.* Ag, respectively, which results in an equivalent cell voltage of *ca.* 1.6 V. The narrow peak separations (<200 mV at 10 mV s^{-1}) of these voltammograms indicate that the polarizations of the electrode reactions were extremely small, suggesting fast electrode reaction kinetics (N-methylphtalimide: $k_0 = 4.6 \times 10^{-2}$ cm s^{-1}; TEMPO: $k_0 = 10^{-1}$ cm s^{-1}) of up to several orders of magnitude higher than those of the V(II)/V(III) reaction ($k_0 = 10^{-5}$ cm s^{-1}) [188, 197, 198].

Charge-discharge cycling tests were conducted in a static cell, which contained a Nepem-117 membrane (BEST, China) separating the two compartments. Carbon felts were used as electrodes and soaked in the corresponding electrolyte for > 1 hour. The electrolyte contained 0.1 mol dm^{-3} active species and 1.0 mol dm^{-3} sodium perchlorate in acetonitrile electrolytes. The battery was charge-discharge cycled at 0.35 mA cm^{-2} between cell voltages limits of 0.45 V and 2.20 V for 20 cycles. The average charge and discharge voltages were 1.65 V and 1.36 V, respectively, and the coulombic efficiency was *ca.* 90%. Despite the promising cycling performance, the duration of each cycle was only 30 minutes [188] and higher cell voltages would be expected since non-aqueous electrolytes were used.

4.1.2. Camphoquinone-oxo-TEMPO redox flow battery

As discussed in Section 4.1.1., TEMPO is an attractive active species in terms of electrode potential (*ca.* +0.3 V *vs.* Ag) and its chemical stability [188]. For these reasons, another TEMPO-based non-aqueous system has been proposed by Park and co-workers [189]. In this system camphoquinone and oxo-TEMPO were used at the negative and positive electrodes, respectively, resulting in an open-circuit voltage of up to 2.12 V, compared to *ca.* 1.6 V of the aforementioned N-methylphtalimide-TEMPO batteries. In the case of the negative electrode reaction, camphoquinone exhibits properties similar to other quinones in non-aqueous electrolytes [128, 129]. In general, quinones form relatively stable radicals with highly electronegative potentials (< –0.2 V *vs.* Ag). The use of camphoquinone leads to an exceptional electrode potential (–1.64 V *vs.* Ag) with relatively high solubility (>1.1 mol dm^{-3}). Similar improvements in terms of the electrode potential were also observed with the use of oxo-TEMPO at the positive electrode. The

redox potentials of oxo-TEMPO and TEMPO were estimated to be +0.48 V *vs.* Ag and +0.3 V vs. Ag, respectively, by cyclic voltammetry. For both the negative and positive electrode reactions, the peak separation was as narrow as *ca.* 90 mV, indicating a highly reversible process. The charge-discharge processes are as follows [189]:

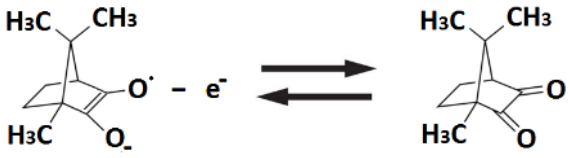

E^o = *ca.* –1.64 V *vs.* Ag

(39)

E^o = *ca.* +0.48 V *vs.* Ag

(40)

During charge, the nitroxyl radical of the oxo-TEMPO molecule undergoes oxidation to form a cation and joins the electrolyte anion to form oxoammonium salt. The reverse reaction takes place during the discharge process. The battery test was conducted in a static cell similar to that of the N-methylphtalimide-TEMPO system, with a symmetric structure containing two carbon felt electrodes separated by a Fumasep®-FAP membrane. The electrolytes contained 0.2 mol dm^{-3} active species and 1.0 mol dm^{-3} tetraethylammonium tetrafluoroborate salts in propylene carbonate. The battery was charge-discharge cycled at 1.0 mA cm^{-2} between 1.3 V and 2.6 V at 30 ºC. The charge

and discharge plateaus appeared at 2.3 V and 2.03 V, respectively. The overall system exhibited coulombic and energy efficiencies of 80.3% and 71.3% at the third cycle. The low coulombic efficiencies were attributed to the crossover of active species as well as poor mass transport within the static cell (zero flow rate) [189]. Optimization of these components and operating parameters would yield improvements.

4.1.3. Trimethylquinoxaline–DBBB redox flow battery

In addition to the TEMPO-based redox flow battery chemistries, one of the earliest organic redox flow battery system was proposed by Brushett and co-workers [180] using quinoxaline and DBBB (2,5-di-tert-butyl-1,4-bis(2-methoxyethoxy)benzene) for the negative and positive electrode reactions, respectively. This system was the first to introduce these active materials for redox flow battery applications. Quinoxaline-derivatives had previously been used as component materials in organic sensitizers in solar cells [199] and organic photovoltics systems [200]. In non-aqueous electrolytes, quinoxaline shows promise due to its high solubility (*ca.* 7 mol dm^{-3} in propylene carbonate), its low molecular weight and its ability to transfer two electrons for each molecule. DBBB is not sensitive to air and exhibits no side-reactions at any potential lower than the redox potential, which has been tested in lithium-ion batteries for 200 cycles of 100% overcharge [184-187]. Unmodified quinoxaline and DBBB exhibit reversible reactions with redox potentials of +2.6 V *vs.* Li and +3.9 V *vs.* Li, respectively.

The cell potential window is still low (*ca.* 1.3 V) considering that non-aqueous electrolytes enable cell voltages above 2 V. Substitutions of methyl groups onto quinoxaline molecules were used to decrease the redox potential (+2.48 V *vs.* Li) and

enhance the redox activity, as a form of 2,3,6-trimethylquinoxaline. The solubility of this quinoxaline derivative is around 0.5 mol dm^{-3} in propylene carbonate [180].

The resulting charge-discharge reactions of this battery are [180]:

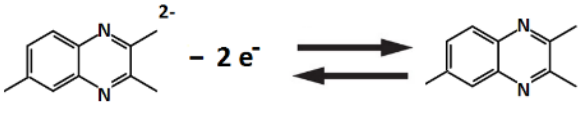

$E^{o} =$ *ca.* +2.48 V *vs.* Li

(41)

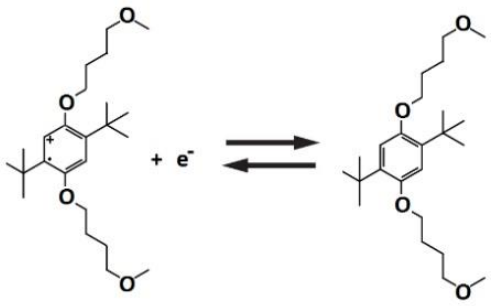

$E^{o} =$ *ca.* +3.9 V *vs.* Li

(42)

The proof-of-concept system was then charge-discharge cycled in a static coin cell, in which two carbon paper electrodes were soaked in the corresponding electrolytes and separated by a Nafion® 117 membrane, as in the configuration for lithium-ion battery testing. A single electrolyte was used, consisting of 0.05 mol dm^{-3} 2,3,6-trimethylquinoxaline, 0.05 mol dm^{-3} DBBB, 0.2 mol dm^{-3} lithium tetrafluoroborate in propylene carbonate. The battery was charge-discharge cycled at 0.0625 mA cm^{-2} between 0.1 V and 2.5 V for 30 cycles. The coulombic efficiency of the first cycle was as low as 43%, which increased and stabilized at *ca.* 70% with a peak of 79%. The low coulombic efficiencies were attributed to the use of a single electrolyte in the coin cell. Based on the experimental cell voltages and the solubilities of the active species, the

theoretical energy density is *ca.* 16 W h dm^{-3} [180], which is still lower than state-of-the-art aqueous technologies (*ca.* 40 W h dm^{-3}) [201]. The performance and operating lifetime should increase with improved cell designs using flowing electrolytes. Further improvements in the energy density can be achieved by increasing the DBBB solubility and the cell voltage through molecular design and electrolyte selection.

4.1.4. Trimethylquinoxaline–trifluoromethyl-ethylphenothiazine redox flow battery

Kaur and co-workers [190] investigated the replacement of DBBB with 3,7-bis(trifluor omethyl)-N-ethylphenothiazine (BCF3EPT) in the trimethylquinoxaline-DBBB redox flow battery. BCF3EPT is highly electropositive with a reversible potential of 3.9 V *vs.* Li, while that of DBBB is at 4.0 V *vs.* Li. The main feature of this active species is its high solubility (1.2 mol dm^{-3}) compared to DBBB (0.18 mol dm^{-3}) and trimethylquinoxaline (0.37 mol dm^{-3}) in propylene carbonate electrolytes, which results in a higher energy density. The reaction mechanism is considered to be [190]:

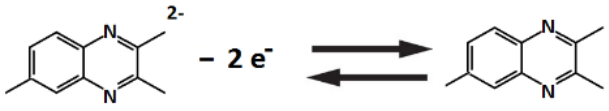

E^o = *ca.* +2.48 V *vs.* Li

(43)

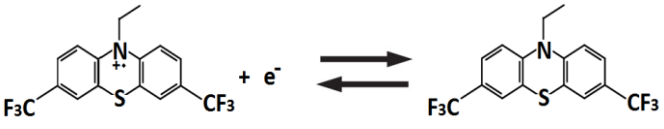

E^o = *ca.* +3.9 V *vs.* Li

(44)

In order to evaluate the stability of the radicals, UV-vis spectroscopy was conducted for the oxidation states of both the BCF3EPT and DBBB molecules obtained through bulk

electrolysis. The spectra collected at regular time intervals over a 5 h period indicated that the radical cation of BCF3FPT was much more stable than that of DBBB in propylene carbonate electrolytes. In the case of BCF3FPT, 80% of the original intensity was observed after 5 h, while for DBBBthe equivalent figure was *ca.* 11%. This observation is consistent with other work using similar organic compounds (e.g. 1,4-bis(tertyl)-2,5-dimethoxybenzene (DDB)) for lithium-ion batteries [202].

Charge-discharge cycling was conducted in a static Swagelok type cell using a single electrolyte, containing the same concentrations of both the negative and positive active species (0.05 mol dm^{-3}, 0.15 mol dm^{-3}, 0.35 mol dm^{-3}) with 0.2 mol dm^{-3} lithium tetrafluoroborate in propylene carbonate. Unlike many previous studies on non-aqueous systems, the static cell was charge-discharged at higher concentrations of active species (from 0.05 to 0.35 mol dm^{-3}) under constant current density (0.14 mA cm^{-2}, 0.71 cm^2) between 0.2 V and 2.5 V [190].

When 0.05 mol dm^{-3} of active species were used, there was a disparity between the plateau voltages during the first charge and discharge cycles. After the first few cycles, the battery transitioned to consistent charging from 1.5 – 2.4 V and discharging from 1.5 – 1.3 V with similar charge and discharge capacities. The coulombic efficiencies stabilized at *ca.* 92% but eventually decayed over subsequent cycles. The performance was superior to that of the previous trimethylquinoxaline-DBBB system under the same operating conditions; the latter system showed a decline in capacity through the first 50 cycles. However, at 0.35 mol dm^{-3}, the capacity of the proposed system decayed rapidly, reaching almost zero after 20 cycles. This is attributable to the increased rate of dimerization of the radicals at higher concentrations, resulting in fewer counter ions available to stabilize these charged species. The cation exchange membrane underwent a colour change during

the process, implying reactions with one or both of the electroactive compounds in their neutral or charged form, leading to a reduced capacity and a higher membrane resistance. It is important to understand the influence of the irreversible second oxidation of both active species on the overall cycling performance [190].

4.1.5. Fluorenone–DBMMB redox flow battery

Based on studies conducted in the past few years, several technical challenges facing non-aqueous organic redox flow battery systems have been identified [41, 43]. Many of these systems suffer from low energy densities and power outputs attributed to low concentrations of the active species [18-23] and a relatively small current density (0.01 – 0.5 mA cm^{-2}) [180, 188, 190]. In addition to the natures of the non-aqueous electrolytes, conventional ion-exchange membranes are another significant factor leading to low current densities. Furthermore, the chemical stability of the charged radicals has been the main research challenge for most non-aqueous systems in relation to reversible cycling in the long-term. Wei and co-workers [58] introduced a new system, in which 9-fluorenone (FL) and 2,5-di-tert-butyl-1-methoxy-4-[2'methoxyethoxy]benzene (DBMMB) were used as the negative and positive electrode species, respectively. Similarly to TEMPO and DBBB, DBMMB has been used for overcharge protection in lithium-ion batteries. As suggested by voltammetric studies, the redox potentials of fluorenone and DBMMB are *ca.* –1.64 V *vs.* Ag and *ca.* +0.73 V *vs.* Ag, respectively, resulting in a cell voltage of *ca.* 2.37 V. Considering that DBMMB is a liquid at room temperature, fluorenone has a solubility of 2.0 mol dm^{-3} in the mixture of acetonitrile and DBMMB. In such an electrolyte, the solubility limit for both redox materials is 0.9 mol

dm^{-3} in 1.2 mol dm^{-3} tetraethylammonium trifluoromethane (TEA-TFSI) sulfonimide in acetonitrile. The resulting battery reactions are [58]:

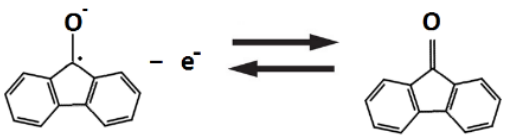

E^o = *ca.* –1.64 V *vs.* Ag

(45)

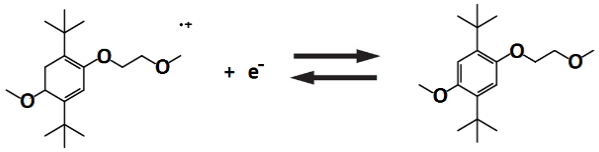

E^o = *ca.* +0.73 V *vs.* Ag

(46)

The battery was charged and discharge at 15 mA cm^{-2} for 100 cycles between 1.7 V and 2.7 V in a parallel plate flow cell, which was the first time such a configuration was used to evaluate a non-aqueous all-organic redox flow battery. The flow cell was assembled with two graphite felts on both sides and separated by a Daramic® microporous polyethylene/silica separator with a median pore size of 0.15 μm and a porosity of 57%. The electrolytes were based on 0.5 mol dm^{-3} active species with 1.0 mol dm^{-3} tetraethylammonium trifluoromethane sulfonimide (TEA-TFSI) in acetonitrile. Under such high current operation, both the coulombic and energy efficiencies remained relatively high (86% and 71%, respectively), even though the highly porous separator tended to allow high crossover rates of the active species; the high coulombic efficiency can be attributed to the increased mass transport of the species under flowing conditions. The energy density of the resulting system was 11 W h dm^{-3}, significantly higher than that of any other non-aqueous all-organic system (2 W h dm^{-3}). The battery suffered from capacity fade, losing 80% of its initial value over 100 cycles [58].

In common with most non-aqueous systems, the capacity fade is attributed to the reactive free radicals of $FL^{\bullet-}$ and $DBMMB^{\bullet+}$. Electron spin resonance (ESR) was used to evaluate the chemical stability of these radicals in a number of electrolytes containing different solvents (dimethoxyethane and acetonitrile) and salts (tetraethylammonium trifluoromethane sulfonimide (TEA-TFSI), tetraethylammonium tetrafluoroborate (TEA-BF4) and lithium trifluoromethane sulfonimide (LiTFSI). The use of DME to test the solvent effect is due to its relatively high stability in the presence of radicals [203]. Figures 6a) and 6b) illustrate the fading of the radical concentration as a function of storage time, indicating that $DBMMB^{\bullet+}$ has much slower fading rates than $FL^{\bullet-}$ in all supporting electrolytes. Moreover, $FL^{\bullet-}$ is much more sensitive to the supporting electrolyte than $DBMMB^{\bullet+}$. The results suggested that the tetraethylammonium cation, the trifluoromethane sulfonimide anion and dimethoxyethane solvents are more suitable for sustaining these two radicals over long periods of time (>10 h) [202, 204]. Since the degradation of radicals is closely associated with the solvents and salts, it is important to identify the degradation mechanisms and to improve the chemical stability by tailoring the structure of the active molecules.

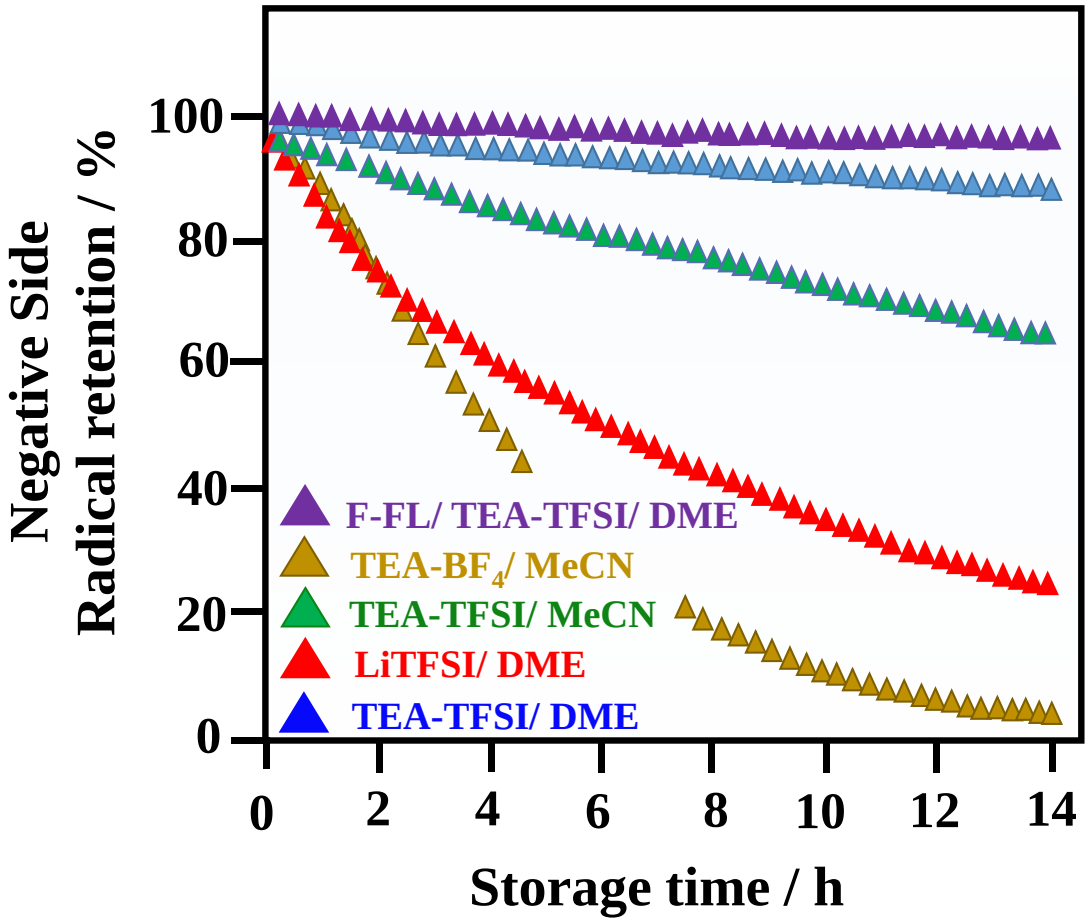
Negative Side
Radical retention / %
100
80
60
40
20
0
0
2
4
6
8
10
12
14
Storage time / h
F-FL/ TEA-TFSI/ DME
TEA-BF4/ MeCN
TEA-TFSI/ MeCN
LiTFSI/ DME
TEA-TFSI/ DME

Figure 6a

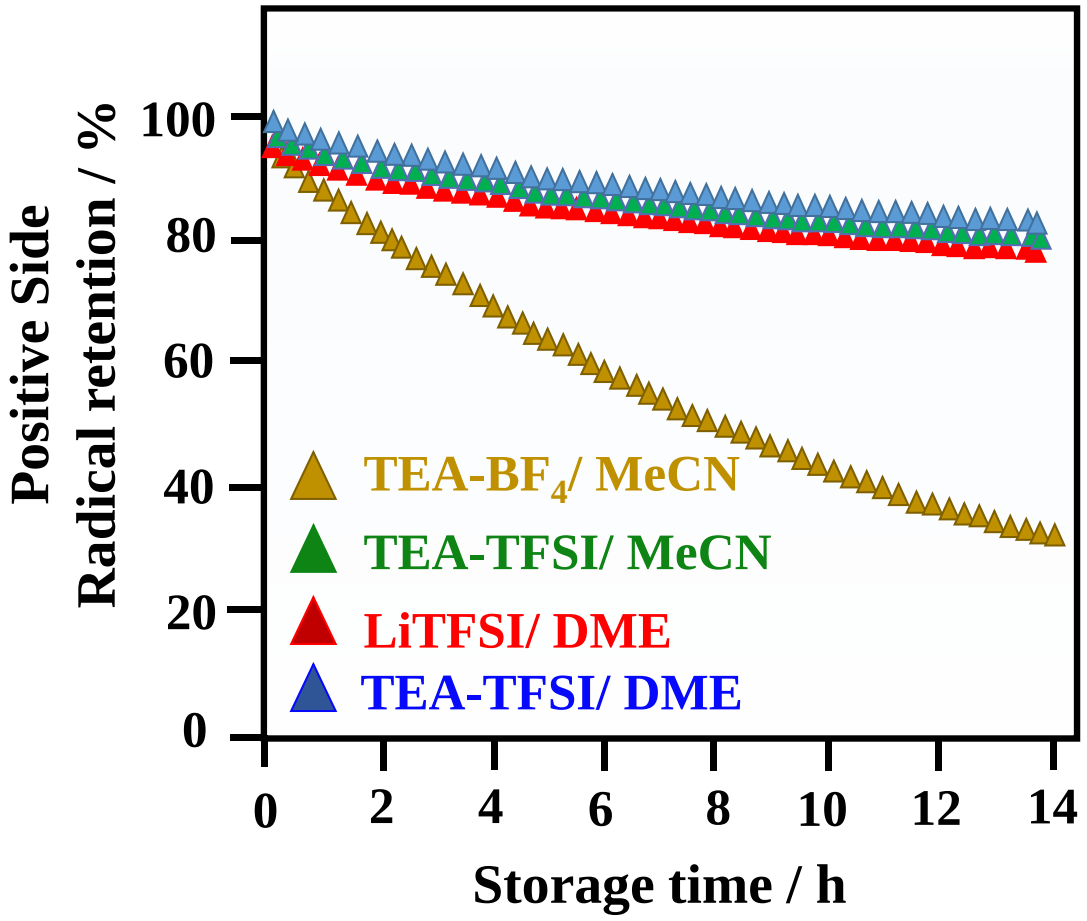

Figure 6b

Figure 6. Fading of the radical concentration as a function of storage time measured by electron spin resonance (ESR) to evaluate the chemical stability/decay of these radicals in a number of electrolytes and salts: a) negative FL^- active radicals; b) positive $DBMMB^+$ active radicals.

4.1.6. *N*-methylphthalimide–DBMMB redox flow battery

Following the introduction of the fluorenone -DBMMB redox flow battery, the same research group developed another DBMMB-based system for even higher current density operation (35 mA cm^{-2}). Rather than fluorenone, commercially available *N*-methylphthalimide was used as the negative redox active species in the proposed system

[179]. As suggested by voltammetric studies, the redox potentials of *N*-methylphthalimide and DBMMB were –1.79 *vs.* Ag and +0.51 V *vs.* Ag, respectively, suggesting a cell-voltage of up to 2.1 V. Both reactions appear to be chemically stable since the redox peaks for both reactions were well-defined even in a mixed-reactant electrolyte (1:1 molar ratio of *N*-methylphthalimide and DBMMB). The authors suggested that the *N*-methylphthalimide radical anion is not likely to undergo any possible side reactions with the sDME and TFSI salts.

Furthermore, these active materials exhibit reasonable solubilities in the DME solvent, with *ca.* 0.7 mol dm^{-3} for the *N*-methylphtalimide, and DBMMB liquid has high miscibility at room temperature. The resulting battery reactions are as follows:

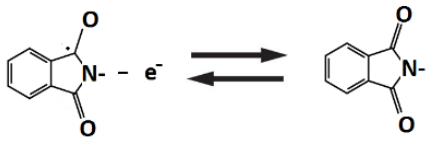

$E^o =$ *ca.* –1.79 V *vs.* Ag (47)

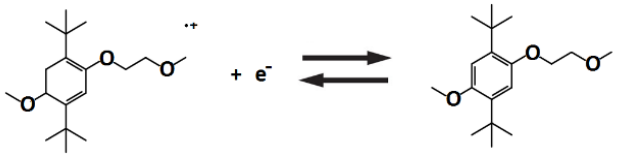

$E^o =$ *ca.* +0.51 V *vs.* Ag (48)

Based on this chemistry, an assessment of different commercial separators (Daramic and Celgard) was carried out in the charge-discharge experiments. Given that Celgard separators (25 µm) are much thinner than Daramic separators (175 – 800 µm), their area specific resistances tend to be relatively low. However, Daramic separators have larger pore size (0.15 mm, *vs.* 28 – 64 nm of Celgard). It has been demonstrated that the thinner version of Daramic (3.8 Ω cm^2 for Daramic-175, 175 µm) has an even lower area

resistance than that of Celgard 2325 (5.1 Ω cm^2). Therefore, a Daramic separator was selected for the flow cell cycling experiment.

In the main cycling test, the battery was charge-discharge cycled at 35 mA cm^{-2} for 50 cycles with the use of 0.3 mol dm^{-3} active species on both sides. The flow cell maintained constant capacities and efficiencies (coulombic efficiencies of *ca.* 90% and energy efficiencies of *ca.* 69%) throughout the test. The average charge and discharge capacities reaches 85% and 77% of the theoretical capacity, indicating a high redox species utilization over prolonged cycling [179].

4.1.7. Symmetric diaminoanthraquinone redox flow battery

In the previous sections, all of the systems were asymmetric, using different active species for the negative and positive electrode reactions. In contrast, the most successful conventional system to date is the all-vanadium redox flow battery, which uses the same element (vanadium) as the active species for both electrode reactions [1-7]. Use of the same element solves the issue of cross-contamination of the electrolytes, thus removing the risk of permanent damage to the battery. No membrane can entirely eliminate the crossover of the species across the electrolyte compartments [147]. Once crossover has take place, there is no straightforward approach to separate the active molecules or elements, which makes it difficult to recondition the electrolyte and return it to its initial state [205, 206].

For these reasons, Potash and co-workers [181, 182] proposed a symmetric system using diaminoanthraquinone derivatives (DAAQ) as the active molecules for both electrode reactions in the initial condition (discharged state). The selected molecule was

commercial ‘DB134’, commonly used as a synthetic fabric dye and as a colourant in pyrotechnics and is produced inexpensively from coal residues on a large scale [207].

In general, many of these diaminoanthraquinone derivatives have more than five discrete redox states over a wide range of potentials. During the charging process, the initial anthraquinone molecule, DAAQ, is reduced or oxidized by two electrons to form $DAAQ^-$ and $DAAQ^+$ species in the negative and positive half-cells, respectively. The reverse reactions take place during the discharge process as follows [181]:

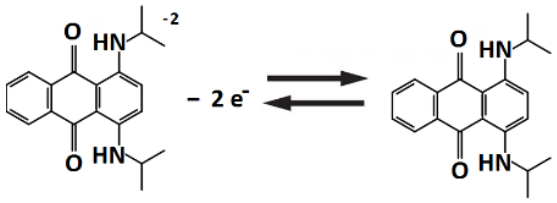

E^o = *ca.* –1.51 to –1.98 V *vs.* Ag

(49)

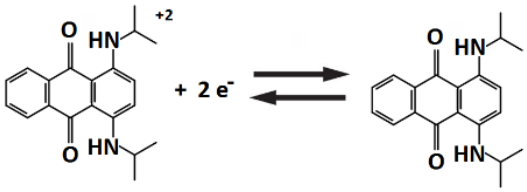

E^o = *ca.* +0.25 to +0.74 V *vs.* Ag

(50)

In acetonitrile electrolytes, DB-134 exhibits four reversible one-electron transfer reactions: two reductions occur at –1.51 to –1.98 V *vs.* Ag and two oxidations occur at +0.25 to +0.74 V *vs.* Ag, respectively. The potential difference between the first and second respective oxidations and reductions are 1.76 V and 2.72 V. These features are superior to those of the conventional all-vanadium redox flow battery using vanadium cations (V^{2+}, V^{3+}, V^{4+} and V^{5+}) since the discharged forms of the electrolytes consist of

V^{3+} and V^{4+} species in the negative and positive electrode compartments, respectively [1-7].

Based on the aforementioned properties, the theoretical energy density of the resulting system is 120 W h mol^{-1}, which is significantly higher than that of all-vanadium electrolytes (34 W h mol^{-1}) [181]. The main drawback of using DB-134 is the limited solubilities in various non-aqueous electrolytes (<10 mmol dm^{-3} in pure acetonitrile). However, a mixture of acetonitrile and toluene can lead to a solubility as high as 100 mmol dm^{-3}. Charge-discharge of a battery was carried out in a static glass cell (H-cell) with agitation at 0.66 mA cm^{-2} (2 mA ÷ 3 cm^2) in an electrolyte containing 3:2 acetronitrile:toluene. The two compartments were separated by a medium porosity glass frit and the electrodes were porous reticulated vitreous carbon. A few cycles were obtained by cycling between 0 and 3 V with charge and discharge voltages of *ca.* 2.3 V and *ca.* 1.3 V, respectively. The coulombic and energy efficiencies need to be further improved (*ca.* 80% and *ca.* 40%, respectively) with the use of optimized cell designs (reduced inter-electrode gap and low resistance separator) [181]. In order to achieve an energy density comparable to existing aqueous systems (40 W h dm^{-3}), the solubilities of the anthraquinone derivatives need to be increased by an order of magnitude.

4.1.8. Symmetric PTIO redox flow battery

In addition to the symmetric diaminoanthraquinone redox flow battery discussed in Section 4.1.7 [181], another symmetric system has been proposed by Duan and co-workers [191]. The proposed system uses 2-phenyl-4,4,5,5-tetramethylimidazoline-1-oxyl-3-oxide (PTIO) as the starting molecule for both the negative and positive electrode reactions. PTIO is a nitronyl nitroxide molecule that has a solubilility of up to 2.6 mol

dm^{-3} in acetonitrile. It has been used in several applications, including batteries, memory devices and molecular magnets [208-211]. During the charging process, the PTIO molecule is reduced and oxidized by one electron to form $PTIO^-$ and $PTIO^+$ species in the negative and positive half-cells, respectively. The reverse reactions take place during the discharge process as follows [191]:

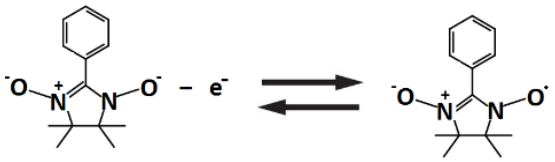

E^o = *ca.* –1.27 V *vs.* Ag

(51)

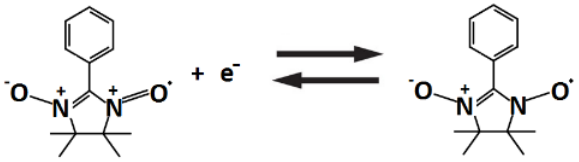

E^o = *ca.* +0.46 V *vs.* Ag

(52)

As suggested by voltammetric studies, both the negative and positive electrode reactions are highly reversible in the electrolytes containing 1.0 mol dm^{-3} tetrabutylammonium hexafluorophosphate in acetonitrile. The voltammograms almost completely overlapped in the first 500 cycles. The active species involved in both electrodes (PTIO, $PTIO^-$ and $PTIO^+$) occur at the same N-O bond. In the case of crossover of the species across the separator, the reaction between $PTIO^-$ and $PTIO^+$ regenerates the original PTIO as confirmed by ESR. Charge-discharge cycling of the battery was conducted in a parallel flow cell at 20 mA cm^{-2} between 0.9 V and 2.1 V for more than 15 cycles using a Daramic microporous separator. Fourier transform infrared spectroscopy (FTIR) was used to determine the state-of-charge of the system (cross-validated with ESR microscopy) [191].

In the case of 0.1 mol dm^{-3}, the average coulombic and energy efficiencies were 96% and 72%, respectively. These efficiencies were higher than those at 0.5 mol dm^{-3}, in which the average coulombic and energy efficiencies were 90% and 60%, respectively. The lower coulombic efficiency at a higher concentration was attributed to the increased crossover during longer charge-discharge times, while the lower voltage efficiency was attributed to the lower ionic conductivity as a result of an increased viscosity. The resulting system at 0.5 mol dm^{-3} had an energy density of 5.0 W h dm^{-3}, which is 43% of the theoretical value (11.6 W h dm^{-3}) [191].

4.2. Polymer organic flow batteries

Polymerized organic active materials involving radicals were introduced following the recent developments in non-aqueous systems. Prior to these developments, radical polymers has been used in other energy storage systems (lithium-organic radical batteries) [36-38] and exhibited attractive electrochemical properties, including high charge-discharge rates at 120 C, e.g.. a full charge-discharge cycle in 30 s, a high capacity (> 140 mA h g^{-1}), and a long cycle life (> 10,000 cycles) [44]. Unlike redox flow batteries, these systems used radical polymers as solid electrodes and swell in the electrolytes to allow redox reactions to take place. For flow battery applications, a first attempt was made to evaluate TEMPO-crowded bottlebrush polymers for the half-cell reactions [212], synthesized through anionic polymerization and ring-opening metathesis polymerization; the system had a plateau cell voltage at 1.0 V *vs.* Ag (in ethylene carbonate/ diethyl carbonate) in a charge-discharge cycling test at a 1 C rate. Other polymerized systems were also based on common stable radicals, such as TEMPO and thiophene [73, 183, 192]. The main challenges in relation to these systems are the high electrolyte viscosities

due to the high molecular masses. The agglomerated particles and conjugated polymers may partially clog the flow channels in the stack, which leads to an unstable cell voltage.

4.2.1. Symmetric polythiophene redox flow battery

Following naturally from the use of polymeric TEMPO in non-aqueous electrolytes, Oh and co-workers [183] investigated polythiophene as the redox couple. Polythiophenes are polymerized thiophene, whose radical-bearing monomers (thiophenes) were proposed after the high-throughput computational screening of Cheng *et al.* [45]. These polymers can become conducting when electron(s) are added or removed from the conjugated π-orbitals via n- and p- dopings. In the conductive polymers, each thiophene repeating unit can accommodate or lose electron(s) at electrode potentials of *ca.* –2.0 V *vs.* Ag and *ca.* +0.45 V *vs.* Ag, respectively. The theoretical specific charge capacity of these materials can reach 319 mA h g^{-1}. The redox reactions are as follows:

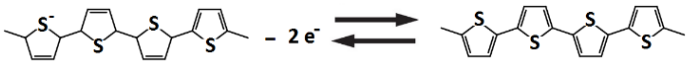

E^o = *ca.*–2.00 V *vs.* Ag

(53)

E^o = *ca.* +0.45 V *vs.* Ag

(54)

Polythiophene can be synthesised by both electrochemical and chemical polymerization. It was found that polythiophene prepared by the electrochemical approach has a lower overpotential and a higher peak current in typical cyclic voltammograms, attributed to the better contact between the particles and the current collector surface. The current densities for both n- and p- doping polymers increased with the thickness of the layer. However,

when the thickness is higher than 500 μm, drastic decreases in current density were observed. These polymers were used as a form of microparticles and acted as initial active species for both the negative and positive electrode reactions. The charge-discharge cycling performance of this chemistry was further tested in both static and flow cells. In the flow cell, carbon felts electrodes were eliminated to prevent interruption of the electrolyte flow. A Fumasep® anion-exchange membrane used as the separator suffered from negligible crossover of polythiophene over 20 h. Electrolytes consisted of 8.41 g dm^{-3} polythiophene, 2 g dm^{-3} of Ketjen black EC600JD in 1.0 mol dm^{-3} tetraethylammonium tetrafluoroborate and propylene carbonate.

The battery was charged to 3.0 V and then discharged to 1.0 V at current densities of 1.0, 0.5 and 0.2 mA cm^{-2} [183]. As shown in Figure 7a), the charge-discharge cycling of this battery was performed for the first eight cycles at 0.5 mA cm^{-2}, utilizing 34.5% of the theoretical capacity. The low utilization can be explained by the low polythiophene conductivities, which are in the range 10^{-10} to 10^{-5} S cm^{-1} in their discharged states (compared up to 1 to 10^{4} S cm^{-1} in charged states through n-doping or p-doping) [213]. This further hinders the discharge reactions of the interior particles; thickness is especially a limiting factor, as determined in the voltammetric studies. The average coulombic and energy efficiencies were *ca.* 77.5% and 60.9%, respectively, with a capacity retention of *ca.* 100 %. Figure 7b) shows the efficiencies of this battery at current densities between 1.0 and 0.2 mA cm^{-2}. Although no carbon felt was used, the voltage efficiencies remained relatively high (>75%) over this range of current densities, while higher coulombic efficiencies were observed at higher current densities due to reduced crossover rates of active species in the shorter charge-discharge cycles [183]. Future improvement in terms of utilization of active materials can be made with the use of nano-particles rather than microparticles as used in this work.

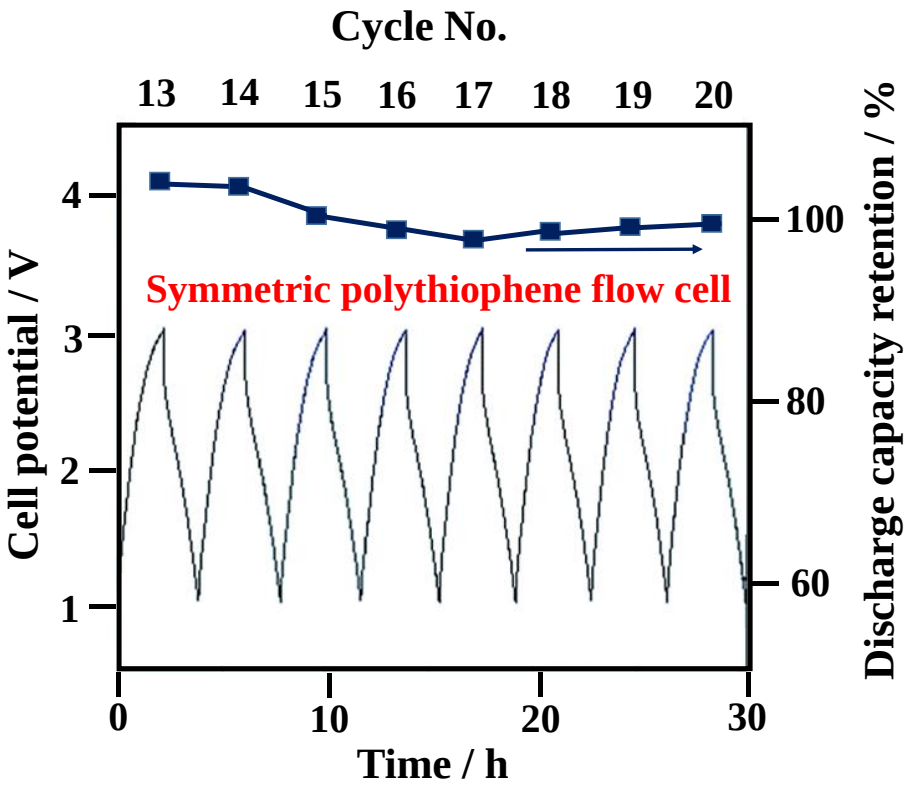
Cycle No.
13 14 15 16 17 18 19 20
Symmetric polythiophene flow cell
Cell potential / V
Discharge capacity retention / %
Time / h
0 10 20 30
1 2 3 4
60 80 100

Figure 7a

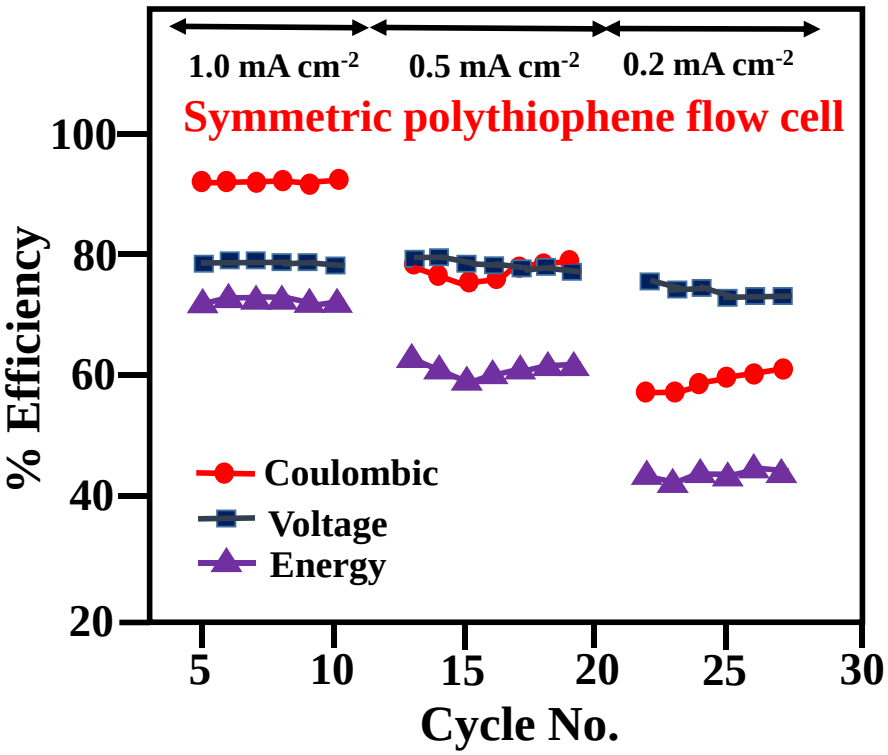
1.0 mA cm-2
0.5 mA cm-2
0.2 mA cm-2
Symmetric polythiophene flow cell
% Efficiency
Cycle No.
Coulombic
Voltage
Energy
20 40 60 80 100
5 10 15 20 25 30

Figure 7b

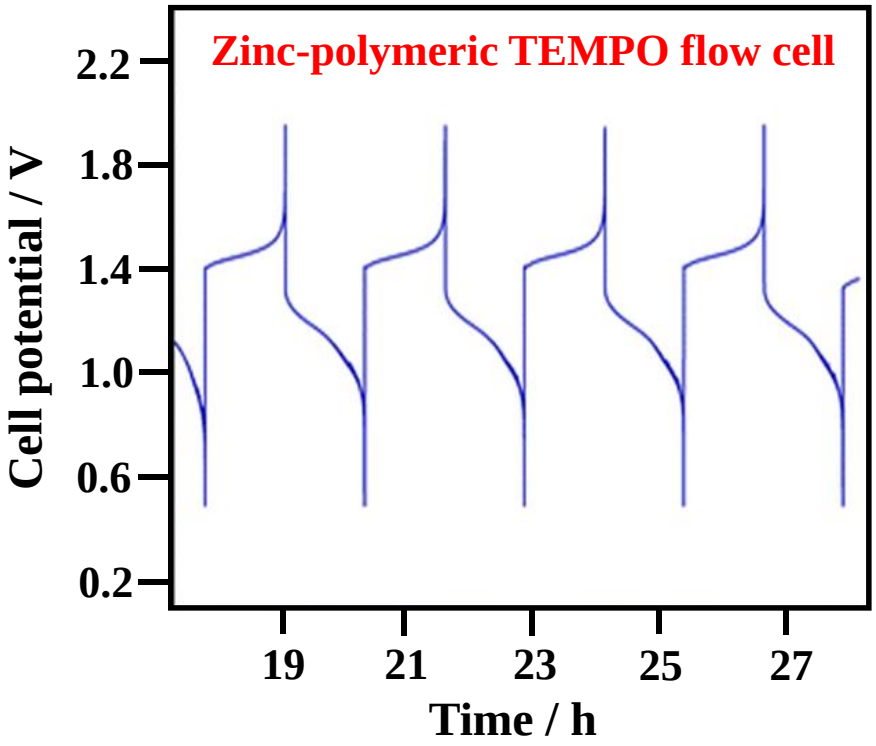

Figure 7c

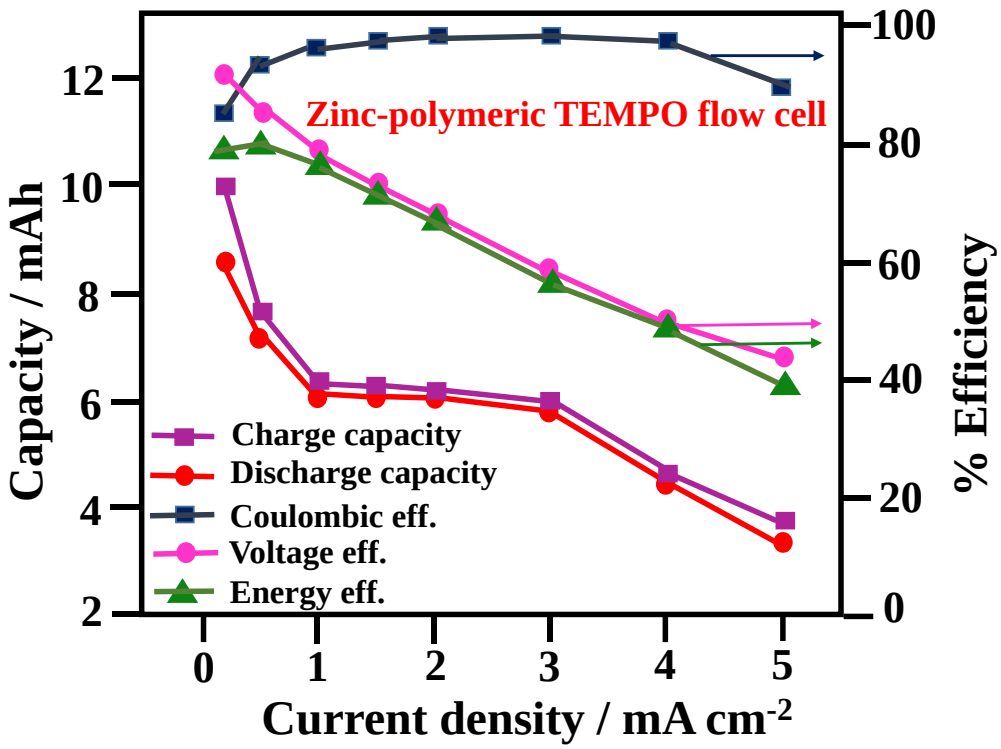
Zinc-polymeric TEMPO flow cell
Charge capacity
Discharge capacity
Coulombic eff.
Voltage eff.
Energy eff.
Capacity / mAh
% Efficiency
Current density / mA cm-2
0
1
2
3
4
5
2
4
6
8
10
12
0
20
40
60
80
100

Figure 7d

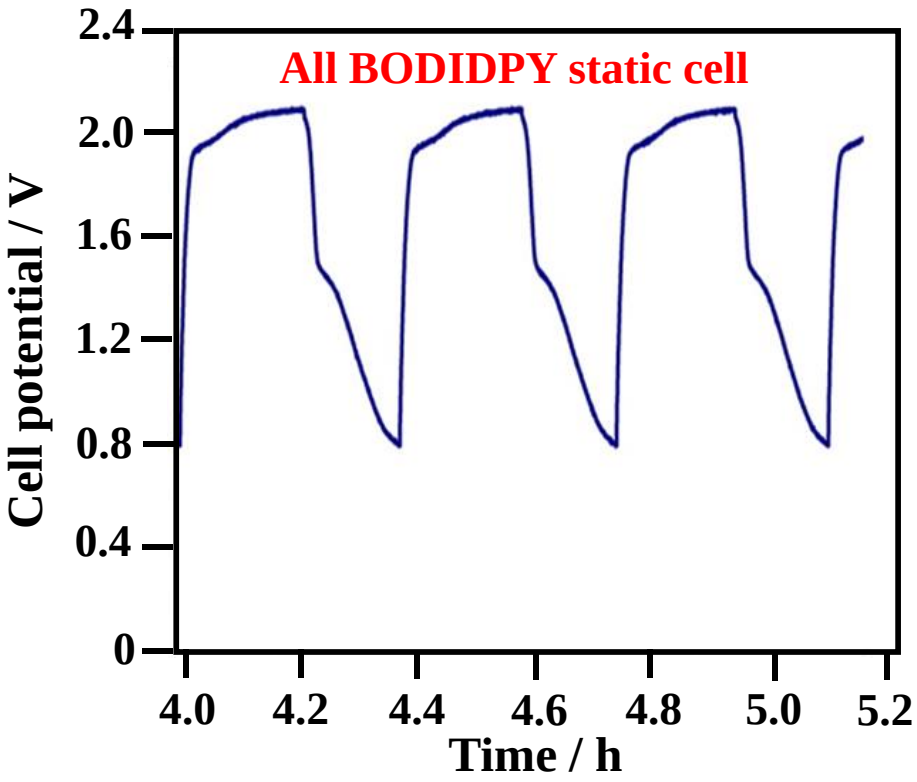
All BODIDPY static cell
Cell potential / V
2.4
2.0
1.6
1.2
0.8
0.4
0
4.0
4.2
4.4
4.6
4.8
5.0
5.2
Time / h

Figure 7e

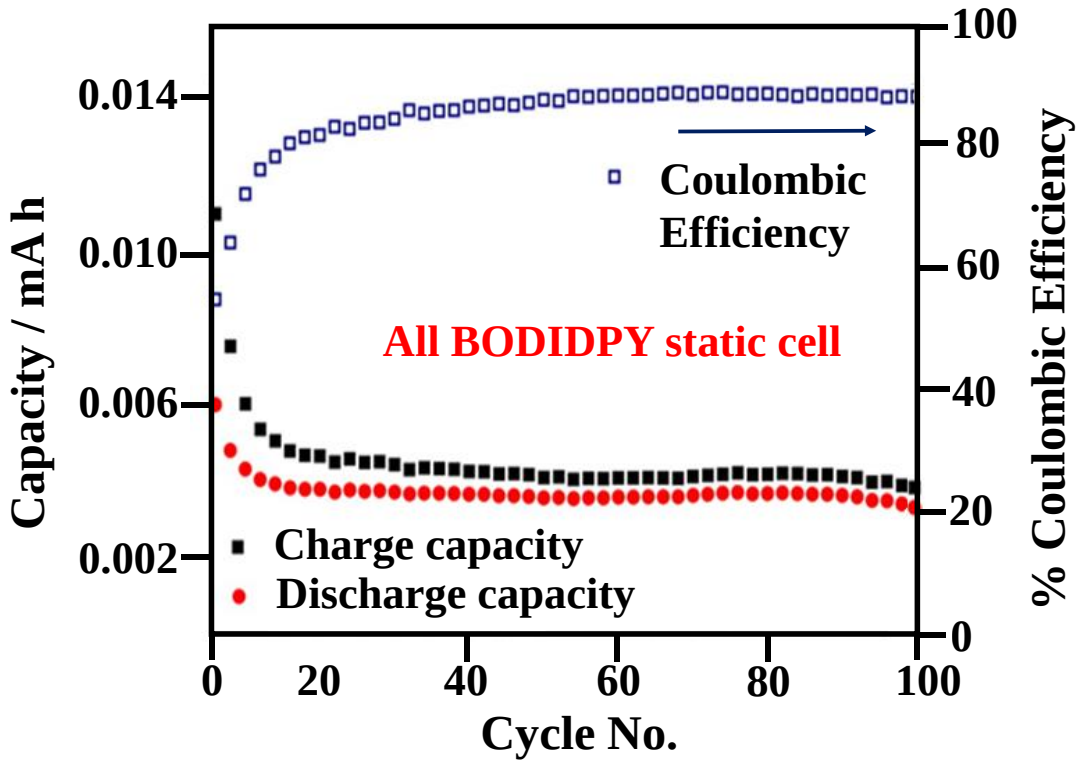

Figure 7f

Figure 7. Charge-discharge cycling performance of several types non-aqueous organic-based flow battery chemistries (flow & static): (1) symmetric polythiophene redox flow battery: (a) charge-discharge cycling profile at 0.5 mA cm^{-2}; (b) system efficiencies at different current densities; (2) zinc-polymeric TEMPO hybrid flow battery: (c) charge-discharge cycling profile at 1 mA cm^{-2}; (d) capacities and system efficiencies at different current densities; (3) all-poly(boron-dipyrromethene) static battery: (e) charge-discharge cycling profiles (cycles 13 to 15) at *c.a.* 0.1 mA cm^{-2}; (f) capacities and coulombic efficiencies over 100 cycles.

4.2.2. Zinc-polymeric TEMPO hybrid flow battery

Polymeric TEMPO has been introduced as the positive active species in both aqueous [71] and non-aqueous systems [212] by virtue of its high electrode potential (*ca.* + 0.4 V *vs.* Ag in carbonate electrolytes) and chemical stability in radical form. The same group [73] proposed aqueous polymer-based viologen-TEMPO and redox flow batteries, introducing a hybrid system using inexpensive zinc metal at the negative electrode, coupled with a polymeric TEMPO reaction at the positive electrode. During the charging process, metallic zinc is deposited on the negative electrode, while the TEMPO molecule is oxidized and forms an oxammonium cation ($TEMPO^+$) in the positive electrode reaction. Reverse reactions take place during discharge as follows [73]:

$$Zn - 2\ e^- \leftrightarrow Zn^{2+} \qquad E^o = \ ca.\ -1.1\ V\ vs.\ Ag \qquad (55)$$

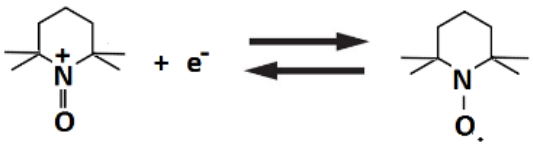

$$E^o = \ ca.\ +0.40\ V\ vs.\ Ag \qquad (56)$$

Rather than using regular, linear polymers, the resulting system used specially shaped polymers with dendrimeric or miscellar structures to minimize the viscosity of the electrolytes. Well-defined TEMPO-methacrylate/styrene block copolymers (PTMA-*b*-PS) were self-assembled into these miscellar structures in the organic carbonate-based electrolytes. Due to the fact that radical polymerization of TEMPO-methacrylate cannot be performed, 2,2,6,6-tetraethyl-4-piperidyl methacrylate (TEMPMA) is polymerised as a precursor and then oxidized to the TEMPO free-radical [214, 215]. $PTMA_{63}$-*b*-PS_{35} was used for all tests, the number in the subscript refers to the average degree of polymerization of the respective block and was determined *via* proton nuclear NMR prior

to the oxidation leading to the TEMPO free-radical. The resulting copolymer ($PTMA_{63}$-*b*-PS_{35}) contains a nonpolar styrene block and a polar TEMPO block, which allow the copolymer to aggregate into miscellar structures when dissolved in a mixture of ethylene carbonate, dimethyl carbonate and diethyl carbonate (1:1:1 volumetric ratio). The resulting miscelles feature a polystyrene (PS) core and a poly-TEMPO-methacrylate (PMA) corona. Transmission electron microscopy (TEM) imaging revealed the presence of a large number of miscelles with a diameter in the range of 50 and 75 nm, and agglomerates of *ca.* 300 nm in size [73].

A charge-discharge experiment was carried out in a flow cell using zinc foil and carbon felt (or paper) as the negative and positive electrode, respectively. The negative electrolyte was a solution containing 0.5 mol dm^{-3} zinc perchlorate in a mixture of organic carbonate electrolytes (1:1:1 volumetric ratio of EC:DMC:DEC), while the positive electrolyte contained the block copolymer miscelles with a maximum concentration of 13 mg cm^{-3} in a solution having the same composition as that of the negative electrolyte. As shown in Figure 7c) stable charge-discharge cycling was performed in a voltage range between 0.5 V and 2.0 V. At 1 mA cm^{-2}, a voltage drop of 280 mV was observed between the charge and discharge plateaux. The resulting voltage efficiencies (*ca.* 80%) decreased linearly with increasing current density (i.e. *ca.* 42% at 5 mA cm^{-2}). However, the coulombic efficiencies were above 90% over a wide range of current densities (0.5 – 5.0 mA cm^{-2}) with a maximum of 98% at 2 mA cm^{-2} (Figure 7d)), A maximum discharge capacity of 8.7 mA h was obtained at 0.2 mA cm^{-2}, corresponding to a material utilization of 93%, while a constant charge capacity of 6.1 mA h was obtained in the current density range 1 to 3 mA cm^{-2} [73].

4.2.3. All-poly(boron-dipyrromethene) redox flow battery (asymmetric)

In addition to the radical molecules (e.g., TEMPO and thiophene) used in non-aqueous redox flow batteries, the same research group [192] proposed the use of boron-dipyrromethenes (BODIDPYs)-containing polymers as both the negative and positive active species. The proposed materials are non-conjugated polymers that aim to avoid the typical challenges of polymeric systems: (1) blockage of flow channels and (2) unstable cell voltages. These materials, which are typically used as laser and fluorescent dyes [216-218], are suitable for redox flow battery applications due to the high degree of reversibility of their redox reactions [219]. The potential gap between the oxidized and reduced species as well as their electrochemical properties can be adjusted by the choice of the substituents decorating the molecular core [220, 221]. The boron-dipyrromethenes containing polymers were synthesized from a sequence of procedures with the use of styrene-based, alkyl-functionalized derivatives as monomers. The monomer was then copolymerized with solubility enhancing comonomers by free radical polymerization procedures and initiated by 2, 2'-azo-bis-(2-methylpropionitrile) (AIBN). The resulting polymers (BODIPY-*co*-TASt and BODIPY-*co*-TEGSt) synthesized from (vinylbenzyl)trimethylammonium perchlorate (TASt) and (vinylbenzyl)-triethylene glycol monomethyl ether (TEGSt) were used as the negative and positive electrode active materials, respectively.

These polymers were used as the starting molecules for the all-organic redox flow battery, which were then reduced or oxidized in the charging process in the negative and positive half-cells, respectively. The reverse reactions take place in the discharge process as follows [192]:

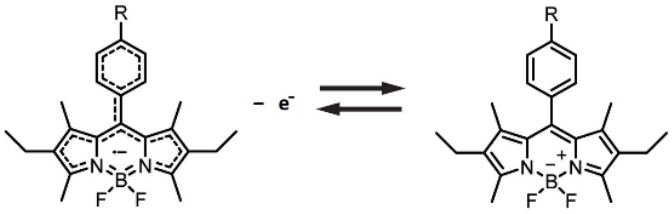

E^o = *ca.* –1.51 V *vs.* Ag

(57)

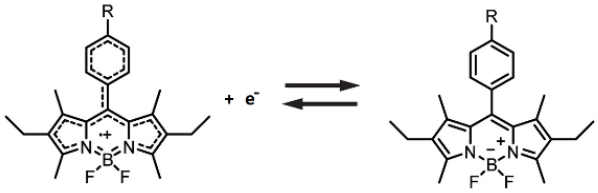

E^o = *ca.* +0.69 V *vs.* Ag

(58)

As suggested by cyclic voltammetry, reversible reactions were observed at –1.51 and +0.69 V *vs.* Ag, respectively. The peak separations were less than 100 mV for both reactions, indicating relatively reversible processes. The charge-discharge performance of this battery was evaluated in a static cell, in which carbon felts were used as the electrodes, together with a size-exclusion membrane with a molecular weight cut-off (MWCO) of 1,000 g mol^{-1}. The electrolytes were prepared with 13 mg cm^{-3} of active polymer with 0.5 mol dm^{-3} tetrabutylammonium perchlorate in propylene carbonate. These polymers were first dialyzed to remove the oligomeric species. As shown in Figure 7e), the resulting system exhibited flat charging plateaus at 2.06 V and a mean discharge voltage of 1.28 V at 0.1 mA cm^{-2}. The average coulombic and energy efficiencies were 89% and 55%, respectively (Figure 7f)). Prolonged cycling led to a discharge capacity fade of 30% in the first 10 cycles, followed by a stable period over the next 90 cycles with steady capacity retention. Further studies should include the development of bipolar copolymers and the utilization of flowing electrolytes to improve electrolyte solubility and overall cell performance [192].

4.3. Lithium-organic hybrid flow batteries

The lithium based redox flow battery is a fast growing technology that combines the advantages of both the redox flow battery and the lithium-ion battery. This type of battery uses electronegative lithium at the negative electrode, while liquid phase redox reactions of active molecules are used for the positive electrode reaction. Some systems also use semi-solid inorganic suspensions containing ion-strong insertion 'flowable electrode materials'. The solid nature of the suspending flowable electrode materials result in an increase in the energy density per electrolyte [56, 61, 171]. In addition to semi-solid suspensions, organometallic or inorganic materials have recently been used in redox-mediated reactions, initially introduced for lithium-based redox flow batteries and subsequently extended to a number of other chemistries (e.g.,. lithium-ion, lithium-sulphur and lithium-air) by different research groups. Many of these systems have been reviewed by Zhao *et al.* [61] and Wang *et al.*. [63].

Lithium-organic hybrid flow batteries									
Chemistries	**Negative active material (at disch. state)**	**Positive active material (at disch. state)**	**Electrolyte & flowing condition**	**Cell components**	**Exp. OCV / V**	**System Efficiencies / %**	**Energy density / W h dm^{-3}**	**No. of cycles**	**Year [Ref]**
Lithium/ dipropoxy-benzoquinone	Li	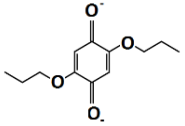	1 M $LiClO_4$ in γ-butyrolactone; 0.01 M positive active material; static	Li foil and carbon paper; LiCGC glsss ceramic	2.8 – 3.0	NG	NG	25	2011 [222]
Lithium/ MEAQ	Li	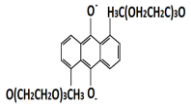	1.0 M $LiPF_6$ in propylene carbonate; 0.25 M positive active material; flowing	Li foil and carbon felt; Celgard 3401	> 2.4	Energy: 82 (0.1 mA cm^{-2})	25	9	2012 [74]
Lithium/ modified DBBB	Li	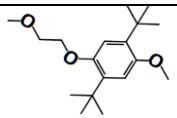	1.0 M $LiBF_4$ in propylene carbonate; 1 mM positive active material; static	Li metal strip and reticulated vitreous carbon; porous glass frit	> 3.9	Energy: 75 (> 0.1 mA cm^{-2})	NG	30	2012 [78]
Lithium/ TEMPO	Li	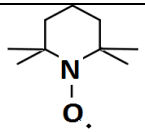	1.0M $LiPF_6$ in EC/PC/EM with 15 % wt. FEC; 0.8 – 2 M active material; flowing	Li foil and carbon felt; polyethylene-based porous separatpr	3.2 – 3.5	Coul.: 84 - 91 Energy: 68 - 76 (1.0 - 5.0 mA cm^{-2})	64 – 126	100	2014 [223]

Lithium/ MeO-TEMPO	Li	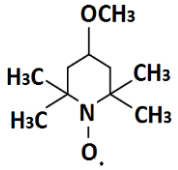	1M LiTFSI in propylene carbonate; 1:1 molar ratio of MeO-TEMPO and LiTFSI with 17% wt. water; flowing	Li foil and carbon felt or paper; LiCGC glsss ceramic	> 3.3	Coul.: > 90 Energy: > 80 (0.1 mA cm^{-2})	200 (static)	20 (static)	2015 [60]

Table 7. Operational parameters and performance of lithium-based organic redox flow battery systems in non-aqueous electrolytes.

Due to the electronegative nature of lithium metal (–3.0 V *vs.* SHE), most systems have cell voltages of > 2.0 V in non-aqueous electrolytes. In these lithium-organic hybrid flow batteries, the positive electrode species are usually based on those with high concentrations and high redox potentials (those previously used in other organic-based systems (Sections 3 and 4). Figure 1a) shows an electrode assembly for this type of flow battery. Without the use of a lithium anode, most of the non-aqueous systems cannot reach the energy densities of aqueous redox flow battery systems (Figure 1b)). In practice, most of those non-aqueous systems have active material concentrations of less than 0.1 mol dm^{-3}, which corresponds to an energy density of less than 10 W h dm^{-3}, even at a high cell voltage [223]. The current densities used in such systems are relatively low (0.5 mA cm^{-2}), with limited cycling performance [180, 188, 190]. The introduction of lithium-organic hybrid flow battery systems can be traced back to the work of Senoh *et al.* in 2011 [222] based on the two-electron reactions of 1,4-benzoquinone and its derivatives for lithium secondary batteries. The reaction mechanisms in non-aqueous media are similar to those of anthraquinone [181, 182], as described in Section 4.1.7. and in the literature [224]:

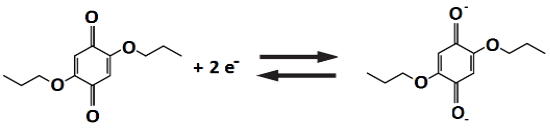

E^o = *ca.* 2.5 to 2.8 V *vs.* Li (59)

The proposed work used a static two-compartment cell containing carbon paper electrodes and a ceramic solid-state electrolyte separator. Peripheral substituents, such as ethoxy and propoxy, were introduced into the benzoquinone molecules to prevent the sublimation of benzoquinone [225], instability of radical anions [226] and low reactivity of the reduction products [227]. The main drawback is the drastic reduction in solubilities

in the corresponding butyrolactone electrolyte (<0.3 mol dm^{-3} compared to 2.6 mol dm^{-3} of unmodified benzoquinone). With a ceramic solid electrolyte separator, improvements in charge capacity were observed. At 50 µA cm^{-2}, the capacity retention against the maximum discharge capacity was over 98% for the two modified benzoquinone species over 25 cycles [222].

Wang and co-workers [74] proposed a lithium-organic hybrid flow battery using modified anthraquinone, 1,5-bis(2-(2-(2-methoxyethoxy)ethoxy)ethoxy)anthracene-9,10-dione (MEAQ). In general, unmodified anthraquinone molecules have very low solubilities (<0.10 mol dm^{-3}) in various electrolytes. The introduction of two triethylene glycol monomethyl ether groups into the anthraquinone molecules improved the solubility (>0.25 mol dm^{-3}) in non-aqueous electrolytes. The redox potential of the modified molecule is similar to that of the aforementioned benzoquinone compounds, with the following discharge reaction [74]:

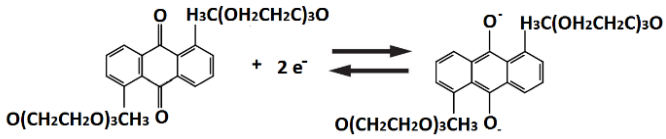

E^o = *ca.* 2.2 to 2.7 V *vs.* Li (60)

The battery was cycled in a static cell with unspecified configuration at 0.1 mA cm^{-2} between 1.8 and 2.8 V for 8 cycles. The electrolytes contained 0.25 mol dm^{-3} active species with 1.0 mol dm^{-3} lithium hexafluorophosphate in propylene carbonate electrolytes. The charge and discharge voltage plateaux were located at *ca.* 2.45 V and *ca.* 2.4 V, respectively, an an energy efficiency of 82% was recorded. Based on the volume of the positive electrolyte, the energy density was *ca.* 25 W h dm^{-3}, higher than that of many previous systems without lithium anodes [74].

In addition, modified DBBB derivatives were proposed by Huang and co-workers [78] for use as positive active species, coupled with a lithium negative electrode. These materials are attractive in terms of electrode potential (4.0 V *vs.* Li), chemical stability and reversibility. In carbonate electrolytes, the solubility of DBBB is *ca.* 0.4 mol dm^{-3}, which needs to be further improved, together with the electrochemical stability. The symmetric aromatic backbone of DBBB is important to maintaining the electrochemical behaviour and chemical stability [228, 229]. The redox centre symmetricity of the DBBB molecule needs to be maintained, while incorporating polyethylene oxide (PEO) to improve the solubility in carbonated-based polar electrolyte solutions. The DBBB molecule with one PEO chain to the redox centre has the same voltammetric performance as its unmodified counterpart without significant changes in molecular weight, diffusion coefficient and viscosity. This molecule was then used as the positive active species in the lithium-organic hybrid flow battery:

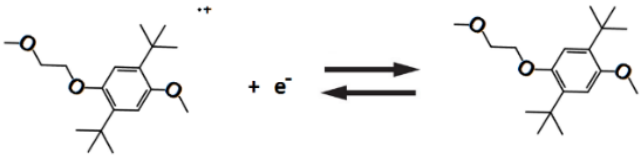

E^o = *ca.* 4.0 V *vs.* Li ((61)

Charge-discharge cycling was carried out in a three-electrode bulk electrolysis cell. Reticulated vitreous carbon was used as the working electrode, and lithium metal strips enclosed in glass tubes with porous glass or ceramic frits were used as reference and counter electrodes. The cell was charge-discharge cycled at 0.4 mA for 30 cycles from 3.8 V to 4.1 V *vs.* Li under agitation at 700 rpm. The electrolyte was 1 mmol dm^{-3} active species with 0.5 mol dm^{-3} lithium hexafluorophosphate salts in propylene carbonate. The average charge and discharge voltage plateaux were *ca.* 4.05 V and *ca.* 3.9 V *vs.* Li, respectively, suggesting reversible reduction of the radical cation. The energy efficiencies

increased from 36.5% in the first cycle to *ca.* 80.9% in subsequent cycles. The inefficiency of the first cycle could be related to the formation of a solid electrolyte interface (SEI), as observed in most lithium batteries [78].

A similar strategy was adopted by Wei and co-workers [223] in their lithium-TEMPO battery. Despite a single electron transfer, the proposed system has a high concentration of active species (2.0 mol dm^{-3}) resulting in a theoretical energy density of 188 W h dm^{-3}. The discharge reaction of TEMPO is similar to those in all-organic redox flow batteries and can be expressed as:

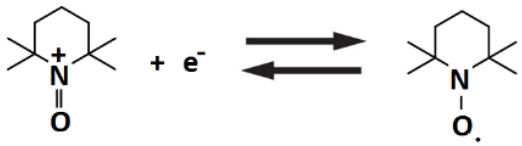

E^o = *ca.* +3.5 V *vs.* Li (62)

Again, in spite of the single electron transfer, the resulting system performance exceeded that of the others in terms of concentration (2.0 mol dm^{-3}) and voltage (3.5 V) in propylene/ethylene/diethyl carbonate electrolytes. Unlike the previous lithium-organic hybrid systems, a fluoroethylene carbonate additive was added to synergistically protect the lithium-metal electrode [97]. The battery was charge-discharge cycled in a flow cell, which comprised a graphite felt as the positive electrode and a polyethylene-based porous separator. The electrolyte contained up to 2.0 mol dm^{-3} of TEMPO and the battery was charge-discharge cycled at low current density (1.0 mA cm^{-2}) due to the high viscosities of the electrolytes. In such an extreme case, the coulombic and energy efficiencies were 84% and 69%, respectively. The energy density was 126 W h dm^{-3}, which is 67 % of the theoretical value of 188 W h dm^{-3} [223].

In the context of lithium-TEMPO redox chemistries, Takechi and co-workers [60] introduced ionic liquids to reach even higher energy densities (200 W h dm^{-3}). Rather than using unmodified TEMPO, methoxy-TEMPO (MeO-TEMPO) was mixed with lithium trifluoromethane (LiTFSI) salt to liquefy the active species. The redox potential of the resulting methoxy-TEMPO was *ca.* 3.6 V vs. Li with a discharge reaction [60]:

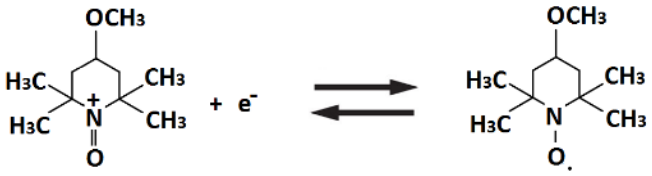

E^o = *ca.* +3.6 V *vs.* Li (63)

At a 1:1 molar ratio of MeO-TEMPO and LiTFSI, the mixture exhibited a self-melting behavior and formed a viscous liquid. By adding 17% wt. water, a highly concentrated (> 2.0 mol dm^{-3}) and less viscous electrolyte with an orange colour was prepared. The phase diagram suggests the appropriate compositions and temperature range to prepare such a liquid and the potential of these active species for applications over a wide range of temperature. The battery was charge-discharge cycled for more than 20 cycles in a flow cell. Carbon papers were used as the active electrodes and a ceramic solid-state separator was used to separate the negative and positive electrolytes. The battery was charge-discharge cycled at 0.1 mA cm^{-2} (1 mA ÷ 9 cm^2) for 2 h for several electrolyte flow rates (5, 2, 1 cm^{-3} min^{-1}). The coulombic and energy efficiencies were higher than 90% and 80%, respectively. Even in a static cell, the energy density was as high as 200 W h dm^{-3}, with a capacity retention of *ca.* 84% after 20 cycles. This value is among one of the highest of organic-based redox flow batteries. The main challenge of this system remains the safety of using metallic lithium, which may be addressed with proper design of the cell architecture and more durable (possibly inorganic) separators between the two electrode compartments [60].

5. Conclusions and future outlook

A number of organic-based flow battery systems have been proposed using aqueous and non-aqueous chemistries in different configurations. These systems would benefit from tailored molecules with low equivalent weights, fast kinetics and a wide window of chemical stability (apart from large corresponding cell voltages). For aqueous systems, the concentration of the organic species used in the reported systems remains relatively low (< 1 mol dm^{-3}, Tables 3 & 4). An open challenge is to obtain high solubility and cell voltage simultaneously to obtain reasonable energy densities comparable to conventional redox flow battery systems. In contrast, non-aqueous systems often suffer from high electrolyte/separator resistances, low utilization, chemical instability and crossover of the active materials.

For extensive market penetration [30, 31], the capital cost should be less than USD$ 150 $(kW\ h)^{-1}$ by 2023. The target for the concentrations of active species should be 5 mol dm^{-3} and 2 mol dm^{-3} for non-aqueous and aqueous systems, respectively [41]. For aqueous systems, previous studies [59] suggests that a more ambitious cost target of USD$ 100 $(kW\ h)^{-1}$ can be achieved with the combination of USD$ 2 Kg^{-1} active material cost, 100 g mol^{-1} molar mass of active material, 0.5 Ω cm^2 area specific resistance of the battery and 0.79 V cell voltage. For non-aqueous systems, the cost is not particularly sensitive to the active material cost (future-state cost: *c.a.* USD$ 5 Kg^{-1}), since they often use expensive solvents (e.g. nitriles, glymes, and carbonates, up to USD$ 20 Kg^{-1}) and fluorinated salts (e.g. tetrafluoroborates, hexafluorophosphates and bis(tri-fluoromethylsulfonyl)imides, USD$ 2 Kg^{-1}). Therefore, increasing the cell voltage is the most effective approach to reduce the overall cost of non-aqueous batteries. It is possible

to achieve a cost target of USD$ 100 $(kW\ h)^{-1}$ with a combination of 100 $g\ mol^{-1}$ molar mass of active material, 2.5 $\Omega\ cm^2$ area specific resistance of the battery, 3.0 V cell voltage, a 0.2 salt ratio and a 3.3 $mol\ kg^{-1}$ active molarity [59].

For both systems [122, 148, 180, 202], the chemical stabilities of the active species and the charge-containing radicals are still the major challenges for long-term cycling and storage stability. Degradation of these active species, particularly radicals, are closely associated with the electrolytes and salts, which are considered as the main factors for inefficiencies and low utilization of active species in the electrolytes. It is important to identify the degradation mechanisms and to improve the chemical stability by tailoring the structures of the active molecules [202]. For non-aqueous chemistries, oxygen and water from ambient atmosphere have substantial impacts on overall performance. For instance, oxygen can passivate the electrode and water can deactivate redox pairs by forming oxo-metal compacts [43].

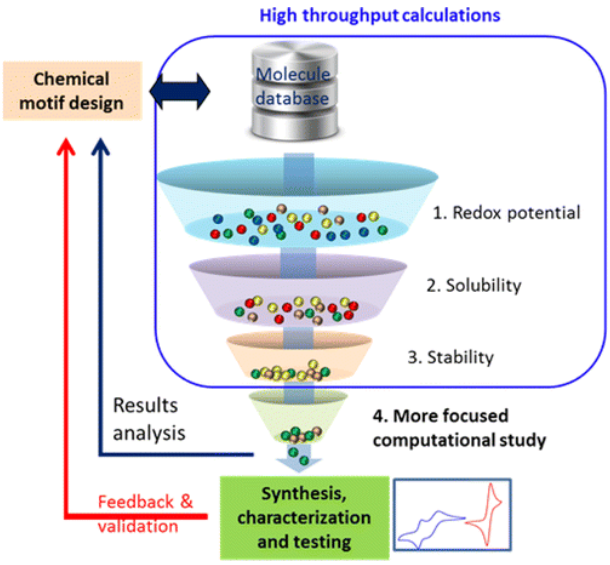

Figure 8a

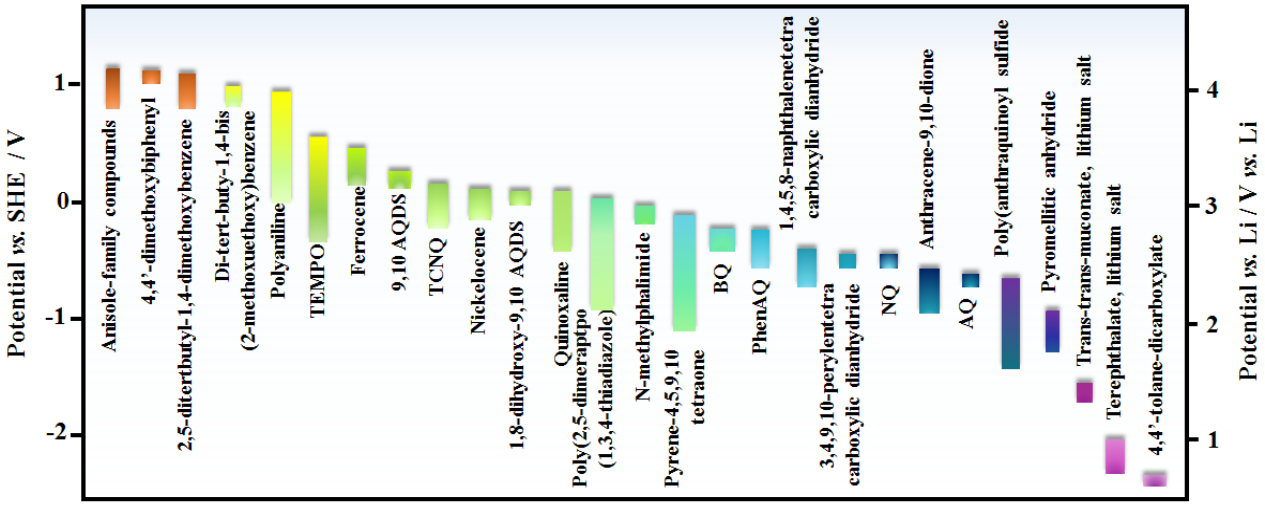

Figure 8b

Figure 8. High-throughput electrolyte screening using (a) a computational modelling using quantum chemical calculations of specific properties through down-selection of candidate molecules for electrical energy storage applications. (b) Redox potential of representative redox-active organic and organometallic compound candidates for non-aqueous redox flow batteries.

Considering that the electrochemical behavior of organic molecules are different from those of their metallic counterparts, development of specific cell components, i.e. electrodes and separators, are necessary to obtain competitive levels of performance. Most of the existing organic based flow batteries use conventional cell component materials, which require further optimization as well as fundamental characterization in terms of their interactions with the organic species. Furthermore, a number of non-aqueous systems have used static electrolyte cells to evaluate the charge-discharge cycling performance. As in the case of coin cells, some of these cells are ineffective at preventing the crossover of the negative and positive active species [180] and at utilizing fluid flow and mass transport to create a more favourable reaction environment.

It is also advisable to reduce the electrolyte resistance by advanced electrode design while controlling the crossover of active species across the separator. For instance, reducing the inter-electrode gap effectively reduces the electrolyte resistance within the electrode. Other strategies include further improvement of the mass transport of species to the electrodes and increased effective surface areas, which can be obtained by flowing electrolytes, implementing flow-through electrodes as well as engineering of the electrode structures. It is also important to reduce the membrane resistance in non-aqueous electrolytes through improving the ionic conductivity and reducing the membrane thickness, without compromising ionic selectivity and other important properties. For non-aqueous systems, it is possible to reduce the viscosity and ionic resistivity through a rational selection of electrolytes [191].

Over the following decades, suitable selections and modifications of organic molecules and the corresponding electrolytes will likely remain the ongoing focus. The properties and electrochemical behaviour of organic materials can be evaluated by mean of high-throughput screening using a modular robotic platform and computational screening to down-select candidate molecules (Figure 8a)) [45, 119, 173]. For non-aqueous systems, the selection of organic active species can be inspired from previous research on organic and lithium-ion batteries [56]. Based on previous research on organic batteries, the following radicals have been evaluated in electrochemical tests: spirobisnitroxide (*ca.* 0.8 V *vs.* Ag) [38], arylnitroxide (*ca.* 0.7 V *vs.* Ag) [230], nitronylnitroxyl (*ca.* 0.7 V *vs.* Ag upon oxidation, *ca.* −0.6 V *vs.* Ag upon reduction) [208], galvinoxyl (*ca.* 0.06 V *vs.* Ag) [231], and PROXYL (2,2,5,5-tetramethyl-2,5-dihydro-1*H*-pyrrol-1-oxyl-3-yl, *ca.* 0.5 V *vs.* Ag) [232].

As summarised in Figure 8b), a number of organic molecules has been proposed elsewhere [56] for lithium-based organic hybrid flow batteries. With recent advances made in computational modelling and synthetic techniques, organic redox flow batteries can eventually meet the proposed cost target of USD$150 (kW h) $^{-1}$ for practical applications at the grid scale and possibly in the automotive sector.

Tables

Parameters	Conventional all-vanadium RFB	Conventional lithium-ion batteries	Projected organic RFB*
Electron stoichiometry	1	< 1	2
Concentration	2 mol dm^{-3}	Nil	6 mol dm^{-3}
Cell potential	1.4 – 1.8 V	3.6 V	1.5 V
Energy efficiency	75 %	90 %	75 %
Charge capacity	54 A h dm^{-3}	70 A h dm^{-3}	320 A h dm^{-3}
Energy density	35 W h dm^{-3}	240 W h dm^{-3}	210 W h dm^{-3}
Specific energy	31 W h kg^{-1}	120 W h kg^{-1}	150 W h kg^{-1}

Table 1. Comparison of the projected organic redox flow battery characteristics with those of the conventional all-vanadium redox flow and lithium-ion batteries. *Assumed performance of projected organic flow battery system: 2-electron transfers, 1.5 V and 75% round trip energy efficiency.

Hydrogen density and Δ*G* dehydrogenation of linear and alicyclic polyolsas organic liquid carrier of hydrogen				
Hydrogenated form	**Dehydrogenated form**	**Hydrogen % wt.**	**Volumetric density / g dm^{-3}**	***ΔG* dehydrogenation / kcal mol^{-1} of hydrogen**
Decaline	Naphtalene	7.29	65.3	20.6
Dehydro-N-ethylcarbazole	N-Ethylcarbazole	5.83	64.2	16.2
2-Propanol	Acetone	3.35	26.4	13.9
2,3-Butanediol	Diacetyl	4.47	44.2	15.2
2,4-Pentanediol	Acetylacetone	3.87	37.2	14.2
2,5-Hexanediol	hexane-2,5-dione	3.41	33.1	12.8
3,5-Hexanediol	1- methylacetylacetone	3.41	33.1	14.9
3-Methyl-2.4-pentanediol	3-methylacetylacetone	3.41	n/a	13.1
5,5-Dimethyl-l,3-cyclohexanediol	Dimedone	2.8	n/a	13.9
1,3-Cyclohexanediol (trans)	1,3-cyclohexanedione	3.47	40.1	14.9
1,3-Cyclohexanediol (cis)	1,3- cyclohexanedione	3.47	40.1	14.9
1,4-Cyclohexanediol trans (quinitol)	1,4-cyclohexanedione	3.47	40.6	15.8
1,4-Cyclohexanediol (cis)	1,4-cycloheXanedione	3.47	40.6	15.6
Heptane-2,4,6-triol	heptane-2,4,6-trione (diacetylacetone)	4.08	45.8	13.9
3,5-Dimethyl-2,4,6-heptanetriol	3,5-dimethyl-2,4,6-heptanetrione	3.43	n/a	14.6
Nonane-2,5,8-triol	nonane-2,5,8-trione	3.43	n/a	12.9
3-Ethylhydroxypentane-2,5-diol	Triacetylmethane	4.08	n/a	13.6
9,10-DihydroXy-9,10-dihydroanthracene	Anthraquinone	1.98	n/a	5.2
Hydrogen density and Δ*G* dehydrogenation of heterocyclic polyols as an organic liquid carrier of hydrogen				
3-Methyltetrahydrofuran-2,5-diol	3-Methylfuran-2,5-dione	5.12	n/a	-14.8
3,4-Di-methyltetrahydrofuran-2,5-diol	3,4-Dimethylfuran-2,5-dione	4.58	n/a	-12.4

Pyranol-2,4,6-triol	Pyranol-2,4,6-trione	4.51	68.1	-10.8
3,5-Dimethylpyranol-2,4,6-triol	3,5-Dimethylpyranol-2,4,6-trione	3.78	n/a	-10.5
Thiotetrahydrofuran-2,5- dial	Thiofuran-2,5-dione	5.04	n/a	-17.2
Perhydropyromellitic dianhydride	Pyromellitic dianhydride	6.08	n/a	-12.0
1,4-Dioxane-2,3,5-triol	1,4-Dioxane-2,3,5- trione	4.44	76.0	-10.8
1,4-Dioxane-2,3,5,6-tetrol	1,4-Dioxane-2,3,5,6-tetrone	5.30	n/a	-12.9
Hydrogen Density and ΔG dehydrogenation of amino alcohols as organic liquid carrier of hydrogen				
1,1'-Iminobisethanol	N-Acetylacetarnide	5.23	n/a	5.0
1-(1-Hydroxyethyl-methyl-amino)ethanol	N-Methyl-N-acetylacetarnide	4.42	46.2	5.8
1,2-Diarninoethane-1,2-diol	Oxarnide	4.47	63.7	-4.9
1,3-Diarninopropane-1,3- diol	Propanediarnide	3.80	49.4	-2.4
1,3-Diarninopropane-1,2- diol	1,3-Diarninopropane-1,2-dione	3.80	49.7	9.8
Perhydro-N-carbarnoylacetarnide	N- Carbarnoylacetarnide	3.80	n/a	2.3
2-Hydroxy-1,4-diarninobutane-1,4-diol	2-Oxopentanediarnide	4.03	53.5	4.6
Piperazine-2,3,5,6-tetrol	Piperazine-2,3,5,6- tetrone	5.37	93.2	6.3
1-Methylpyrrolidine-2,3 ,4,5-tetro	1-Methylpyrrolidine- l 2,3,4,5-tetrone	5.41	n/a	14.9
Piperidine-2,3,4,5-tetrol	Piperidine-2,3,4,5- tetrone	5.41	89.1	18.7
1-(1-Hydroxyethylarnino)ethanol	N-Acetylacetarnide	3.83	40.6	5.0
1-(1-Hydroxyethyl-methyl-arnino)ethanol	N-Acetyl-N-methyl-acetarnide	3.38	35.3	5.8
1H-Tetrahydropyrrole-2,5-diol	1H-Pyrrole-2,5-dione (maleimide)	5.86	76.8	12.4
Perhydropyrornellitic diimide	Pyrornellitic diimide	6.13	n/a	8.8

Table 2. Hydrogen density and ΔG dehydrogenation of linear and alicyclic polyols, heterocyclic polyols and amino alcohols organic liquid carrier of hydrogen [51].

All-organic redox flow batteries									
Chemistries	**Negative active material (in discharged state)**	**Positive active material (in discharged state)**	**Electrolyte & flow conditions**	**Cell components**	**Experimental OCV / V**	**Approx. % System efficiencies**	**Energy density / W h dm^{-3}**	**Number of cycles**	**Year [Ref:]**
Anthraquinone/ benzoquinone (acid)	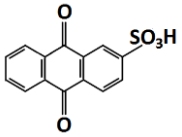	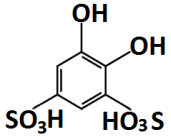	1 M H_2SO_4; 0.2 M active materials; up 1.0 M active materials in recent work; flowing	Carbon papers/ Nafion 117	0. 76 (100 % SOC)	Coulombic: > 95% (8 – 10 mA cm^{-2})	4.1	> 12	2014 [121]
Quinoxaline/ benzoquinone (alkaline-acid)	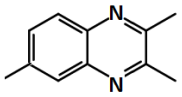	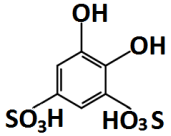	0.2 M KOH + 0.067 M KCl + 0.5 M K_2SO_4 ; 0.4 M H_2SO_4 + 0.5 M K_2SO_4; 0.1 M active materials; static	Carbon felts / lithiated Nafion 117	1.4 – 1.5	Coulombic: > 70% (0.35 mA cm^{-2})	N.G.	> 10	2015 [126]
Polymer-based viologen/ TEMPO (neutral)	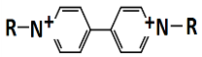	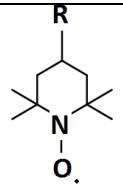	2 M NaCl; 15 mL negative active materials; 10 mL positive active materials; flowing	Carbon felts/ cellulose-based dialysis membrane	1.1	Coulombic: 99% Energy: > 75% (20 – 40 mA cm^{-2})	8.0	10,000 cycles (static cell)	2015 [71]
Methyl viologen / hydroxyl-TEMPO (neutral)	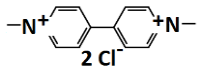	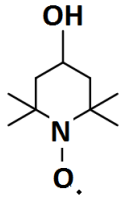	1 M NaCl; 0.1 M active materials; flowing.	Carbon felts / Selemion	1.25	Coulombic. 99% Energy: 45 – 82% (20 – 100 mA cm^{-2})	8.4	100	2016 [57]

Table 3. Operational parameters and performance of all-organic redox flow battery systems in aqueous electrolytes. N.G.: not given.

Organic-inorganic redox flow batteries									
Chemistries	**Negative active (in discharged state)**	**Positive active material (in discharged state)**	**Electrolyte & flowing condition**	**Cell components**	**Experimental OCV / V**	**Approx. % System efficiencies**	**Energy density /W h dm^{-3}**	**Number of cycles**	**Year [Ref]**
Cadmium / chloro-benzoquinone (acid)	Cd^{2+}	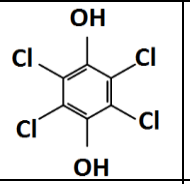	1 M $(NH_4)_2SO_4$ + 0.5 M H_2SO_4; 0.5 M negative active materials; flowing	Cadmium, chloranil/ No separator	1.2	Coulombic: 99 Energy: 82 (10 mA cm^{-2})	N.G.	100	2009 [72]
Lead/ benzoquinone (acid)	$PbSO_4$	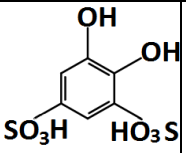	1 M H_2SO_4; 0.25 M positive active materials; flowing	Carbon felts/ Nafion 115	1.1	Coulombic: > 99 Energy: > 80 (10 mA cm^{-2})	7.2	10	2010 [72]
Anthraquinone-bromide (acid)	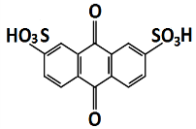	HBr	1 M H_2SO_4; 0.1 – 1 M negative active material; 0.5 – 2.5 M positive active material; flowing	Carbon papers/ Nafion 212	0.86	Coulombic: 99 (200 – 500 mA cm^{-2})	12 - 16	> 10	2014 [40]
Anthraquinone-ferricyanide (alkaline)	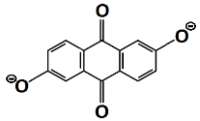	$Fe(CN)_6^{4-}$	1 M KOH; 0.5 M negative active material; 0.4 M positive active material; flowing.	Carbon papers/ Nafion 212	*c.a.* 1.2	Coulombic: > 99 Energy: 84 (100 mA cm^{-2})	6.8	100	2015 [75]
Quinoxaline/ ferricyanide (alkaline)	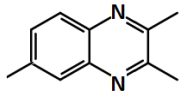	$Fe(CN)_6^{4-}$	0.2 M KOH + 0.067 M KCl + 0.5 M K_2SO_4 ; 0.2 M KOH + 0.5 M K_2SO_4; 0.1 M negative active material; 0.08 M positive	Carbon felts / lithiated Nafion 117	*c.a.* 1.4	Coulombic: > 92 Energy: > 83 (1.76 mA cm^{-2})	N.G.	200	2015 [126]

			active material; flowing.						
Alloxazine/ ferricyanide (alkaline)	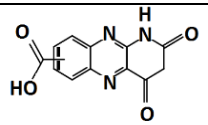	$Fe(CN)_6^{4-}$	pH 14 adjuested by KOH; 0.5 M negative active material; 0.08 M positive active material; flowing.	Carbon papers/ Nafion 212	1.1 – 1.2 V	Coulombic: > 99 Energy: > 60 (100 mA cm^{-2})	N.G.	400	2016 [150]
Zinc/ benzoquinone	Zn^{2+}	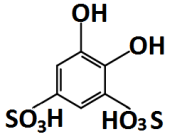	pH 7, 1.5 M $ZnCl_2$; 1.5 M negative active material; 50 mM positive active material	Carbon, carbon felt	*c.a.* 1.52	Coulombic: > 78 Energy: > 70 (30 mA cm^{-2})	N.G.	12	2016 [152]

Table 4. Operational parameters and performance of organic-inorganic redox flow battery systems in aqueous electrolytes.

	Electrolytes	Conductivity / mS cm^{-1}
1	1 M TEA-BF_4/ acetonitrile	56
2	1.5 M TEA-BF_4/ acetonitrile	60
3	1 M TEA-TFSI/ acetonitrile	45
4	1 M $LiBF_4$/ acetonitrile	16
5	1 M LiClO/ acetonitrile	34
6	1 M $LiPF_6$/ acetonitrile	50
7	1 M LiTFSI/ acetonitrile	36
8	1 M LiTFSI/ diethylene glycol dimethyl ether	7
9	1 M LiTFSI/ 1,2-dimethoxyethane (DME)	14
10	1 M TEA-TFSI/ 1,2-dimethoxyethane (DME)	17
11	1 M TEA-TFSI/ dimethyl sulfoxide (DMSO)	9
12	1 M TEA-TFSI/ tetrahydrofuran (THF)	10

Table 5. Ionic conductivities of different supporting electrolytes and conducting salts used in non-aqueous systems.

Non-aqueous organic redox flow batteries						
Chemistries	**Negative active material (at disch. state)**	**Positive active material (at disch. state)**	**Electrolyte & flowing condition**	**Cell components**	**Exp. OCV / V**	**Approx. % System Efficiencies**
N-methyl-phtalimide / TEMPO	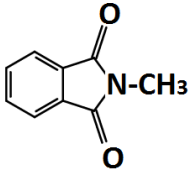	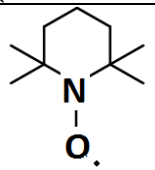	1 M $NaClO_4$ in acetonitrile; 0.1 M active materials; static.	Carbon papers/ Nepem-117	*ca.* 2.0	Coulombic: > 90 Energy: > 60 (0.35 mA cm^{-2})
Camphoquinone/ oxo-TEMPO	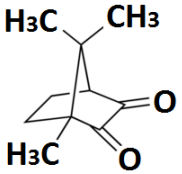	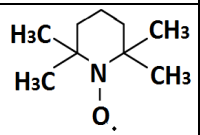	1.0 M $TEABF_4$ in propylene carbonate; 0.2 M active materials; static	Carbon felts/ Fumasep FAP	*ca.* 2.1 – 2.3 V	Coulombic: > 80 Energy: > 71 (1.0 mA cm^{-2})
Trimethyl-quinoxaline/ DBBB	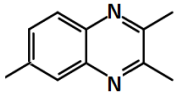	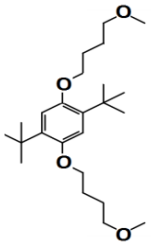	0.2 M $LiBF_4$ in propylene carbonate; 0.05 M active materials; static	Carbon papers/ Nafion 117	1.6 – 2.4	Coulombic: 70 Energy: 37 (0.0625 mA cm^{-2})
Trimethyl-quinoxaline/ trifluoromethyl-ethyl-phenothiazine	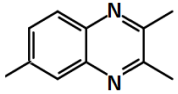	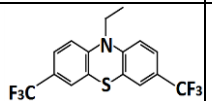	0.2 M $LiBF_4$ in propylene carbonate; 0.05 – 0.35 M active materials; static	Carbon felts/ Nafion	1.5 – 2.4	Coulombic: > 80 (0.14 mA cm^{-2})
Fluorene / DBMMB	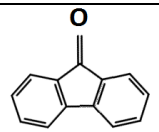	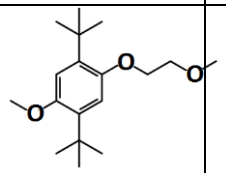	1.0 M TEA-TFSI in acetonitrile; 0.5 M active materials; flowing	Carbon felts/ Daramic microporous polyethylene / silica separator	2.2 – 2.7	Coulombic:. 86 Energy: 71 (15 mA cm^{-2})

N-methyl-phthalimide/ DBMMB	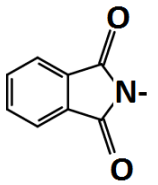	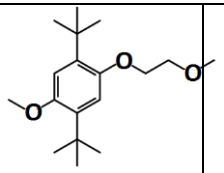	1 M LiTFSI in DME; 0.3 M active materials;	Graphite felts/ Daramic 175	2.0 – 2.4	Coulombic: 90 Energy: 69 (35 mA cm^{-2})
Symmetric diamino-anthraquinone	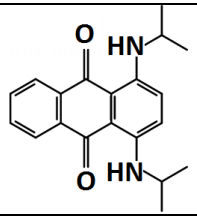	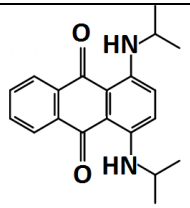	100 mM TBAP in acetronitrile /toluene; 50 mM active materials; static	Reticulated vitreous carbon / medium porosity glass frit	> 1.1	Coulombic: 60 – 80 Energy: 28 – 40 (0.66 mA cm^{-2})
Symmetric PTIO	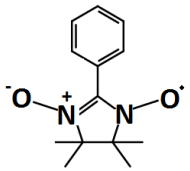	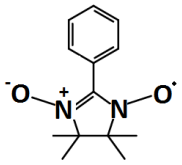	1 M $TBAPF_6$ in acetronitrile; 0.5 M active materials; flowing	Carbon felts/ Daramic porous separator	1.5 – 1.9	Coulombic: 90 Energy: 60 (20 mA cm^{-2})
Symmetric polythiophene	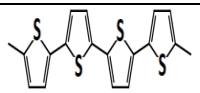	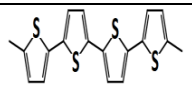	1.0 M $TEAPF_6$ in propylene carbonate; 8.41 g dm^{-3} active materials; flowing	Carbon & Ketjen black / Fumasep FAP	2.6 – 3.0	Coulombic: 78 Energy: 61 (0.5 mA cm^{-2})
Zinc/ polymeric TEMPO	Zn	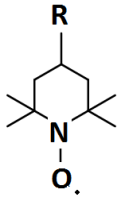	0.5 M $Zn(ClO_4)_2$ in EC:DMC:DEC; flowing	Zinc and carbon felt or paper / dialysis membrane	1.3 – 1.7	Coulombic: > 90 Energy: > 70 (1.0 mA cm^{-2})
All-poly(boron-dipyrromethene)	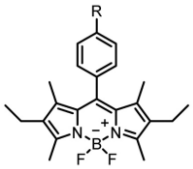	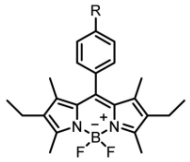	0.5 M Bu_4NClO_4 in propylene carbonate; static	Carbon felts/ dialysis membrane	> 1.28	Coulombic: 89 Energy: 55 (0.1 mA cm^{-2})

Table 6. Operational parameters and performance of organic redox flow battery systems in non-aqueous electrolytes (excluding lithium-based systems).

Lithium-organic hybrid flow batteries									
Chemistries	**Negative active material (at disch. state)**	**Positive active material (at disch. state)**	**Electrolyte & flowing condition**	**Cell components**	**Exp. OCV / V**	**System Efficiencies / %**	**Energy density / W h dm^{-3}**	**No. of cycles**	**Year [Ref]**
Lithium/ dipropoxy-benzoquinone	Li	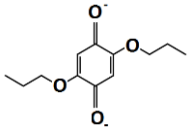	1 M $LiClO_4$ in γ-butyrolactone; 0.01 M positive active material; static	Li foil and carbon paper; LiCGC glsss ceramic	2.8 – 3.0	NG	NG	25	2011 [222]
Lithium/ MEAQ	Li	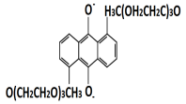	1.0 M $LiPF_6$ in propylene carbonate; 0.25 M positive active material; flowing	Li foil and carbon felt; Celgard 3401	> 2.4	Energy: 82 (0.1 mA cm^{-2})	25	9	2012 [74]
Lithium/ modified DBBB	Li	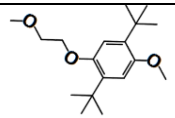	1.0 M $LiBF_4$ in propylene carbonate; 1 mM positive active material; static	Li metal strip and reticulated vitreous carbon; porous glass frit	> 3.9	Energy: 75 (> 0.1 mA cm^{-2})	NG	30	2012 [78]
Lithium/ TEMPO	Li	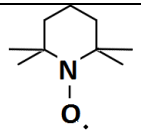	1.0M $LiPF_6$ in EC/PC/EM with 15 % wt. FEC; 0.8 – 2 M active material; flowing	Li foil and carbon felt; polyethylene-based porous separatpr	3.2 – 3.5	Coul.: 84 - 91 Energy: 68 - 76 (1.0 - 5.0 mA cm^{-2})	64 – 126	100	2014 [223]
Lithium/ MeO-TEMPO	Li	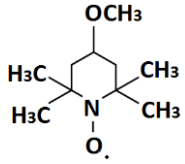	1M LiTFSI in propylene carbonate; 1:1 molar ratio of MeO-TEMPO and LiTFSI with 17% wt. water; flowing	Li foil and carbon felt or paper; LiCGC glsss ceramic	> 3.3	Coul.: > 90 Energy: > 80 (0.1 mA cm^{-2})	200 (static)	20 (static)	2015 [60]

Table 7. Operational parameters and performance of lithium-based organic redox flow battery systems in non-aqueous electrolytes.

References

References

1. M. Skyllas-Kazacos, M.H. Chakrabarti, S.A. Hajimolana, F.S. Mjalli, M. Saleem, 'Progress in Flow Battery Research and Development', *J. Electrochem. Soc.*, **158** (2011) R55-R79.

2. A.Z. Weber, M.M. Mench, J.P. Meyers, P.N. Ross, J.T. Gostick, Q. Liu, 'Redox flow batteries: a review', *J. Appl. Electrochem*, **41** (2011) 1137-1164.

3. P. Leung, X. Li, C. Ponce de Leon, L. Berlouis, C.T.J. Low, F.C. Walsh, 'Progress in redox flow batteries, remaining challenges and their applications in energy storage', *RSC Adv*, **2** (2012) 10125-10156.

4. C. Ponce de Leon, A. Frias-Ferrer, J. Gonzalez-Garcia, D.A. Szanto, F.C. Walsh, 'Redox flow cells for energy conversion', *J. Power Sources*, **160** (2006) 716-732.

5. J. Noack, N. Roznyatovskaya, T. Herr, P. Fischer, 'The Chemistry of Redox-Flow Batteries', *Angew. Chem. Int. Ed.*, **54** (2015) 9776-9809.

6. W. Wang, Q. Luo, B. Lin, X. Wei, L. Li, Z. Yang, 'Recent Progress in Redox Flow Battery Research and Development', *Adv. Funct. Mater.*, **23** (2013) 970-986.

7. C. Ding, H. Zhang, X. Li, T. Liu, F. Xing, 'Vanadium Flow Battery for Energy Storage: Prospects and Challenges', *J. Phys. Chem. Lett.*, **4** (2013) 1281-1294.

8. G.L. Soloveichik, 'Flow Batteries: Current Status and Trends', *Chem. Rev.*, **115** (2015) 11533-11558.

9. 'Grid Energy Storage, U.S. Department of Energy, 2013'. http://energy.gov/oe/downloads/grid-energy-storage-december-2013.

10. 'Joint EASE/EERA recommendations for a European Energy Storage Technology Development Roadmap towards 2030, The European Association for Storage of Energy (EASE)'. http://www.eera-set.eu/wp-content/uploads/148885-EASE-recommendations-Roadmap-04.pdf.

11. D. Pletcher, R. Wills, 'A novel flow battery: A lead acid battery based on an electrolyte with soluble lead(II) Part II. Flow cell studies', *Phys. Chem. Chem. Phys.*, **6** (2004) 1779-1785.

12. N.H. Hagedorn, L.H. Thaller, 'Redox storage systems for solar applications, ' *Power Sources: Research and Development in Non-Mechanical Electrical Power Sources*, (1981) 227-243.

13. E. Sum, M. Rychcik, M. Skyllas-Kazacos, 'Investigation of the V(V)/V(IV) system for use in the positive half-cell of a redox battery', *J. Power Sources,* **16** (1985) 85-95.

14. A. Price, S. Bartley, S. Male, G. Cooley, 'A novel approach to utility-scale energy storage', *Power Engineering Journal,* **13** (1999) 122-129.

15. H.S. Lim, A.M. Lackner, R.C. Knechtli, 'Zinc-Bromine Secondary Battery', *J. Electrochem. Soc.,* **158** (2011) R55-R79.

16. P.K. Leung, C. Ponce de Leon, C.T.J. Low, A.A. Shah, F.C. Walsh, 'Characterization of a zinc-cerium flow battery', *J. Power Sources,* **196** (2011) 5174-5186.

17. S.H. Shin, S.H. Yun, S.H. Moon, 'A review of current developments in non-aqueous redox flow batteries: characterization of their membranes for design perspectives', *RSC Adv.,* **3** (2013) 9095-9116.

18. Y. Matsuda, K. Tanaka, M. Okada, Y. Takasu, M. Morita, T. Matsumura-Inoue, 'A rechargeable redox battery utilizing ruthenium complexes with non-aqueous organic electrolyte', *J. Appl. Electrochem.,* **18** (1988) 909-914.

19. A.E.S. Sleightholme, A.A. Shinkle, Q. Liu, Y. Li, C.W. Monroe, L.T. Thompson, 'Non-aqueous manganese acetylacetonate electrolyte for redox flow batteries', *J. Power Sources,* **196** (2011) 5742-5745.

20. Q. Liu, A.E.S. Sleightholme, A.A. Shinkle, Y. Li, L.T. Thompson, 'Non-aqueous vanadium acetylacetonate electrolyte for redox flow batteries', *Electrochem. Commun.,* **11** (2009) 2312-2315.

21. Q. Liu, A.A. Shinkle, Y. Li, C.W. Monroe, L.T. Thompson, A.E.S. Sleightholme, 'Non-aqueous chromium acetylacetonate electrolyte for redox flow batteries', *Electrochem. Commun.,* **12** (2010) 1634-1637.

22. J.H. Kim, K.J. Kim, M.S. Park, N.J. Lee, U. Hwang, H. Kim, Y.-J. Kim, 'Development of metal-based electrodes for non-aqueous redox flow batteries', *Electrochem. Commun.,* **13** (2011) 997-1000.

23. A.A. Shinkle, A.E.S. Sleightholme, L.T. Thompson, C.W. Monroe, 'Electrode kinetics in non-aqueous vanadium acetylacetonate redox flow batteries', *J. Appl. Electrochem.,* **41** (2011) 1191-1199.

24. P. Leung, J. Palma, E. Garcia-Quismondo, L. Sanz, M.R. Mohamed, M. Anderson, 'Evaluation of electrode materials for all-copper hybrid flow batteries', *J. Power Sources,* **310** (2016) 1-11.

25. L. Wei, T.S. Zhao, L. Zeng, Y.K. Zeng, H.R. Jiang, 'Highly catalytic and stabilized titanium nitride nanowire array-decorated graphite felt electrodes for all vanadium redox flow atteries', *J. Power Sources*, **341** (2017) 318-326.

26. Y. Zeng, T. Zhao, X. Zhou, L. Wei, H. Jiang, 'A low-cost iron-cadmium redox flow battery for large-scale energy storage', *J. Power Sources*, **330** (2016) 55-60.

27. L. Wei, T.S. Zhao, Q. Xu, X.L. Zhou, Z.H. Zhang, 'In-situ investigation of hydrogen evolution behavior in vanadium redox flow batteries', *Appl. Energy*, **190** (2017) 1112-1118.

28. L. Wei, T.S. Zhao, L. Zeng, X.L. Zhou, Y.K. Zeng, 'Copper nanoparticle-deposited graphite felt electrodes for all vanadium redox flow batteries', *Appl. Energy*, **180** (2016) 386-391.

29. M.C. Wu, T.S. Zhao, H.R. Jiang, Y.K. Zeng, Y.X. Ren, 'High-performance zinc bromine flow battery via improved design of electrolyte and electrode', *J. Power Sources*, **355** (2017) 62-68.

30. R.F. Service, 'Tank for the Batteries', *Science*, **344,** (2014) 352-354.

31. G. Kear, A.A. Shah, F.C. Walsh, 'Development of the all-vanadium redox flow battery for energy storage: a review of technological, financial and policy aspects', *Int. J. Energy Res.*, **36** (2012) 1105-1120.

32. S. Eckroad, 'Handbook of Energy Storage for Transmission or Distribution Applications', *Electric Power Research Institute Report*, (2002) http://www.sandia.gov/ess/publications/ESHB%201001834%20reduced%20size.pdf.

33. L. Joerissen, J. Garche, Ch. Fabjan, G. Tomazic, 'Possible use of vanadium redox flow batteries for energy storage in small grids and stand-alone photovoltaic systems', *J. Power Sources*, **127** (2004) 98-104.

34. T. Janoschka, M.D. Hager, U.S. Schubert, 'Powering up the future: radical polymers for battery applications', *Adv. Mater.*, **24** (2012) 6397-6409.

35. H. Nishide, K. Koshika, K. Oyaizu, 'Environmentally benign batteries based on organic radical polymers', *Pure Appl. Chem.*, **81** (2009) 1960-1970.

36. K. Oyaizu, T. Kawamoto, T. Suga, H. Nishide, 'Synthesis and Charge Transport Properties of Redox-Active Nitroxide Polyethers with Large Site Density', *Macromolecules*, **43** (2010) 10382-10389.

37. K. Nakahara, J. Iriyama, S. Iwasa, M. Suguro, S. Masaharu, E.J. Cairns, 'High-rate capable organic radical cathodes for lithium rechargeable batteries', *J. Power Sources*, **165** (2007) 870-873.

38. P. Nesvadba, L. Bugnon, P. Maire, P. Novak, 'Synthesis of A Novel Spirobisnitroxide Polymer and its Evaluation in an Organic Radical Battery', *Chem. Mater.*, **22** (2010) 783-788.

39. 'Organic-Based Aqueous Flow Batteries for Massive Electrical Energy Storage'. Presentation of M. Aziz at Princeton University, 20/10/2014, http://nuweb9.neu.edu/mres/wp-content/uploads/2014/11/Michael-Aziz-presentation.pdf.

40. B. Huskinson, M.P. Marshak, C.W. Suh, S. Er, M.R. Gerhardt, C.J. Galvin, X.D. Chen, A. Aspuru-Guzik, R.G. Gordon, M.J. Aziz, 'A metal-free organic-inorganic aqueous flow battery', *Nature*, **505** (2014) 195-198.

41. R.M. Darling, K.G. Gallagher, J.A. Kowalski, S. Ha, F.R. Brushett, 'Pathways to low-cost electrochemical energy storage: a comparison of aqueous and nonaqueous flow batteries', *Energy Environ. Sci.*, **7** (2014) 3459-3477.

42. P.K. Leung, T. Martin, A.A. Shah, M.R. Mohamed, M.A. Anderson, J. Palma, 'Membrane-less hybrid flow battery based on low-cost elements', *J. Power Sources*, **341** (2017) 36-45.

43. K. Gong, Q.R. Fang, S. Gu, S.F.Y. Li, Y.S. Yan, 'Nonaqueous Redox-Flow Batteries: Organic Solvents, Supporting Electrolytes, and Redox Pairs', *Energy Environ. Sci.*, **8** (2015) 3515-3530.

44. T.B. Schon, B.T. McAllister, P.-F. Li, D.S. Seferos, 'The rise of organic electrode materials for energy storage', *Chem. Soc. Rev.*, **45** (2016) 6345-6404.

45. L. Cheng, R.S. Assary, X.H. Qu, A. Jain, S.P. Ong, N.N. Rajput, K. Persson, L.A. Curtiss, 'Accelerating Electrolyte Discovery for Energy Storage with High-Throughput Screening', *J. Phys. Chem. Lett.*, **6** (2015) 283-291.

46. S.D. Pineda Flores, G.C. Martin-Noble, R.L. Phillips, J. Schrier, 'Bio-Inspired Electroactive Organic Molecules for Aqueous Redox Flow Batteries. 1. Thiophenoquinones', *J. Phys. Chem. C.*, **119** (2015) 21800-21809.

47. Y. Moon, Y.K. Han, 'Computational screening of organic molecules as redox active species in redox flow batteries', *Current Applied Physics*, **1** (2016) 939-943.

48. K. Xu, 'Nonaqueous Liquid Electrolytes for Lithium-Based Rechargeable Batteries', *Chem. Rev.*, **104** (2004) 4303-4418.

49. W. Wang, V. Sprenkle, 'Energy storage: Redox flow batteries go organic', *Nature Chemistry*, **8** (2016) 204-206.

50. C.S. Sevov, R.E.M. Brooner, E. Chenard, R.S. Assary, J.S. Moore, J. Rodriguez-Lopez, M.S. Sanford, 'Evolutionary Design of Low Molecular Weight Organic Anolyte Materials for Applications in Nonaqueous Redox Flow Batteries', *J. Am. Chem. Soc.,* **137** (2015) 14465-14472.

51. G.L. Soloveichik, 'System and method for electrochemical energy conversion and storage', US Patent 8338055 B2, 25 Dec 2012.

52. Q. Xu, F. Zhang, L. Xu, P. Leung, C. Yang, H. Li, 'The applications and prospect of fuel cells in medical field: A review', *Renewable and Sustainable Energy Reviews,,* **67** (2017) 574-580.

53. M.H. Osman, A.A. Shah, F.C. Walsh, 'Recent progress and continuing challenges in bio-fuel cells. Part I: Enzymatic cells', *Biosensors and Bioelectronics,* **26** (2011) 3087-3102.

54. J.D. Milshtein, L. Su, C. Liou, A.F. Badel, F.R. Brushett, 'Voltammetry study of quinoxaline in aqueous electrolyte', *Electrochim. Acta,* **180** (2015) 695-704.

55. D.R. García, P.G. Romero, P.L. Cabot. 'Design of new electroactive fluids for redox flow batteries based on quinones', Universitat de Barcelona, 2014.

56. Y. Zhao, Y. Ding, Y. Li, L. Peng, H.R. Byon, J.B. Goodenough, G. Yu, 'A chemistry and material perspective on lithium redox flow batteries towards high-density electrical energy storage', *Chem. Sov. Rev.,* **44** (2015) 7968-7996.

57. T. Liu, X. Wei, Z. Nie, V. Sprenkle, W. Wang, 'A Total Organic Aqueous Redox Flow Battery Employing a Low Cost and Sustainable Methyl Viologen,anolyte and 4-HO-TEMPO catholyte', *Adv. Energy. Mater.,* **6** (2016) 1501449-1501456.

58. X. Wei, W. Xu, J. Huang, L. Zhang, E. Walter, C. Lawrence, M. Vijayakumar, W. Henderson, T. Liu, L. Cosimbescu, B. Li, V. Sprenkle, W. Wang, 'Radical Compatibility with Nonaqueous Electrolytes and Its Impact on an All-Organic Redox Flow Battery', *Angew. Chem. Int. Ed.,* **127** (2015) 1-5.

59. R. Dmello, J.D. Milshtein, F.R. Brushett, K.C. Smith, 'Cost-driven materials selection criteria for redox flow battery electrolytes', *J. Power Sources,* **330** (2016) 261-272.

60. K. Takechi, Y. Kato, Y. Hase, 'A Highly Concentrated Catholyte Based on a Solvate Ionic Liquid for Rechargeable Flow Batteries', *Adv. Mater.,* **27** (2015) 2501-2506.

61. M. Duduta, B. Ho, V.C. Wood, P. Limthongkul, V.E. Brunini, W.C. Carter, Y.M. Chiang, 'Semi-Solid Lithium Rechargeable Flow Battery', *Adv. Energy Mater.,* **1** (2011) 511-516.

62. F. Pan, Q. Wang, 'Redox Species of Redox Flow Batteries: A Review', *Molecules,* **20** (2015) 20499-20517.

63. Q. Huang, Q. Wang, 'New-Generation, High-Energy-Density Redox Flow Batteries', *ChemPlusChem,* **80** (2015) 312-322.

64. A. Parasuraman, T.M. Lim, C. Menictas, M. Skyllas-Kazacos, 'Review of material research and development for vanadium redox flow battery applications', *Electrochim. Acta,* **101** (2013) 27-40.

65. P. Alotto, M. Guarnieri, F. Moro, 'Redox flow batteries for the storage of renewable energy: A review', *Renewable and Sustainable Energy Reviews,,* **29** (2014) 325-335.

66. Q. Xu, T.S. Zhao, 'Fundamental models for flow batteries', *Prog. Energy Combust. Sci.,* **49** (2015) 40-58.

67. S.M. Laramie, J.D. Milshtein, T.M. Breault, F.R. Brushett, L.T. Thompson, 'Performance and cost characteristics of multi-electron transfer, common ion exchange non-aqueous redox flow batteries', *J. Power Sources,* **327** (2016) 681-692.

68. J.A. Kowalski, L. Su, J.D. Milshtein, F.R. Brushett, 'Recent advances in molecular engineering of redox active organic molecules for nonaqueous flow batteries', *Current Opinion in Chemical Engineering,* **13** (2016) 45-52.

69. J. Winsberg, T. Hagemann, T. Janoschka, M.D. Hager, U.S. Schubert, 'Redox-Flow Batteries: From Metals to Organic Redox-Active Materials', *Angew. Chem. Int. Ed.,* **56** (2016) 686-711.

70. M. Park, J. Ryu, W. Wang, J. Cho, 'Material design and engineering of next-generation flow battery technologies', *Nature Reviews,* article-in-press.

71. T. Janoschka, N. Martin, U. Martin, C. Friebe, S. Morgenstern, H. Hiller, M.D. Hager, U.S. Schubert, 'An aqueous, polymer-based redox-flow battery using non-corrosive, safe, and low-cost materials', *Nature,* **527** (2015) 78-81.

72. Y. Xu, Y. Wen, J. Cheng, G.G.Y. Yang, 'Study on a single flow acid Cd-chloranil battery', *Electrochemistry Communications,* **11** (2009) 1422-1424.

73. J. Winsberg, S. Muench, T. Hagemann, S. Morgenstern, T. Janoschka, M. Billing, F.H. Schacher, G. Hauffman, J.F. Gohy, S. Hoeppener, M.D. Hager, U.S. Schubert, 'Polymer/ zinc hybrid-flow battery using block copolymer micelles featuring a TEMPO corona as catholyte', *Polym. Chem.,* **7** (2016) 1711-1718.

74. W. Wang, W. Xu, L. Cosimbescu, D.W. Choi, L.Y. Lib, Z.G. Yang, 'Anthraquinone with tailored structure for a nonaqueous metal–organic redox flow battery', *Chem. Commun.,* **48** (2012) 6669-6671.

75. K.X. Lin, Q. Chen, M.R. Gerhardt, L.C. Tong, S.B. Kim, L. Eisenach, A.W. Valle, D. Hardee, R.G. Gordon, M.J. Aziz, M.P. Marshak, 'Alkaline quinone flow battery', *science,* **349** (2015) 1529-1532.

76. P.J. Cappillino, H.D. Pratt, N.S. Hudak, N.C. Tomson, T.M. Anderson, M.R. Anstey, 'Application of Redox Non-Innocent Ligands to Non-Aqueous Flow Battery Electrolytes', *Adv. Energy Mater.*, **4** (2014) 1-4.

77. M.H. Chakrabarti, E.P.L. Roberts, C.B.M. Saleem, 'Ruthenium based redox flow battery for solar energy storage', *Energy Convers. Manage,* **52** (2011) 2501-2508.

78. J. Huang, L. Cheng, R.S. Assary, P. Wang, Z. Xue, A.K. Burrell, L.A. Curtiss, L. Zhang, 'Liquid Catholyte Molecules for Nonaqueous Redox Flow Batteries', *Adv. Energy Mater.,* **5** (2015) 1-6.

79. C.H. Bae, E.P.L. Roberts, R.A.W. Dryfe, 'Chromium redox couples for applicaton to redox flow batteries', *Electrochim. Acta,* **48** (2002) 279-287.

80. J.G. Ibanez, C.S. Choi, R.S. Becker, 'Aqueous redox transition metal complexes for electrochemical applications as a function of pH', *J. Electrochem. Soc.,* **134** (1987) 3083-3089.

81. Y.W.D. Chen, K. Santhanam, A.J. Bard, 'Solution Redox Couples for Electrochemical Energy Storage I. Iron(III)-Iron(II) Complexes with O-Phenanthroline and Related Ligands', *J. Electrochem. Soc.,* **128** (1981) 1460-1467.

82. Y.H. Wen, H.M. Zhang, P. Qian, H.T. Zhou, P. Zhao, B.L. Yi, Y.S. Yang, 'A study of the Fe(III)/Fe(II)-triethanolamine complex redox couple for redox flow battery application', *Electrochim. Acta,* **94** (2013) 336-343.

83. A.S.N. Murthy, T. Srivastava, 'Fe(III)/Fe(II) - Ligand systems for use as negative half-cells in redox-flow cells', *J. Power Sources,* **27** (1989) 119-126.

84. P. Modiba, M. Matoetoe, A.M. Crouch, 'Kinetics study of transition metal complexes (Ce-DTPA, Cr-DTPA and V-DTPA) for redox flow battery applications', *Electrochim. Acta,* **94** (2013) 336-343.

85. M.H. Chakrabarti, R.A.W. Dryfe, E.P.L. Roberts, 'Evaluation of electrolytes for redox flow battery applications', *Electrochim. Acta,* **52** (2007) 2189-2195.

86. J. Mun, M.J. Lee, J.W. Park, D.J. Oh, D.Y. Lee, S.G. Doo, 'Non-Aqueous Redox Flow Batteries with Nickel and Iron Tris(2,2'-bipyridine) Complex Electrolyte', *Electrochem. Solid-State Lett.,* **15** (2012) A80-A82.

87. P.K. Leung, C. Ponce de Leon, C.T.J. Low, F.C. Walsh, 'Ce(III)/Ce(IV) in methanesulfonic acid as the positive half cell of a redox flow battery', *Electrochim. Acta,* **56** (2011) 2145-2153.

88. A. Hazza, D. Pletcher, R. Wills, 'A novel flow battery: A lead acid battery based on an electrolyte with soluble lead(II) Part I: Preliminary studies', *Phys. Chem. Chem. Phys.,* **6** (2004) 1773-1778.

89. P.K. Leung, M.R. Mohamed, A.A. Shah, Q. Xu, M.B. Conde-Duran, 'A mixed acid based vanadium-cerium redox flow battery with a zero-gap serpentine architecture', *J. Power Sources,* **274** (2015) 651-658.

90. P.K. Leung, C. Ponce de Leon, C.T.J. Low, F.C. Walsh, 'Zinc deposition and dissolution in methanesulfonic acid onto a carbon composit electrode as the negative electrode reactions in a hybrid redox flow battery', *Electrochim. Acta,* **18** (2011) 6536-6546.

91. G.P. Rajarathnam, A.M. Vassallo, 'The Zinc/Bromine Flow Battery: Materials Challenges and Practical Solutions for Technology Advancement', Springer, (2016) 1-97.

92. G.P. Rajarathnam, M.E. Easton, M. Schneider, A.F. Masters, T. Maschmeyer, A.M. Vassallo, 'The influence of Ionic Liquid Additives on Zinc Half-Cell Electrochemical Performance in Zinc/Bromine Flow Batteries', *RSC Adv.,* **6** (2016) 27788-27797.

93. M.H. Chakrabarti, F.S. Mjalli, I.M. AlNashef, M.A. Hashim, M.A. Hussain, L. Bahadori, C.T.J. Low, 'Prospects of applying ionic liquids and deep eutectic solvents for renewable energy storage by means of redox flow batteries, Renewable & Sustainable Energy Reviews', **30** (2014) 254-270.

94. G.B. Adams, 'Electrically rechargeable batteries', US Patent 4180623, 25 Dec 1979, (1979).

95. L. Zhang, Z. Zhang, K. Amine, 'Redox Shuttle Additives for Lithium-Ion Battery, Lithium Ion Batteries - New Developments', *Publ. InTech,* 173-188.

96. Y. Ding, Y. Zhao, Y. Li, J.B. Goodenough, G. Yu, 'A high-performance all-metallocene-based non-aqueous redox flow battery', *Energy Environ. Sci.,* **10** (2017) 491-497.

97. X. Wei, L. Cosimbescu, W. Xu, J.Z. Hu, M. Vijayakumar, J. Feng, M.Y. Hu, X. Deng, J. Xiao, J. Liu, 'Towards High-Performance Nonaqueous Redox Flow

Electrolyte via Ionic Modification of Active Species', *Adv. Energy Mater.*, **5** (2015) 1400678.

98. Y. Zhao, Y. Ding, J. Song, G. Li, G. Dong, J.B. Goodenough, G. Yu, 'Sustainable Electrical Energy Storage through the Ferrocene/Ferrocenium Redox Reaction in Aprotic Electrolyte', *Angew. Chem. Int. Ed.*, **53** (2014) 11036-11040.

99. Q. Huang, H. Li, M. Gratzel, Q. Wang, 'Reversible chemical delithiation/lithiation of LiFePO4: towards a redox flow lithium-ion battery', *Phys. Chem. Chem. Phys.*, **15** (2013) 1793-1797.

100. F. Pan, J. Yang, Q. Huang, X. Wang, H. Huang, Q. Wang, 'Redox Targeting of Anatase TiO2 for Redox Flow Lithium-Ion Batteries', *Adv. Energy Mater.*, **4** (2014) 1400567.

101. F. Pan, Q. Huang, H. Huang, Q. Wang, 'High-Energy Density Redox Flow Lithium Battery with Unprecented Voltage Efficiency', *Chem. Mater.*, **28** (2016) 2052-2057.

102. Q. Huang, J. Yang, C.B. Ng, C. Jia, Q. Wang, 'A redox flow lithium battery based on the redox targeting reactions between LiFePO4 and iodide', *Energy Environ. Sci.*, **9** (2016) 917-921.

103. C. Jia, F. Pan, Y.G. Zhu, Q. Huang, L. Lu, Q. Wang, 'High-energy density nonaqueous all redox flow lithium battery enabled with a polymeric membrane', *Sci. Adv.*, **1** (2015) e1500886.

104. Q. Wang, S.M. Zakeeruddin, D. Wang, I. Exnar, M. Gratzel, 'Redix Targeting of Insulating Electrode Materials: A New Approach to High-Energy-Density Batteries', *Angew. Chem. Int. Ed.*, **118** (2006) 8377-8380.

105. Y.G. Zhu, C. Jia, J. Yang, F. Pan, Q. Huang, Q. Wang, 'Dual Redox Catalysts for oxygen reduction and evolution reactions: towards a redox flow Li-O2 battery', *Chem. Commun.*, **51** (2015) 9451-9454.

106. Y.G. Zhu, X. Wang, C. Jia, J. Yang, Q. Wang, 'Redox-mediated ORR and OER Reactions: Redox Flow Lithium Oxygen Batteries Enabled with a Pair of Soluble Redox Catalysts', *ACS Catalysis*, **6** (2016) 6191-6197.

107. Y.G. Zhu, Q. Liu, Y. Rong, H. Chen, J. Yang, C. Jia, L.J. Yu, A. Karton, Y. Ren, X. Xu, S. Adams, Q. Wang, 'Proton enhanced dynamic battery chemistry for aprotic lithium-oxygen batteries', *Nat. Comm.*, **8** (2017) 14308.

108. J. Li, L. Yang, S. Yang, J.Y. Lee, 'The application of redox targeting principles to the design of rechargeable Li-S flow batteries', *Adv. Energy Mater.*, **5** (2015) 1501808.

109. H. Chen, W. Zou, Z. Liang, H. Liu, Q. Li, Y.C. Lu, 'Sulphur-Impregnated Flow Cathode to Enable High-Energy-Density Lithium Flow Batteries', *Nat. Comm.,* **6** (2015) 5877.

110. L. Fan, J.R. Jennings, S.M. Zakerruddin, M. Gratzel, Q. Wang, 'Redox Catalysis for Improved Counter-Electrode Kinetics in Dye-Sensistized Solar Cells', *ChemElectroChem,* (2017) accepted.

111. P. Peljo, M. Bichona, H.H. Girault, 'Ion transfer battery: storing energy by transferring ions across liquid–liquid interfaces', *Chem. Commun.,* **52** (2016) 9761-9764.

112. J.B. Conant, H.M. Kahn, L.F. Fieser, S.S. Kurtz Jr., 'An electrochemical study of the reversible reduction of organic compounds', *J. Am. Chem. Soc.,* **44** (1992) 1382-1396.

113. L.F. Fieser, 'The tautomerism of hydroxyl quinones', *J. Am. Chem. Soc.,* **50** (1928) 439-465.

114. G.L. Soloveichik, J.C. Zhao, 'Method and apparatus for electrochemical energy conversion', US Patent 20080248345 A1, 09 Oct 2008.

115. G.L. Soloveichik, 'Liquid fuel cells', *Beilstein J. Nanotechnol,* **5** (2014) 1399-1418.

116. C. Moyses Araujo, D.L. Simone, S.J. Konezny, A. Shim, R.H. Crabtree, G.L. Soloveichik, V.S. Batista, 'Fuel selection for a regenerative organic fuel cell / flow battery: thermodynamic considerations', *Energy Environ. Sci.,* **5** (2012) 9534-9542.

117. S. Er, C. Suh, M.P. Marshak, A. Aspuru-Guzik, 'Computational design of molecules for an all-quinone redox flow battery', *Chem. Sci.,* **6** (2015) 885-893.

118. E.V. Carino, J. Staszak-Jirkovsky, R.S. Assary, L.A. Curtiss, N.M. Markovic, F.R. Brushett, 'Tuning the Stability of Organic Active Materials for Nonaqueous Redox Flow Batteries via Reversible, Electrochemically Mediated Li+ Coordination', *Chem. Mater.,* **28** (2016) 2529-2539.

119. Y. Ding, Y.F. Li, G.H. Yu, 'Exploring bio-inspired quinone-based organic redox flow batteries: A combined experimental and computational study', *Chem,* **1** (2016) 790-801.

120. Q. Chen, M.R. Gerhardt, L. Hartle, M.J. Aziz, 'A Quinone-Bromide Flow Battery with 1 W cm-2 Power Density', *J. Electrochem. Soc.,* **163** (2016) A5010-A5013.

121. B. Yang, L. Hoober-Burkhardt, F. Wang, G.K. Surya Prakash, S.R. Narayanan, 'An Inexpensive Aqueous Flow Battery for Large-Scale Electrical Energy Storage

Based on Water-Soluble Organic Redox Couples', *J. Electrochem. Soc.*, **161** (2014) A1371-A1380.

122. B. Yang, L. Hoober-Burkhardt, S. Krishnamoorthy, A. Murali, G.K. Surya Prakash, S.R. Narayanan, 'High-Performance Aqueous Organic Flow Battery with Quinone-Based Redox Couples at Both Electrodes', *J. Electrochem. Soc.*, **163** (2016) A1442-A1449.

123. S. Zhang, X. Lin, D. Chu, 'An organic Electroactive Material for Flow Batteries', *Electrochim. Acta*, **190** (2016) 737-743.

124. X. Li, 'Modeling and simulation study of a metal free organic–inorganic aqueous flow battery with flow through electrode', *Electrochim. Acta*, **170** (2015) 98-109.

125. S. Nawar, B. Huskinson, M. Aziz, 'Benzoquinone-Hydroquinone Couple for Flow Battery', *Mater. Res. Soc. Symp. Proc.*, **1491** (2013) 1-6.

126. F.R. Brushett, A.N. Jansen, J.T. Vaughey, L. Su, J.D. Milshtein, 'Materials for use with aqueous redox flow batteries and related methods and systems', US Patent 2015/0236543 A1, 20 Aug 2015.

127. S.I. Bailey, I.M. Ritchie, F.R. Hewgill, 'The Construction and Use of Potential-pH Diagrams in Organic Oxidat ion-Reduct ion React ions', *J. CHEM. SOC. PERKIN TRANS.*, **11** (1983) 645-652.

128. M. Quan, D. Sanchez, M.F. Wasylkiw, D.K. Smith, 'Voltammetry of Quinones in Unbuffered Aqueous Solution: Reassessing the Roles of Proton Transfer and Hydrogen Bonding in the Aqueous Electrochemistry of Quinones', *J. Am. Chem. Soc.*, **129** (2007) 12847-12856.

129. J.Q. Chambers, 'Electrochemistry of quinones', John Wiley & Sons Ltd, **Chapter 12** (1988) 719-751.

130. E.M. Thurman, 'Organic Geochemistry of Natural Waters', Kluwer Academic Publishers, Hingham, (1985) 94-98.

131. 'Chemical property of anthraquinone-2,6-disulfonic acid disodium salt (853-68-9)'. http://www.chemicalbook.com/ProductChemicalPropertiesCB5481901_EN.htm.

132. S. Narayan, S.G.K. Prakash, B. Yang, L. Hoober-Burkhardt, S. Krishnamoorthy, 'Inexpensive metal-free organic redox flow battery (orbat) for grid-scale storage', US Patent 20140370403 A1, 18 Dec, 2014.

133. S. Miertus, E. Scrocco, J. Tomasi, 'Electrostatic interaction of a solute with a continuum. A direct utilization of AB initio molecular potetentials for the prevision of solvent effects', *Chemical Physics*, **1** (1981) 117-129.

134. E. Biilmann, 'Oxidation and reduction potentials of organic compounds', *Trans. Faraday Soc.,* **19** (1924) 676-691.

135. J.M. Hale, R. Parsons, 'Reduction of p-quinones at a dropping mercury electrode', *Trans. Faraday Soc.,* **59** (1963) 1429-1437.

136. R.H. Philip Jr., R.L. Flurry, R.A. Day Jr., 'The Polarographic Reduction of Some Aryl Diketones', *J. Electrochem. Soc.,* **111** (1964) 328-334.

137. B.K. Sharma, 'Electrochemical Reduction and Oxidation, Electro Chemistry', 5th edition ed. GOEL Publishing House, **Chapter 20** (1997) 249-258.

138. E.A. Cepeda, B. Gomez, M. Diaz, 'Solubility of anthracene and anthraquinone in some pure and mixed solvents', *J. Chem. Eng. Data,* **34** (1989) 273-275.

139. D. Aaron, Q. Liu, Z. Tang, G. Grim, A. Papandrew, A. Turhan, T. Zawodzinski, M. Mench, 'Dramatic performance gains in vanadium redox flow batteries through modified cell architecture', *J. Power Sources,* **206** (2012) 450-453.

140. M.P. Strier, J.C. Cavagnol, 'The Polarography of Quinoxaline', *J. Am. Chem. Soc.*, **79** (1957) 4331-4335.

141. M. Aleksic, J. Pantic, V. Kapetanovic, 'Evaluation of kinetic parameters and redox mechanism of quinoxaline at glassy carbon electrode', *Facta Univ. Ser. Phys. Chem. Technol,* **12** (2014) 55-63.

142. S.I. Imabayashi, N. Kitamura, S. Tazuke, K. Tokuda, 'Substituent effects on electrochemical reduction of viologen dimer and trimer with ethylene spacer', *J. Electroanal. Chem.,* **239** (1988) 397-403.

143. S.I. Imabayashi, N. Kitamura, S. Tazuke, K. Tokuda, 'The role of intramolecular association in the electrochemical reduction of viologen dimers and trimers', *J. Electroanal. Chem.,* **243** (1988) 143-160.

144. W. Silwa, B. Bachowska, N. Zelichowicz, 'Chemistry of Viologens', *Heterocycles,* **11** (1991) 2241-2273.

145. C.L. Bird, A.T. Kuhn, 'Electrochemistry of the viologens', *Chem. Soc. Rev.,* **10** (1981) 49-82.

146. R.J. Mortimer, 'Organic electrochromic materials', *Electrochim. Acta.,* **44** (1990) 2971-2981.

147. X. Li, H. Zhang, Z. Mai, H. Zhang, I. Vankelecom, 'Ion exchange membranes for vanadium redox flow battery (VRB) applications', *Energy Environ. Sci.,* **4** (2011) 1147-1160.

148. Y. Xu, Y.H. Wen, J. Cheng, G.P. Cao, Y.S. Yang, 'A study of tiron in aqueous solutions for redox flow battery application', *Electrochim. Acta*, **55** (2010) 715-720.

149. A. Orita, M.G. Verde, M. Sakai, Y.S. Meng, 'A biomimetic redox flow battery based on flavin mononucleotide', *Nat. Comm.*, **7** (2016) 13230 https://www.nature.com/articles/ncomms13230.

150. K.X. Lin, R. Gómez-Bombarelli, E.S. Beh, L.C. Tong, Q. Chen, A. Valle, A. Aspuru-Guzik, M.J. Aziz, R.G. Gordon, 'A redox-flow battery with an alloxazine-based organic electrolyte', *Nature Energy*, **Article No.: 16102, DOI: 10.1038/NENERGY.2016.102** (2016) 1-8.

151. J. Winsberg, T. Janoschka, S. Morgenstern, T. Hagemann, S. Muench, G. Hauffman, J. Gohy, M.D. Hager, U.S. Schubert, 'Poly(TEMPO)/Zinc Hybrid-Flow Battery: A Novel, "Green," High Voltage, and Safe Energy Storage System', *Adv. Mater.*, **28** (2016) 2238-2243.

152. P.K. Leung, T. Martin, A.A. Shah, M.A. Anderson, J. Palma, 'Membrane-less organic-inorganic aqueous flow batteries with improved cell potential', *Chem Comm.*, (2017) article in press.

153. H. Alt, H. Binder, A. Köhling, G. Sandstede, 'Investigation into the use of quinone compounds-for battery cathodes', *Electrochim. Acta*, **17** (1972) 873-887.

154. F.R. McLarnon, 'The Secondary alkaline zinc electrode', *J. Electrochem. Soc.*, **138** (1991) 645-664.

155. P.K. Leung, C. Ponce de Leon, F.C. Walsh, 'An undivided zinc-cerium redox flow battery operating at room temperature (295 K)', *Electrochemistry Communications*, **13** (2011) 770-773.

156. L.P. Papauchado, 'Anodic oxidation pathways of phenolic compounds. Part I. Anodic hydroxylation reactions', *J. Electroanal. Chem.*, **38** (1972) 389-395.

157. B. Huskinson, M. Marshak, M.J. Aziz, R.G. Gordon, 'Small organic molecule based flow battery', US 20160043423 A1, 3 April 2014.

158. B. Huskinson, M. Marshak, M.J. Aziz, R.G. Gordon, A. Aspuru-Guzik, S. Er, C. Suh, L. Tong, K. Lin, 'Quinone and Hydroquinone Based Flow Battery', Patent WO2015048550, 02 April 2015.

159. W.O. Gordon, E. Plattner, F. Doppenberg, 'Production of pulp by the soda-anthraquinone process (SAP) with recovery of the cooking chemicals', US Patent 5,595,628, 21 Jan 1997.

160. M.L. Crossley, 'The separation of mono-β, 2,6- and 2,7-sulfonic acids of anthraquinone', *J. Am. Chem. Soc.*, **37** (1915) 2178-2181.

161. 'US Geological Survey 2010 Minerals Yearbook: Bromine'. http://minerals.usgs.gov/minerals/pubs/commodity/bromine/myb1-2010-bromi.pdf.

162. G.G. II. Joseph, A.J. Gotcher, G. Sikha, G.J. Wilson, 'High performance flow battery', US Patent 20110244277 A1, 6 Oct 2011.

163. J.R. Goldstein, 'Novel flow battery and usage thereof', US Patent 20150048777 A1, 19 Feb 2015.

164. 'Seventeenth Report of the Joint FAO/WHO Expert Committee on Food Additives. Report No. 539', *Wld Hlth Org. Techn. Rep. Ser., World Health Organization, Geneva,* (1974).

165. C. Giacomelli, K. Ckless, D. Galato, F.S. Miranda, A. Spinelli, 'Electrochemistry of caffeic acid aqueous solutions with pH 2.0 to 8.5', *J. Braz. Chem. Soc.*, **13** (2002) 332-338.

166. M. Lee, J. Hong, D.H. Seo, D.H. Nam, K.T. Nam, K. Kang, C.B. Park, 'Redox Cofactor from Biological Energy Transduction as Molecularly Tunable Energy-Storage Compound', *Angew. Chem. Int. Ed.*, **52** (2013) 8322-8328.

167. S. Chen, M.S. Hossain, F. W. Jr. Foss, 'Organocatalytic Dakin oxidation by nucleophilic flavin catalysts', *Org. Lett.*, **14** (2012) 2806-2809.

168. G. de Gonzalo, C. Smit, J. Jin, A.J. Minnaard, M.W. Fraaije, 'Turning a riboflavin-binding protein into a self-sufficient monooxygenase by cofactor redesign', *Chem. Commun.*, **47** (2011) 11050-11052.

169. A.A. Linden, M. Johnsson, N. Hermanns, J.E. Backvall, 'Efficient and selective sulfoxidation by hydrogen peroxide, using a recyclable Flavin-[BMIm]PF_6 catalytic system', *J. Org. Chem.*, **71** (2006) 3849-3853.

170. T. Yamamura, Y. Shiokawa, H. Yamana, H. Moriyama, 'Electrochemical investigation of uranium β-diketonates for all-uranium redox battery', *Electrochim. Acta*, **48** (2002) 43-50.

171. Y. Yang, G. Zheng, Y. Cui, 'A membrane-free lithium/polysulfide semi-liquid battery for large-scale energy storage', *Energy Environ. Sci.*, **6** (2013) 1552-1558.

172. F.Y. Fan, W.H. Woodford, Z. Li, N. Baram, K.C. Smith, A. Helal, G.H. McKinley, W.C. Carter, Y.-M. Chiang, 'Polysulfide Flow Batteries Enabled by Percolating Nanoscale Conductor Networks', *Nano Lett.*, **14** (2014) 2210-2218.

173. L. Su, M. Ferrandon, J.A. Kowalski, J.T. Vaughey, F.R. Brushett, 'Electrolyte Development for Non-Aqueous Redox Flow Batteries Using a High-Throughput Screening Platform', *J. Electrochem. Soc.,* **161** (2014) A1905-A1914.

174. K. Hayashi, Y. Nemoto, S.I. Tobishima, J.I. Yamaki, 'Electrolyte for high voltage Li/LiMn1.9Co0.1O4 cells', *J. Power Sources,* **68** (1997) 316-319.

175. A. Poisson, 'Conductivity/Salinity/Temperature Relationship of Diluted and Concentrated Standard Seawater', *IEEE J. Ocean. Eng.,* **5** (1980) 41-50.

176. J.D. Milshtein, A.P. Kaur, M.D. Casselman, J.A. Kowalski, S. Modekrutti, P.L. Zhang, N.H. Attanayake, C.F. Elliott, S.R. Parkin, C. Risko, F.R. Brushett, S.A. Odom, 'High current density, long duration cycling of soluble organic active species for non-aqueous redox flow batteries', *Energy Environ. Sci.,* **9** (2016) 3531-3543.

177. R. Darling, K. Gallagher, W. Xie, L. Su, F. Brushett, 'Transport Property Requirements for Flow Battery Separators', *J. Electrochem. Soc.,* **163** (2016) A5029-A5040.

178. L. Su, R.M. Darling, K.G. Gallaher, W. Xie, J.L. Thelen, A.F. Badel, J.L. Badel, J.L. Barton, K.J. Cheng, N.P. Balsara, J.S. Moore, F.R. Brushett, 'An investigation of the Ionic Conductivity and Species Crossover of Lithiated Nafion 117 in Nonaqueous Electrolyte', *J. Electrochem. Soc.,* **163** (2016) A5253-A5262.

179. X.L. Wei, W.T. Duan, J.H. Huang, L. Zhang, B. Li, D. Reed, W. Xu, V. Sprenkle, W. Wang, 'A High-Current, Stable Nonaqueous Organic Redox Flow Battery', *ACS Energy Lett.,* **1** (2016) 705-711.

180. F.R. Brushett, J.T. Vaughey, A.N. Jansen, 'An All-Organic Non-aqueous Lithium-Ion Redox Flow Battery', *Adv. Energy Mater.,* (2012) 1390-1396.

181. R.A. Potash, J.R. McKone, S. Conte, H.D. Abruna, 'On the Benefits of a Symmetric Redox Flow Battery', *J. Electrochem. Soc.,* **163** (2016) A338-A344.

182. R. Potash, J.R. Mckone, H.D. Abruna, S. Conte, 'Symmetric Redox Flow Battery containing organic redox active molecule', WO 2015/148357 A1, 1 Oct 2015, (2015).

183. S.H. Oh, C.W. Lee, D.H. Chun, J.D. Jeon, J. Shim, K.H. Shin, J.H. Yang, 'Metal-free and all-organic redox flow battery with polythiophene as the electroactive species', *J. Mater. Chem. A,* **2** (2014) 19994-19998.

184. Z. Chen, Y. Qin, K. Amine, 'Redox shuttles for safer lithium-ion batteries', *Electrochim. Acta,* **54** (2009) 5605-5613.

185. W.K. Behl, D.T. Chin, 'Electrochemical Overchage Protection of Rechargeable Lithium Batteries I. Kinetics of Iodide/ Tri-Iodide/ Iodine Redox Reactions on Platinum in LiAsF6/Tetrahydrofuran Solutions', *J. Electrochem. Soc.,* **135** (1988) 16-21.

186. K.M. Abraham, D.M. Pasquariello, E.B. Willstaedt, 'n - Butylferrocene for Overcharge Protection of Secondary Lithium Batteries', *J. Electrochem. Soc.*, **137** (1990) 1856-1857.

187. L.M. Moshurchak, W.M. Lamanna, M. Bulinski, R.L. Wang, R.R. Garsuch, J. Jiang, D. Magnuson, M. Triemert, J.R. Dahn, 'High-Potential Redox Shuttle for Use in Lithium-Ion Batteries', *J. Electrochem. Soc.*, **156** (2009) A309-A312.

188. Z. Li, S. Li, S.Q. Liu, K.L. Huang, D. Fang, F.C. Wang, S. Peng, 'Electrochemical Properties of an All-Organic Redox Flow Battery Using 2,2,6,6-Tetramethyl-1-Piperidinyloxy and N-Methylphthalimide', *Electrochem. Solid-State Lett.,* **14** (2011) A171-A173.

189. S.K. Park, J. Shim, J. Yang, K.H. Shin, C.S. Jin, Y.S. Lee, J.D. Jeon, 'Electrochemical properties of a non-aqueous redox battery with all-organic redox couples', *Electrochemistry Communications,* **59** (2015) 68-71.

190. A.P. Kaur, N.E. Holubowitch, S. Ergun, C.F. Elliott, S.A. Odom, 'A Highly Soluble Organic Catholyte for Non-Aqueous Redox Flow Batteries. Energy Technol', **3** (2015) 476-480.

191. W. Duan, R. Vemuri, J.D. Milshtein, S. Laramie, R.D. Dmello, J. Huang, L. Zhang, D. Hu, M. Vijayakumar, W. Wang, J. Liu, R.M. Darling, L. Thompson, K. Smith, K. Smith, J.S. Moore, F.R. Brushett, X. Wei, 'A symmetric organic-based non-aqueous redox flow battery and its state of charge diagnostics by FTIR', *J. Mater. Chem. A*, **4** (2016) 5448-5456.

192. J. Winsberg, T. Hagemann, S. Muench, C. Friebe, B. Haupler, T. Janoschka, S. Morgensterm, M.D. Hager, U.S. Schubert, 'Poly(boron-dipyrromethene) - A Redox-Active Polymer Class for Polymer Redox-Flow Batteries', *Chem. Mater.*, **28** (2016) 3401-3405.

193. A.R. Forrester, R.H. Thomson, 'Stable Nitroxide Radicals', *Nature,* **203** (1964) 74-75.

194. H. Nishide, S. Iwasa, J.Y. Pu, T. Suga, K. Nakahara, M. Satoh, 'Organic radical battery: nitroxide polymers as a cathode-active material', *Electrochim. Acta,* **50** (2004) 827-831.

195. K. Nakahara, S. Iwasa, M. Satoh, Y. Morioka, J. Iriyama, M. Suguro, E. Hasegawa, 'Rechargeable batteries with organic radical cathodes', *Chem. Phys. Lett.,* **359** (2002) 351-354.

196. D.W. Leedy, D.L. Muck, 'Cathodic reduction of phthalimide systems in non-aqueous solutions', *J. Am. Chem. Soc.*, **93** (1971) 4263-4270.

197. K. Oyaizu, A. Hatemata, W. Choi, H. Nishide, 'Redox-active polyimide/ carbon nanocomposite electrodes for reversible charge storage at negative potentials: expanding the functional horizon of polyimides', *J. Mater. Chem.,* **20** (2010) 5404-5410.

198. A. Bourke, M.A. Miller, R.P. Lynch, X. Gao, J. Landon, J.S. Wainright, R.F. Savinell, D.N. Buckley, 'Electrode Kinetics of Vanadium Flow Batteries: Contrasting Responses of VII - VIII and VIV - VV to electrochemical pretreatment of carbon', *J. Electrochem. Soc.,* **163** (2016) A5097-A5105.

199. D.W. Chang, H.J. Lee, J.H. Kim, S.Y. Park, S.M. Park, L. Dai, J.B. Baek, 'Novel quinoxaline-based organic sensitizers for dye-sensitized solar cells', *Org. Lett.,* **13** (2011) 3880-3883.

200. J.Y. Lee, W.S. Shin, J.R. Haw, D.K. Moon, 'Low Band-gap Polymers Based on Quinoxaline Derivatives and Fused Thiophene as Donor Materials for High Efficiency Bulk-heterojunction Photovoltaic Cells', *J. Mater. Chem.,* **19** (2009) 4938-4945.

201. L. Li, S. Kim, W. Wang, M. Vijayakumar, Z. Nie, B. Chen, J. Zhang, G. Xia, J. Hu, G. Graff, J. Liu, Z. Yang, 'A Stable Vanadium Redox-Flow Battery with High Energy Density for Large-Scale Energy Storage', *Adv. Energy Mater.,* **1** (2011) 394-400.

202. A.P. Kaur, S. Ergun, C.F. Elliott, S.A. Odom, '3,7-Bis(trifluoromethyl)-N-ethylphenothiazine: a redox shuttle with extensive overcharge protection in lithium-ion batteries', *J. Mater. Chem. A,* **2** (2014) 18190-18193.

203. K.U. Schwenke, S. Meini, X. Wu, H.A. Gasteiger, M. Piana, 'Stability of superoxide radicals in glyme solvents for non-aqueous Li-O2 battery electrolytes', *Phys. Chem. Chem. Phys.,* **15** (2013) 11830-11839.

204. E. Nasybulin, W. Xu, M.H. Engelhard, Z. Nie, S.D. Burton, L. Cosimbescu, M.E. Gross, J. Zhang, 'Effects of Electrolyte Salts on the Performance of Li- O2 Batteries', *J. Phys. Chem. C,,* **117** (2013) 2635-2645.

205. S.J. Lee, B.G. Kim, 'Method for preparing electrolyte for vanadium redox flow battery using vanadium oxide', US Patent 20150056525 A1, 26 Feb ,2015.

206. M.R. Mohamed, P.K. Leung, M.H. Sulaiman, 'Performance characterization of a vanadium redox flow battery at different operating parameters under a standardized test-bed system', *Appl. Energy,* **147** (2015) 402-412.

207. J.A. Conkling, C.J. Mocella, 'Chapter 7 - Chemistry of Pyrotechnics', CRC Press Ltd. United States, (1985) 159-178.

208. T. Suga, S. Sugita, H. Ohshiro, K. Oyaizu, H. Nishide, 'p- and n-Type Bipolar Redox-Active Radical Polymer: Toward Totally Organic Polymer-Based Rechargeable Devices with Variable Configuration', *Adv. Mater.,* **23** (2011) 751-754.

209. J. Lee, E. Lee, S. Kim, G.S. Bang, D.A. Shultz, R.D. Schmidt, M.D.E. Forbes, H. Lee, 'Nitronyl Nitroxide Radicals as Organic Memory Elements with Both n- and p- Type Properties', *Angew. Chem. Int. Ed.,* **50** (2011) 4414-4418.

210. T. Akita, K. Kobayashi, 'Magnetic properties of nitronyl nitroxide radicals substituted in phenylboronic acid the BOH O hydrogen bond as a constituent unit of a one-dimensional suprastructure exhibiting a ferromagnetic spin interaction', *Adv. Mater.,* **9** (1997) 346-349.

211. Q. Huang, D.W. Choi, L. Cosimbescu, J.P. Lemmon['Multi-electron redox reaction of an organic radical cathode induced by a mesopore carbon network with nitroxide polymers', *Phys. Chem. Chem. Phys.,* **15** (2013) 20921-20928.

212. T. Sukegawa, I. Masuko, K. Oyaizu, H. Nishide, 'Expanding the Dimensionality of Polymers Populated with Organic Robust Radicals toward Flow Cell Application: Synthesis of TEMPO-Crowded Bottlebrush Polymers Using Anionic Polymerization and ROMP, Macromolecules', **47** (2014) 8611-8617.

213. C. Li, H. Bai, G. Shi, 'Conducting polymer nanomaterials: electrosynthesis and applications', *Chem. Soc. Rev.,* **38** (2009) 2397-2409.

214. G. Hauffman, Q. Maguin, J.P. Bourgeois, A. Vlad, J.F. Gohy, 'Micellar Cathodes from Self-Assembled Nitroxide-Containing Block Copolymers in Battery Electrolytes', *Macromol. Rapid Commun.,* **35** (2014) 228-233.

215. G. Hauffman, J. Rolland, J.P. Bourgeois, A. Vlad, J.F. Gohy, 'Synthesis of nitroxide-containing block copolymers for the formation of organic cathodes', *J. Polym. Sci., Part A: Polym. Chem.,* **51** (2013) 101-108.

216. N. Boens, B. Verbelen, W. Dehaen, 'Postfunctionalization of the BODIPY Core: Synthesis and Spectroscopy', *Eur. J. Org. Chem.,* **30** (2015) 6577-6595.

217. S.P. Singh, T. Gayathri, 'Evolution of BODIPY Dyes as Potential Sensitizers for Dye-Sensitized Solar Cells', *Eur. J. Org. Chem.,* **22** (2014) 4689-4704.

218. T. Kowada, H. Maeda, K. Kikuchi, 'BODIPY-based probes for the fluorescene imaging of biomolecules in living cells', *Chem. Soc. Rev.,* **44** (2015) 4953-4972.

219. F. Harnisch, U.P.D. Schroder, M.P.D. Broring, 'Use of metal-free organonitrogen compound as redox-active Substance used in redox electrolyte for energy storage accumulator, fuel ell and redox flow battery, contains two five- or six- diatomic annealed rings', German Patent DE102012015176A1, 6 Feb 2014.

220. S. Kim, J. Bouffard, Y. Kim, 'Tailoring the Solid-State Fluorescene Emission of BODIPY Dyes by meso Substitution', *Chem. - Eur. J.*, **21** (2015) 17459-17465.

221. A.B. Nepomnyashchii, S. Cho, P.J. Rossky, A.J. Bard, 'Dependence of Electrochemical and Electrogenerated Chemiluminescene Properties on the Structure of BODIPY Dyes, Unusually Large Separation between Sequential Electron Transfers', *J. Am. Chem. Soc.,* **132** (2010) 17550-17559.

222. H. Senoh, M. Yao, H. Sakaebe, K. Yasuda, Z. Siroma, 'A two-compartment cell for using soluble benzoquinone derivatives as active materials in lithium secondary batteries', *Electrochim. Acta,* **56** (2011) 10145-10150.

223. X. Wei, W. Xu, M. Vijayakumar, L. Cosimbescu, T. Liu, V. Sprenkle, W. Wang, 'TEMPO-Based Catholyte for High-Energy Density Nonaqueous Redox Flow Batteries', *Adv. Mater.,* **26** (2014) 7649-7653.

224. Y. Wang, E.I. Rogers, S.R. Belding, R.G. Compton, 'The electrochemical reduction of 1,4-benzoquinone in 1-ethyl-3-methylimidazolium bis(trifluoromethane-sulfonyl)-imide, [C2mim][NTf2]: A voltammetric study of the comproportionation between benzoquinone and the benzoquinone dianion', *J. Electronal. Chem.,* **648** (2010) 134-142.

225. J.F. Xiang, C.X. Chang, M. Li, S.M. Wu, L.J. Yuan, J.T. Sun, 'A novel coordination polymer as positive electrode material for lithium ion battery', *Cryst. Growth Des.,* **8** (2008) 280-282.

226. T. Nagaoka, S. Okazaki, T. Fujinaga, 'Ion-pair effects on the electroreduction of carbonyl compounds in N,-Dimethylformamide', *J. Electroanal. Chem.,* **133** (1982) 89-99.

227. K.J. Stutts, G.W. Eastland, 'The lithium salt of benzoquinone radical anion and voltammetric anomalies', *J. Electroanal. Chem.,* **234** (1987) 357-359.

228. Z. Zhang, L. Zhang, J.A. Schlueter, P.C. Redfern, L. Curtiss, K. Amine, 'Understanding the redox shuttle stability of 3,5-di-tert-butyl-1,2-dimethoxybenzene for overcharge protection of lithium-ion batteries', *J. Power Sources,* **195** (2010) 4857-4962.

229. L. Zhang, Z. Zhang, P.C. Redfern, L.A. Curtiss, K. Amine, 'Molecular engineering towards safer lithium-ion batteries: A highly stable and compatible redox shuttle for overcharge protection', *Energy Environ. Sci.,* **5** (2012) 8204-8207.

230. T. Suga, Y.J. Pu, S. Kasatori, H. Nishide, 'Cathode- and Anode-Active Poly(nitroxylstyrene)s for Rechargeable Batteries: p- and n-Type Redox Switching via Substituent Effects, Macromolecules', *Macromolecules,* **40** (2007) 3167-3173.

231. T. Suga, H. Ohshiro, S. Sugita, K. Oyaizu, H. Nishide, 'Emerging N-Type Redox-Active Radical Polymer for a Totally Organic Polymer-Based Rechargeable Battery', *Adv. Mater.,* **21** (2009) 1627-1630.

232. J. Qu, T. Fujii, T. Katsumata, Y. Suzuki, M. Shiotsuki, F. Sanda, M. Satoh, J. Wada, T. Masuda, 'Helical polyacetylenes carrying 2,2,6,6-tetramethyl-1-piperidinyloxy and 2,2,5,5-tetramethyl-1-pyrrolidinyloxy moieties: Their synthesis, properties, and function', *J. Polym. Sci., Part A: Polym. Chem.,* **45** (2007) 5431-5445.